Titre: Title:	Modeling and Simulation of an Aircraft Environmental Control System
Auteur: Author:	Daniel Perez Linares
Date:	2016
Type:	Mémoire ou thèse / Dissertation or Thesis
Référence: Citation:	Perez Linares, D. (2016). Modeling and Simulation of an Aircraft Environmental Control System [Mémoire de maîtrise, École Polytechnique de Montréal]. PolyPublie. https://publications.polymtl.ca/2277/

UNIVERSITÉ DE MONTRÉAL

MODELING AND SIMULATION OF AN AIRCRAFT ENVIRONMENTAL CONTROL SYSTEM

DANIEL PEREZ LINARES

DÉPARTEMENT DE GÉNIE CHIMIQUE

ÉCOLE POLYTECHNIQUE DE MONTRÉAL

MÉMOIRE PRÉSENTÉ EN VUE DE L'OBTENTION

DU DIPLÔME DE MAÎTRISE ÈS SCIENCES APPLIQUÉES

(GÉNIE CHIMIQUE)

AOÛT 2016

UNIVERSITÉ DE MONTRÉAL

ÉCOLE POLYTECHNIQUE DE MONTRÉAL

Ce mémoire intitulé :

MODELING AND SIMULATION OF AN AIRCRAFT ENVIRONMENTAL CONTROL SYSTEM

présenté par : PEREZ LINARES Daniel

en vue de l'obtention du diplôme de : Maîtrise ès sciences appliquées

a été dûment accepté par le jury d'examen constitué de :

M. PERRIER Michel, Ph. D, président

M. SRINIVASAN Bala, Ph. D., membre et directeur de recherche

M. BEAULAC Sébastien, membre

DEDICATION

To my brother

ACKNOWLEDGEMENTS

Je tiens à remercier tout d'abord mon directeur Bala Srinivasan pour la confiance qu'il m'a accordée durant ce projet. Ses conseils m'ont beaucoup guidé et son support m'a encouragé dans les moments les plus difficiles. J'en suis grandement reconnaissant.

Merci à mes collègues chez Bombardier : Amir, Pascal, Yannick, André, Hongzhi, Tariq, Benoit, Amine, Walid et Sébastien. Par votre présence, vous avez rendu mon projet des plus agréables. Merci de m'avoir initié à Clash of Clans auquel je joue toujours d'ailleurs.

Merci à mes amis colocataires qui m'ont encouragé lorsque la motivation n'était pas au rendez-vous. Merci pour les bons moments passés ensemble.

Finalement, je tiens à remercier ma famille et proches pour toujours avoir été là pour moi, je vous en suis très reconnaissant.

RÉSUMÉ

Dans ce mémoire, on traite de la modélisation du Système de contrôle de l'environnement (SCE) des avions CS300 de Bombardier en se basant sur des données de vol et des modèles analytiques. Plus précisément, les données de vol et l'analyse dimensionnelle sont utilisées pour créer des modèles des composantes du SCE. La principale fonctionnalité du SCE est de fournir les conditions optimales dans les cabines afin d'assurer le confort des passagers. Ainsi, ce système assure une pressurisation convenable, régule la température et fournit une ventilation adéquate en fonction du nombre de passagers en traitant l'air provenant des moteurs à réaction. Les composantes principales du SCE comprennent quatre échangeurs de chaleur à plaques et ailettes, un ventilateur, un compresseur, une turbine, des vannes de régulation, des sources et des puits de chaleur, et les conduites faisant circuler l'air. Pour chaque composante mécanique, les paramètres de performance ont été adimentionnalisés et cartographiés. Lorsque des surfaces tridimensionnelles étaient requises, les paramètres de performances issus des données de vol ont été complémentés avec des hypothèse de lissage de surface. En procédant de cette façon, un problème de régularisation a pu être résolu. L'architecture du SCE a été créée et résolu à l'aide du logiciel Flowmaster® (FM). En effet, le logiciel permet d'intégrer des scripts personnalisés au modèle ce qui le rend très flexible. Les résultats de simulation du modèle ont été comparés aux données de vol et les deux convergent vers des valeurs similaires. Seuls les résultats de simulation des cas avec beaucoup d'humidité (HD et XHD) n'ont pas convergé vers les températures attendues parce que le calcul de transfert thermique dans Flowmaster néglige la chaleur latente de l'eau. Néanmoins, un algorithme Matlab est suggéré dans ce mémoire afin d'améliorer celle du logiciel. Pour tous les autres cas de vol (XCD, CD et ISA), le modèle est capable de prédire les conditions dans les cabines selon l'altitude, la température extérieure, et la vitesse de l'avion.

ABSTRACT

In this memoir we address the task of modeling Bombardier's CSeries 300 aircraft environmental control system (ECS) based on flight data. That is, flight data and dimensional analysis is used to model the system main components. The function of the ECS is to supply optimal cabin conditions to the passengers' cabin (ventilation, pressurization, temperature control and best possible humidity) using bleed air coming from the engines. The system components comprise four heat exchangers, a fan, a compressor, a turbine, control valves, cabin heat sources and sinks and the interconnecting piping. For each component analogous to a mechanical machine, the performance parameters were adimensionalized and their respective performance maps were built. When tridimensional reliable maps were required, flight data was augmented with smoothing assumptions. By doing so, a regularized optimization problem could be solved. The ECS network was built and solved with Flowmaster® software (FM). In fact, the software allows for customized scripts and performance maps to be easily imported to the model. The simulation of the final model was compared with flight data and converged to very similar results. Only simulations with very high humidity (HD and XHD cases) failed to converge to the expected temperature because Flowmaster's heat exchanger calculation neglected water latent heat. Nevertheless, code is suggested in this work to improve the software calculation method. For all the other cases (XCD, CD and ISA), the model is able to predict cabin conditions at any permitted altitude and aircraft speed. Moreover, the model and can be used as a design tool or analysis tool within Bombardier's support team.

TABLE OF CONTENTS

LIST OF TABLES

LIST OF FIGURES

LIST OF SYMBOLS AND ABBREVIATIONS

Acronyms

A/C	Aircraft
ACM	Air Cycle Machine
ACU	Air Conditioning Unit
APU	Auxiliary Power Unit
BA	Bombardier Aerospace
CD	Cold Day conditions
Cd	Coefficient of discharge
CDS	Condenser
CDTS	Compressor Discharge Temperature Sensor
CMFR	Corrected Mass Flow Rate
CS	Corrected Speed
DART	Dry Air Rated Temperature
DBT	Dry Bulb Temperature
DTS	Duct Temperature Sensor
ECS	Environmental Control System
EOS	Equation of State
FCV	Flow Control Valve
FSV	Flow Sensor Venturi
FWD	Forward Part of Cabin
GND	Ground
HAAO	High Altitude Airport Operation
HD	Hot Day conditions
HX	Heat Exchanger
IAMS	Integrated Air Management System
IASC	Integrated Air System Controller
ITD	Inlet Temperature Difference
LPDS	Low Pressure Distribution System
ISA	Standard day conditions

LTS	Liebherr Aerospace Toulouse S.A.S
MFR	Mass Flow Rate
MHX	Main Heat Exchanger (same as SHX)
MIXTS	Mix manifold Temperature Sensor
NTU	Number of Transfer Units
OAT	Outside Ambient Temperature
OFV	Outflow Valve
PAX	Passengers
PDTS	Pack Discharge Temperature Sensor
PHX	Primary Heat Exchanger
PR	Pressure Ratio
PRSOV	Pressure Regulating and Shut-Off Valve
PTS	Pack Temperature Sensor
RARV	Ram Air Regulating Valve
REH	Reheater
SHX	Secondary Heat Exchanger
TACKV	Trim Air Check Valve
TAV	Trim Air Valve
TAPRV	Trim Air Pressure Regulating Valve
TCV	Temperature Control Valve
VENTS	Ventilated Temperature Sensor
WE	Water Extractor

Symbols

A	Area
C_p	Specific heat capacity at constant pressure
C_r	Ratio of capacity coefficients
D	Diameter
h	Specific enthalpy
M	Mach number
$\dot{m}$	Mass flow rate

N	Rotational speed
P	Pressure
$\dot{Q}$	Volumetric flow rate
$\dot{Q}$	Heat flow
R	Specific gas constant
T	Temperature
U	Overall heat transfer coefficient
V	Velocity
W	Power
Z	Compressibility factor
Z	Fan correction factor
α	Speed of sound
ρ	Density
γ	Heat capacity ratio of air

Subscripts

0	Total or stagnation condition
1	Inlet
2	Outlet
ise	Isentropic
s	Static

LIST OF APPENDICES

CHAPTER 1 INTRODUCTION

1.1 Problematic and hypothesis

Simulation-based engineering (SBE) focuses on the computational tools and techniques to evaluate performance parameters of complex systems and has become the primary means of analysis in the industry. The advantages of SBE are numerous: minimal time spent on analysis, reduced costs, and less planning and logistics compared to bench-testing. Ultimately, it improves decision-making among designers and engineers. For example, in the automotive industry, crash worthiness analysis allows engineers to predict the effects of a car crash on the vehicle body by means of computer simulation. This is a major improvement in the automobile design process since, previously, the vehicle had to be crashed in a controlled environment in the real world, which can be expensive and requires considerable planning.

Aircraft simulation modeling consists on creating a digital prototype of a given system in order to predict and evaluate its performance. When such models attain a certain level of maturity, they can become a design tool. The model can be used to discard poor designs early during the design process and achieve significant customer satisfaction.

One of the main concerns in commercial aircraft design is to achieve passenger comfort during flight by providing adequate ventilation, temperature control and pressurization. The system responsible of providing these optimal cabin conditions is called the Environmental Control System (ECS). During a typical flight where ambient conditions change tremendously (altitude, ambient temperature, aircraft speed), this system is to supply adequate heating or cooling to the cabin in the most efficient manner.

Currently, Bombardier's aircraft ECSs are designed by third parties. Thus, thermodynamic analysis with regard to the ECS relies greatly on data not readily available by Bombardier. Moreover, no in-house ECS model is available to predict cabin conditions for every flight case. However, data consisting on 236 different flight cases provided by CS100/300 ECS manufacturer is available. The data comprise Auxiliary Power Unit (APU), one engine and two engines cases in-ground or in-flight under various ambient conditions. For each case, data on the inlet and outlet conditions (mass

flow rate, temperature, pressure) and efficiencies (if applicable) of the main components of the ECS are given.

Given this amount of information, it was postulated that an ECS model could be reverse engineered by modeling each main component and connecting them. Consequently, the motivation on developing an ECS model to predict cabin conditions ensued.

1.2 Objectives

In light of what's been previously mentioned, the general objective of this thesis is to:

1. Develop a model of the environmental control system based on analytical models that are derived from physical principles, conservation laws for instance, and data-based models obtained from flight-testing. Use Flowmaster software to build the model.
2. Predict temperature and pressure at various points of the system under different flight conditions with a reasonable accuracy.

The sub-objectives can be detailed as follows:

1. Verification of each component presented in the schematic of the ECS.
2. Validation of the model by comparing with data.

1.3 Methodology and organisation

Flowmaster software is used to model the system. The choice of this modeling tool was made prior to the beginning of this project. Nevertheless, one of the reasons for choosing this platform is based on its modular approach in opposition to written code. In fact, the ECS components can be connected to each other in a very intuitive and user-friendly manner. Moreover, the model can be understood more easily by other people without the considerable effort in decrypting lines of code.

In theory, highly accurate modeling of components such as pipes and heat-exchangers could be undertaken by considering two-dimensional or three-dimensional flow, but the data available to us assumes the flow is directed to only one direction, i.e. the direction of the flow. Thus, in this work

the ECS is considered as a 1D thermo-fluid system that could be solved in principle with Flowmaster, a 1D thermo-fluid software.

This master's thesis is divided in 5 chapters. Chapter 2 presents the state of the art with regards to ECS modeling. A review of literature is reported and the governing equations of the main components of the ECS model are introduced.

In Chapter 3, the developed model is presented by describing its internal and external inputs. In the chapter afterward, the performance maps obtained and simulation results are stated. Finally, in chapter 5, discussion with regard to the results is presented.

CHAPTER 2 STATE OF THE ART

2.1 Environmental control system description

Many aircraft systems carry different functions to ensure safe flight. To name some examples we can think of propulsion, avionics, fuel, landing gear, auxiliary power unit (APU) and pneumatics. The Environmental Control System (ECS) is another example of great importance. In this section, we will describe its function, explain what its components are and how it works.

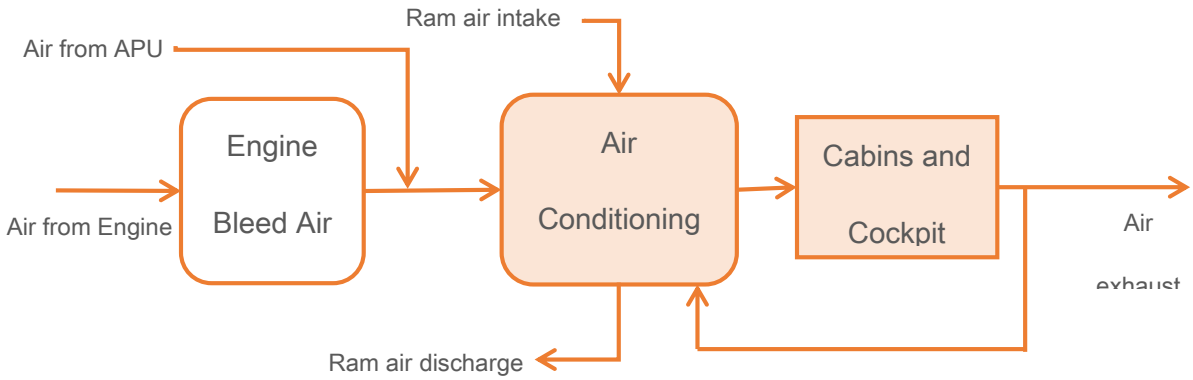

Figure 1 Simplified ECS block diagram

The main function of the Environmental Control System is to provide the conditions for comfortable travelling of passengers. This includes optimum cabin air pressure, cooling, heating and ventilation within the passengers' cabin compartment, cockpit and cargo compartments. [1] The technology of an ECS is based on air-cycle refrigeration process. Such process is called the reversed Brayton cycle. [2] Although, it is important to remember that an ECS is not a closed system as the Brayton cycle, but is often considered as so in thermodynamic analysis.

In Figure 1, the ECS is schematically represented by the Engine Bleed Air System, the Air Conditioning System and the cabins and cockpit. Air is first extracted from the engine or APU and flows to the Wing Anti-ice system (WAIS) and Air conditioning system. The air conditioning system is composed of many units processing hot and pressurized bleed air. Here, air is ultimately cooled down and expanded down to a pressure around 1 atm. Thereafter, the breathable gas is sent

to passenger cabins, cockpit and cargo compartments. Approximately, one half of the amount of air sent to cabins is recycled while the other half is exhausted to the ambient. [3]

Air conditioning system

Air entering the air conditioning system comes from the engine bleed. The first unit the air encounters is the primary heat-exchanger where heat is removed with ambient air (ram air) as the coolant fluid. Next, air pressure is increased by a centrifugal compressor, part of the Air Cycle Machine (ACM). Since this step increases the temperature, air is passed through a secondary heat-exchanger. Air is cooled in the primary heat-exchanger prior to being compressed because the amount of work required to compress a gas decreases as the temperature of the gas decreases. [4]

After passing through the secondary heat-exchanger, air flows through two other heat-exchangers: the reheater and condenser. In the reheater, a small amount of heat is transferred to the cold fluid. In the condenser, air is cooled as much as possible so as to condense the water vapor that air might carry. The condensed water is then removed by the water extractor. Removal of water is very important in order to avoid icing that can break the turbine. It also enables the turbine outlet temperature to reach sub-zero state. [4]

At this point, air is very cold so it is warmed in the reheater (in case some icing has formed) prior to be expanded in the turbine. At the turbine exit, air might be below the target temperature. Therefore, it is heated with a small amount of non-conditioned hot engine bleed air. The non-conditioned flow is controlled by the Temperature Control Valve (TCV) coupled to the Integrated Air System Controller (IASC). The last unit is the mix manifold where air is mixed with recycled cabin air. As a matter of fact, without recirculation, a greater fuel penalty on the aircraft would be imposed. [5]

The central component of the air conditioning system is the three-wheel ACM unit comprising the turbine, compressor and fan mounted on the same shaft. [3] It is the power output from the turbine that drives the compressor and fan. The fan is located in the ram air channel and its purpose is to ensure there is sufficient flow in the channel when aircraft is on ground. Because of space and weight constraints imposed in new generation aircrafts, the rotating elements in the ACM are very small. As a result, ACMs must handle significant air mass flows with large enthalpy drops. These constraints can be achieved with high rotational speeds ranging from 60 000 to 90 000 RPM.

Note that since there are two engines in the CSeries aircrafts, there are two identical packs, each containing one ACM and all the other components described previously. The left pack is supplied with air from the left engine and the other from the right engine. The mix manifold mixes air coming from both packs in addition to the recycled cabin air. Figure 2 illustrates the ECS flow diagram, while Figure 3 shows the equivalent Catia drawing of the left and right packs.

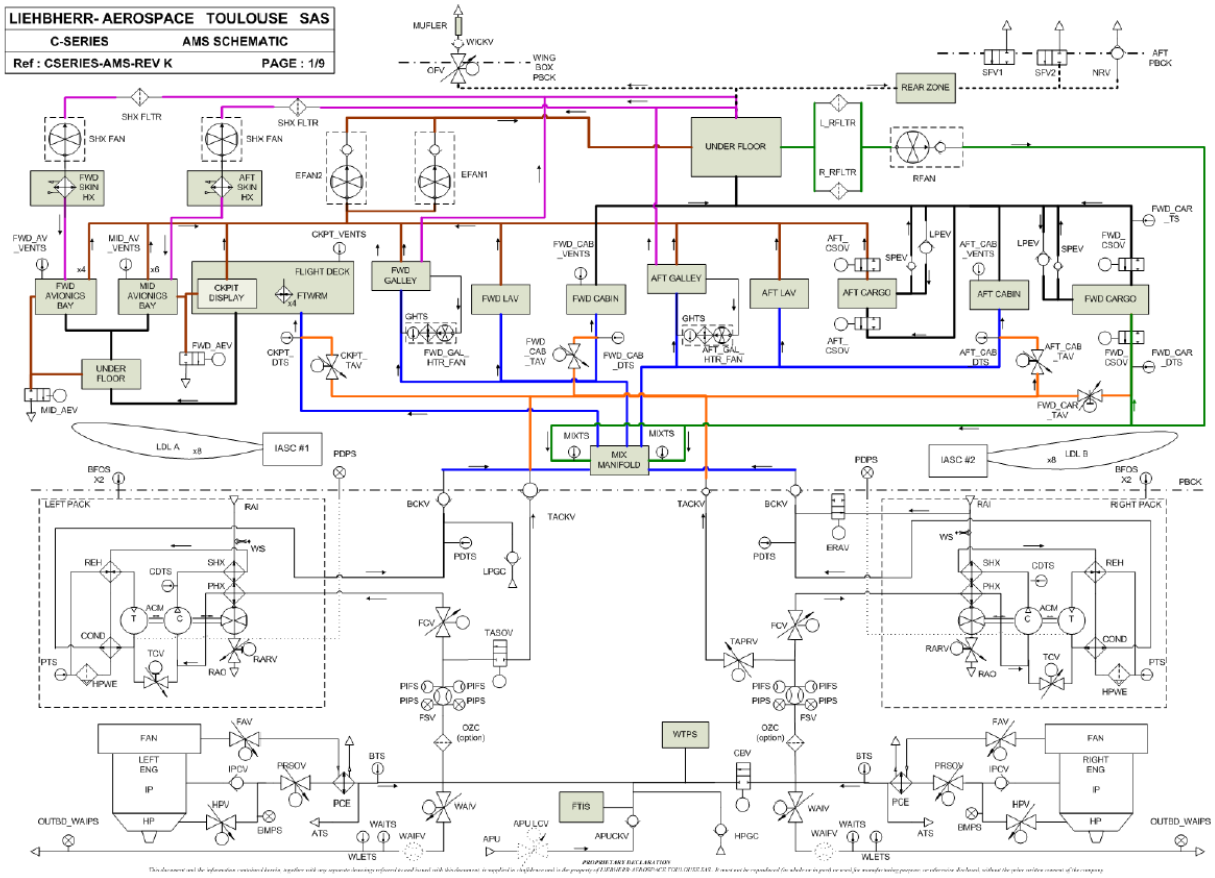

Figure 2 Ecs schematic [6]

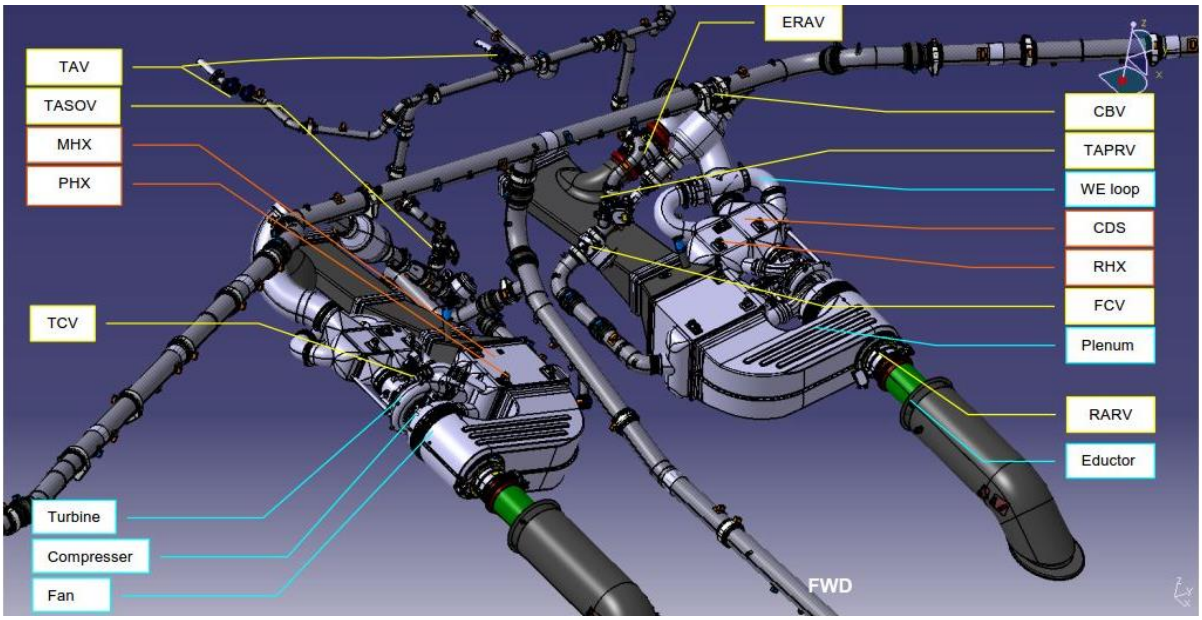

Figure 3 Right and left packs [7]

Integrated air management system

Flow control within the packs and cabins is monitored by the *Integrated Air Management System* (IAMS). Flow is controlled by action of the *Flow Control Valve* (FCV) and will depend on the flow schedule, which in turn depends on flight conditions such as the altitude, number of passengers, number of packs available, cargo heating, etc.

Temperature is also monitored by the IAMS. For this task, temperature sensors are installed at specific locations in the cabin, cockpit, packs and ducts. The ECS temperature readings are regulated by action of three valves: TAV, TCV and RARV. For example, the temperature at the *Compressor Discharge Temperature Sensor* (CDTS) must be kept at 148°C when possible. When the temperature is higher, the RARV position is changed to keep the temperature at its target value. However, RARV action is limited. If the temperature cannot be regulated and exceeds 220°C, then the flow through the pack is reduced by action of the FCV. As last resort, if the temperature goes above 232°C, the FCV is completely closed and the pack is turned down. [6] Clearly, every control action described so far is performed automatically by the IAMS reducing the pilot load tremendously.

Another example of temperature control performed by action of the TCV can be found at the outlet of the water extractor. In fact, the temperature at this location is measured by the Pack Temperature Sensor (PTS) and must not go below a limit to avoid freezing. This temperature limit depends on the aircraft altitude and it is programmed in the IASC. [6]

Low pressure distribution system

The LPDS consists of all the ducts and control valves used to regulate pressure inside the cabin downstream of the mix manifold. The cabin pressure is controlled by modulating pressure drop at the outflow valve (OFV). In addition, positive pressure relief valves prevent over-pressurizing the passengers' cabin.

Dynamic control of ECS

Control of the most important cabin parameters, pressure and temperature, is carried out by manipulation of the outflow valve (OFV) and TCV, respectively. For temperature control, it might also be necessary to open one of the three trim air valves (TAVs) if TCV action is not sufficient. Figure 4 illustrates cabin control inputs and outputs. Note that humidity is not a controlled parameter but rather a passive parameter.

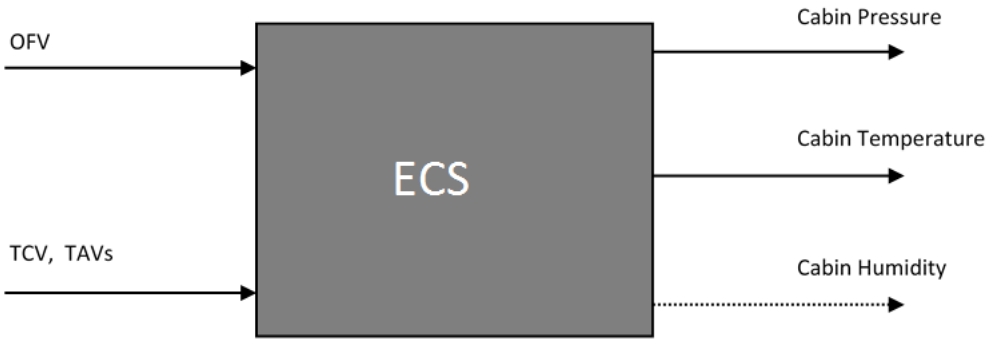

Figure 4 Cabin Control

2.2 Review of literature

Experimental study of aircraft ECS performance have been undertaken by Zhao et al. [2] during off-design conditions and the system response by changing bleed air flow rate and altitude was investigated.

With regard to ECS modeling, one of the first ECS models mentioned in literature dates back to 1975. Eichler [8] developed dynamic models for each component and studied the stability of the whole system. However, the mathematical base of such component models are undescribed. Thus, one can hardly assess the validity of his results. Moreover, time constants were held constant although these happen to be function of flow rate.

Santos, Andrade and Zaparoli [1, 9] developed an air-cycle machine model to simulate the effects of changing Mach number, cabin altitude and cabin recirculation air. However, their model assumed constant efficiencies with regard to the main components (heat-exchangers effectiveness, compressor and turbine efficiencies), whereas these are function of multiple parameters.

More recently, Lin and Tu [10, 11] integrated cabin temperature control based on Fuzzy method to a dynamic ECS model. Furthermore, their heat exchanger is more elaborated as it is a two-dimensional transient model. In order to derive such model, they used a discretized lumped parameter method where heat and mass transfer phenomena were simplified by assuming the Lewis number was equal to one.

On a more specific level, Vargas and Bejan [12-14] have been conducted research on heat-exchanger optimization. They advanced a method for optimal sizing of ECS cross flow heat exchangers by minimisation of ACM entropy generation. Their heat-exchanger model consisted of a specific well-known effectiveness-NTU relation. Perez-Grande and Leo [15] accomplished a similar study by considering two optimum functions: the entropy generation and heat-exchanger weight.

Comini et al. [16, 17] have addressed the heat and mass transfer description in air-cooling applications where latent (condensation and evaporation) and sensible heat transfer is involved. Their analysis can be used to develop more accurate geometrical heat-exchanger models, as it is a three-dimensional approach. Nevertheless, they assumed heat and mass transfer analogy for simplification and their description only applies to laminar flow.

2.3 Mathematical background

In this section, the mathematical model of each ECS component is presented. An assessment is also performed to validate Flowmaster software by comparing FM's results to hand calculations. This step will help the reader get familiar with the way FM solves systems that are more complex and verify that the solution is in agreement with theory.

2.3.1 Pressure drop model

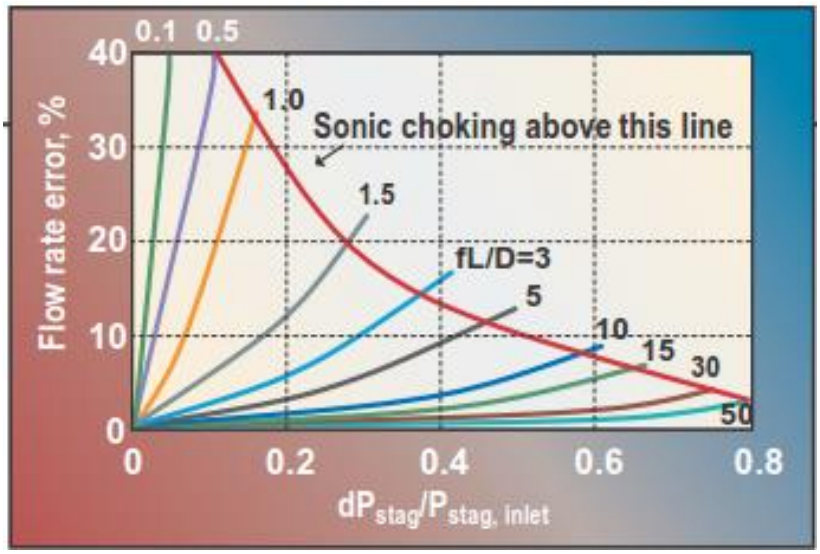

Figure 5 Error in flow rate prediction for a single pipe due to using incompressible flow assumptions [18]

Designing gas-piping networks requires mathematical models that address all the relevant phenomena like sonic choking, accurate pressure drop and psychrometrics. Compressible flow simulation takes into account all of these phenomena whereas incompressible simulations cannot predict choking and are inherently inaccurate with respect to flow rate or pressure drop prediction. Figure 5 illustrate the incompressible flow rate error for different fL/D (Equation 10) ratios as a function of pressure drop over inlet *pressure ratio* (PR). Therefore, a compressible model is preferred for ECS modeling.

The drawback of compressible flow modeling is that it is a challenging technical application because of the couple nature of the governing equations. When a real gas model is included, the complications compound even further. However, FM software can accurately calculate pressure drop, flow rates and temperatures in gas systems by solving the coupled governing equations simultaneously.

The *Cylindrical gas pipe component* as shown in Figure 6 is used to model pressure drop in cylindrical pipes. Friction, heat transfer and variation in cross sectional area affect the flow of a compressible fluid in pipes. Nevertheless, only the adiabatic, constant cross section area with friction is analyzed here, as this is the most common occurrence for ECS piping.

Pipes and ducts

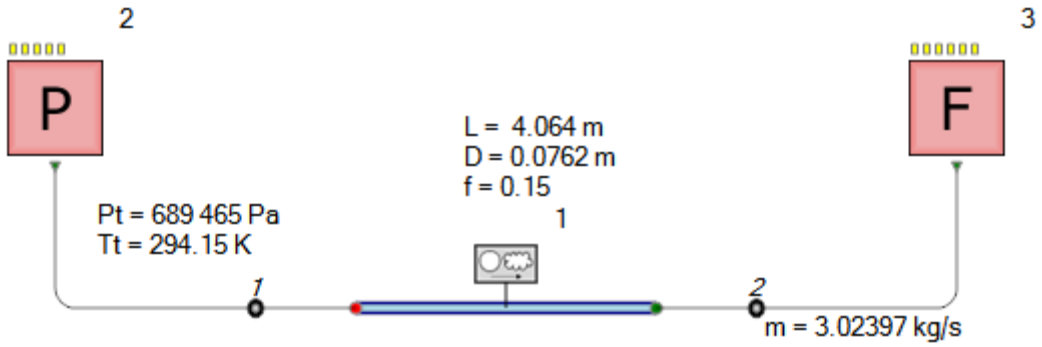

Figure 6 Pipe component

The equations governing steady-state compressible fluids flow in pipes are derived from mass, momentum and energy balance [19]. An equation of state (EOS) that relates gas intensive properties as well as the second law are also required. [20]

$$\boldsymbol{Mass\ balance}: \frac{d\rho}{\rho} + \frac{dV}{V} = 0 \qquad (1)$$

$$\boldsymbol{Momemtum}: dP + \frac{1}{2}\rho V^2 \frac{f}{D} dx + \rho V dV + \rho g dz = 0 \qquad (2)$$

$$\boldsymbol{First\ law}: dq = dh + VdV \qquad (3)$$

$$\boldsymbol{Equation\ of\ state}: P = Z\rho RT \qquad (4)$$

$$\boldsymbol{Mach\ number}:\ \boldsymbol{M = \frac{V}{\sqrt{\gamma ZRT}}} \quad (5)$$

$$\boldsymbol{Second\ law}:\ \boldsymbol{ds \geq 0} \quad (6)$$

Depending on the Equation of State (EOS) selected for the working fluid, FM can evaluate the compressibility factor, *Z*, in Equation 4 and 5. The available EOSs include Redlich-Kwong-Soave (RKS), London Research Station (LRS), Peng-Robinson (PR), the Corresponding States Principle and Chao-Seader-Grayson-Streed. Z can also be defined as a constant. The air heat capacity ratio, γ, is a function of temperature and the relationship can be defined in the working fluid options. However, Z and γ have both been assumed as constants in our model with values of 1 and 1.4, respectively.

Stagnation properties are extensively used in air systems and thus are presented below. [21]

$$\boldsymbol{\frac{T_t}{T} = 1 + \frac{\gamma - 1}{2} M^2} \quad (7)$$

$$\boldsymbol{\frac{P_t}{P} = \left[1 + \frac{\gamma - 1}{2} M^2\right]^{\frac{\gamma}{\gamma - 1}}} \quad (8)$$

$$\boldsymbol{dq = dh_0 = C_{p0} dT_t} \quad (9)$$

The hand solution method consists on rewriting all the governing equations in terms of the Mach number and use the length of the pipe to compute the increase in Mach number. Therefore, the following equation is derived from Equations 1 to 6 assuming an adiabatic process with no change in potential energy ($dq = 0, \rho g dz = 0$).

$$\int_0^L \frac{f}{D} dx = \int_{M_1}^{M_2} \frac{(1 - M^2)}{\gamma M^3 \left(1 + \frac{\gamma - 1}{2} M^2\right)} dM$$

After integration,

$$\boldsymbol{Pressure\ drop\ coefficient}:\ \boldsymbol{\frac{\bar{f}}{D} L = \frac{1}{\gamma}\left(\frac{1}{M_1^2} - \frac{1}{M_2^2}\right) + \frac{\gamma + 1}{2\gamma} ln\left[\frac{M_1^2}{M_2^2}\left(\frac{1 + \frac{\gamma - 1}{2} M_2^2}{1 + \frac{\gamma - 1}{2} M_1^2}\right)\right]} \quad (10)$$

Where $\bar{f} L = \int_0^L f dx$.

For accurate results, FM uses the Swamee-Jain equation [22] to compute the Darcy friction factor, *f*, for turbulent flow in circular pipes. It approximates the implicit Colebrook-White equation. However, FM can also use a constant average value throughout the pipe specified by the user.

$$\boldsymbol{Swamee - Jain\ relation}: \boldsymbol{f} = \frac{\mathbf{0.25}}{\left[log_{10}\left(\frac{k}{3.7D}+\frac{5.74}{Re^{0.9}}\right)\right]^2} \tag{11}$$

Where *k* is the roughness of the pipe and *Re* is the Reynolds number.

At last, the following equation derived from the continuity and stagnation properties is introduced:

$$\dot{\boldsymbol{m}} = \boldsymbol{AP_t}\sqrt{\frac{\gamma}{ZRT_t}}\boldsymbol{M}\left(\mathbf{1}+\frac{\gamma-1}{2}\boldsymbol{M^2}\right)^{\frac{-(\gamma+1)}{2(\gamma-1)}} \tag{12}$$

Where A is the cross section area.

In most cases, the inlet Mach number at one end of a pipe is subsonic. Hence, from Equation 6, it can be shown that the gas flow can only accelerate along the length a pipeline of constant cross section area resulting in an increase of the Mach number. However, the maximum value M can take, given a subsonic initial condition, is 1. When the velocity reaches sonic speed (Mach=1), the flow is said to choke, i.e. the mass flow rate (MFR) in Equation 12 reaches its maximum value. If the flow chokes before the end of the pipe, a shock wave forms, resulting in a pressure discontinuity.

From Equation 6, it can also be stated that air flows from high to low pressure. This will be important for our discussion on ram air flight data in Section 5.2.

Curve loss component

When the exact pressure drop through a given unit is known, it is more convenient to model it with the *Curve loss component* illustrated in Figure 7. The main difference between the pipe and the curve loss component is that the latter does not require a friction factor nor a pipe length since Equation 10 is not required to solve for the flow variables.

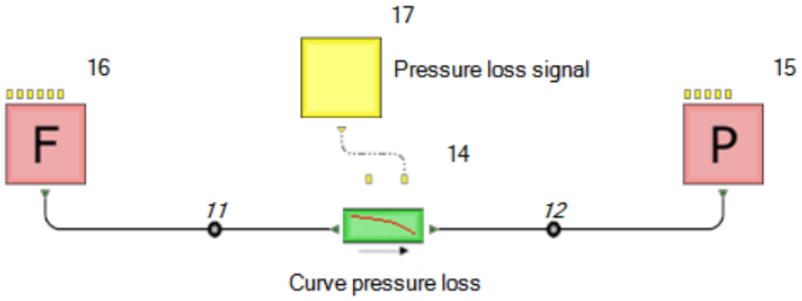

Figure 7 Curve pressure loss component

Pressure drop assessment

Table 1 Pressure drop Input data

		Inputs
$P_{t\ inlet}$	Pa	689 465
T_t	K	294.15
$\dot{m}$	kg/s	3.02395
$\bar{f}$	-	0.15
L	m	4.064
D	m	0.0762

Table 2 Pressure drop Output Values

		Inlet			Outlet		
		FM	**Hand calculation**	**Deviation**	**FM**	**Hand calculation**	**Deviation**
Mach		0.244756	0.244761	0.00%	0.516405	0.516482	0.01%
T_s	K	290.67	290.67	0.00%	279.248	279.247	0.00%
P_t	Pa				368456	368430	0.01%
P	Pa	661 314	661 315	0.00%	307 154	307 132	-0.01%

From comparison between FM results and the hand calculations, FM gives accurate results in agreement with theory.

2.3.2 Heat transfer model

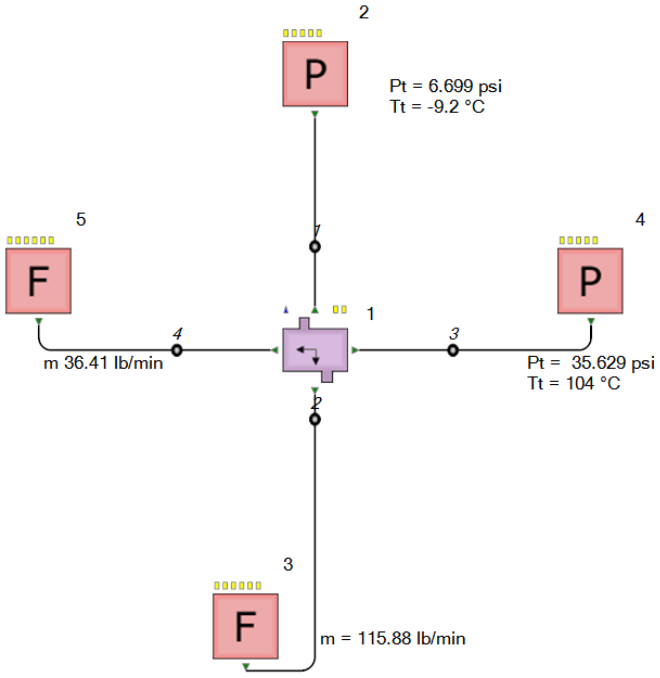

Figure 8 Heat-exchanger component

The type of heat exchanger used in the ECS model is the Flowmaster *Thermal Heat-Exchanger*. This component can be inserted in compressible simulations to model the heat exchange between two gas streams. The amount of heat transfer is defined by the effectiveness or the heat load (also called thermal duty), *Q*, and the pressure drop is calculated by specifying a constant pressure drop coefficient for each stream.

Thermal simulation with dry air

The maximum possible heat transfer rate in a heat exchanger (HX) is calculated assuming an ideal heat exchanger of infinite area where one of the outlet streams (cold or hot) reaches the inlet temperature of the opposite stream, i.e. the maximum temperature difference $\left|T_{0,1,H} - T_{0,1,C}\right|$ is

reached. It can be shown that the stream undergoing the maximum temperature difference has also the minimum $\dot{m}\cdot C_p$ value. [23] Assuming constant heat capacities, the maximum heat transfer can be written as

$$\dot{\boldsymbol{Q}}_{\boldsymbol{max}} = \left(\dot{\boldsymbol{m}}\boldsymbol{C_p}\right)_{\boldsymbol{min}}\left(\boldsymbol{T_{0,1,H}} - \boldsymbol{T_{0,1,C}}\right) \tag{13}$$

To calculate the minimum value of $\dot{m}\cdot C_p$, values for the hot and cold streams must be compared.

$$\left(\dot{\boldsymbol{m}}\cdot\boldsymbol{C_p}\right)_{\boldsymbol{min}} = \boldsymbol{Min}\left\{\left(\dot{\boldsymbol{m}}\cdot\boldsymbol{C_p}\right)_{\boldsymbol{H}}, \left(\dot{\boldsymbol{m}}\cdot\boldsymbol{C_p}\right)_{\boldsymbol{C}}\right\} \tag{14}$$

Integrating the First law (Equation 9) with respect to total temperature and assuming constant heat capacity, it follows that the energy expression for the cold and hot streams are

$$\boldsymbol{Q_H} = \left(\dot{\boldsymbol{m}}\boldsymbol{C_p}\right)_{\boldsymbol{H}}\left(\boldsymbol{T_{0,2}} - \boldsymbol{T_{0,1}}\right)_{\boldsymbol{H}} \tag{15}$$

$$\boldsymbol{Q_C} = \left(\dot{\boldsymbol{m}}\boldsymbol{C_p}\right)_{\boldsymbol{C}}\left(\boldsymbol{T_{0,2}} - \boldsymbol{T_{0,1}}\right)_{\boldsymbol{C}} \tag{16}$$

The heat exchanger's thermal effectiveness, ε, is defined as the ratio of the actual heat transfer rate over the maximum possible heat transfer rate.

$$\boldsymbol{\varepsilon} = \frac{|\dot{\boldsymbol{Q}}|}{\dot{\boldsymbol{Q}}_{\boldsymbol{max}}} \tag{17}$$

The effectiveness can be related to two parameters referred to as the *Number of Transfer Units* (NTU) and the *ratio of Capacity coefficients* (C_r).

$$NTU = \frac{UA}{\left(\dot{m}C_p\right)_{min}}$$

$$C_r = \frac{\left(\dot{m}C_p\right)_{min}}{\left(\dot{m}C_p\right)_{max}}$$

Thus, it is possible to characterize the thermal performance of a heat exchanger with the functional relation

$$\varepsilon = f(NTU, C_r)$$

Thermal performance can also be presented in terms of the ratio $Q/(ITD \cdot A)$, where *ITD* stands for *Inlet Temperature Difference*, $(T_{0,1,H} - T_{0,1,C})$, and A is the exchange area.

From now, the parameter $Q/(ITD \cdot A)$ will be referred to as the *performance capability*. Its derivation is a direct consequence of the ε-NTU method. [24] As a matter of fact, the performance capability is simply $\varepsilon \cdot \frac{(\dot{m}C_p)_{min}}{A}$ and the functional relationship is that of the effectiveness multiplied by $\varepsilon \cdot \frac{(\dot{m}C_p)_{min}}{A}$.

$$Q/(ITD \cdot A) = f(NTU, C_r) \cdot \frac{(\dot{m}C_p)_{min}}{A}.$$

Humid air mixture

The presence of humidity in the air has a great impact on heat-exchangers performance, essentially when condensation or evaporation occurs.

The water content in the air can be specified by the humidity ratio, the relative humidity or the specific humidity. The humidity ratio, w, is defined as the ratio of the amount of water vapor (mass) by the amount of dry air. The fact that the humidity ratio is defined with respect to dry air and not the total gas mixture (dry air and water vapor) is advantageous because dry air component of the mixture is generally conserved, while water vapor can easily change between process units.

Humidity ratio: $w = \frac{m_v}{m_a}$

The relative humidity is defined by considering the maximum amount of water vapor that dry air can dissolve at a given temperature and pressure.

Relative humidity: $\phi = \frac{P}{P^0(T)}$

P is the partial pressure of water vapor in the gas mixture and $P^0(T)$ is the saturation vapor pressure of water at the temperature of the gas mixture.

Finally, the specific humidity is defined with respect to the total amount (mass) of gas mixture.

Specific humidity: $x = \frac{m_v}{m_a + m_v}$

Thermal simulation with humid air

To develop the thermal equation using humid air, we first need to choose reference values for energies for water and air. The most common choice is to assign zero enthalpy for liquid water at 0°C, and zero enthalpy for dry air at 0°C. Then, the enthalpy of the gas mixture per unit mass of dry air can be defined as, [25]

$$\boldsymbol{h \equiv \frac{\dot{H}}{\dot{m}_a} = C_{p_{air}}(T - T_{ref}) + w\left[h_{latent} + C_{p_{vapor}}(T - T_{ref})\right]} \quad (18)$$

Applying mass and energy balance between the heat exchanger, the following relations are obtained:

- mass balance on dry air: $\dot{m}_{a,1} = \dot{m}_{a,2}$
- mass balance for water: $\dot{m}_{a,1}w = \dot{m}_{a,2}w$
- Energy balance = $\dot{m}_{a,1}h_1 + \dot{Q} = \dot{m}_{a,1}h_2$

Thus, when Q and T_1 are known and no condensation or evaporation occurs, the following equation must be solved to find the outlet temperature T_2

$$\boldsymbol{\dot{Q} = \dot{m}_{a,1}\left(C_{p_{air}}(T_2 - T_1) + w\left[C_{p_{vapor}}(T_2 - T_1)\right]\right)} \quad (19)$$

When there is liquid water at the inlet or outlet, the problem becomes more complex as evaporation or condensation can occur. An additional term must be added to Equation 18 to take into account the liquid water content.

Flow pressure simulation

The same governing equations for pipes (Equations 1 to 9) can be used to model heat exchangers' pressure loss. The heat duty must be taken into account by using Equation 15 or Equation 16. The assumption of no change in potential energy, constant compressibility factor and constant heat capacity ratio remains.

After algebraic manipulation of Equations 1, 2, 4, and 5, we can finally write the following differential equation.[26]

$$\frac{dM^2}{M^2} = F_{T0}\frac{dT_o}{T_o} + F_f\frac{fdx}{D}$$

Where $F_{T0} = \frac{(1+\gamma M^2)\left(1+\frac{\gamma-1}{2}M^2\right)}{1-M^2}$ and $F_f = \frac{\gamma M^2\left(1+\frac{\gamma-1}{2}M^2\right)}{1-M^2}$.

After integration,

$$\boldsymbol{ln}\left(\frac{M_2^2}{M_1^2}\right) = \bar{F}_{T0}\,\boldsymbol{ln}\left(\frac{T_{0,2}}{T_{0,1}}\right) + \bar{F}_f\frac{\bar{f}L}{D} \tag{20}$$

Where $\bar{F}_{T0}$ and $\bar{F}_f$ are the average values of F_{T0} and F_f between M_1 and M_2, respectively. Besides, unlike the pipe component, the friction factor is not calculated by FM as a function of the Reynolds number in heat exchangers. In fact, the pressure drop coefficient, $\frac{\bar{f}L}{D}$, is simply assumed as a constant average value throughout the entire stream and must be entered in FM by the user. At last, the total temperature at the outlet $T_{0,2}$ can be calculated independently using Equation 15 or Equation 16.

Heater-cooler component

The *Heater-cooler component* allows heating or cooling of a fluid in a straightforward manner when the exact heating flow is known. The heat flow (positive or negative) is entered and FM computes the outlet temperature according to Equation 15 if heat is removed from the fluid (Equation 16 if heat is added).

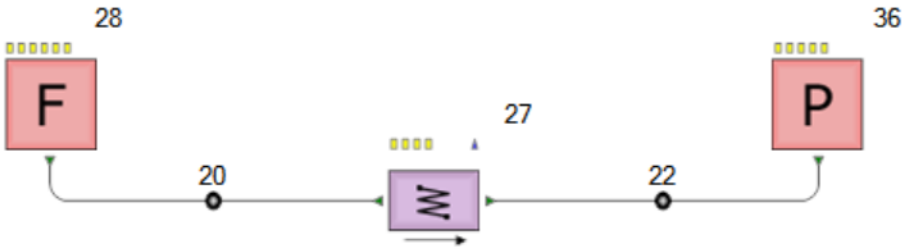

Figure 9 heater-cooler component

Heat-exchanger assessment

Table 3 Heat-Exchanger Input data

		Cold Stream	**Hot Stream**
$T_{t\ inlet}$	K	328.75	497.65
$P_{t\ inlet}$	Pa	82 937	272 335
$\dot{m}$	kg/s	1.796075	0.441421
$\bar{f}L/D$	-	4.435	55.455
A	m^2	0.0645161	0.0135484
Q	W	66220	

Table 4 Hot stream outputs

		Hot stream					
		Inlet			**Outlet**		
		FM	Hand calculation	Deviation	FM	Hand calculation	Deviation
Mach		0.038259	0.038250	-0.03%	0.033615	0.033773	0.47%
T_t	K				350.96	351.04	0.02%
T_s	K	497.50	497.50	0.00%	350.88	350.96	0.02%
P_t	Pa				259 170	258 970	-0.08%
P_s	Pa	271 959	272 056	0.04	258 965	258 763	-0.08

Table 5 Cold stream outputs

		Cold stream					
		Inlet			Outlet		
		FM	Hand calculation	Deviation	FM	Hand calculation	Deviation
Mach		0.086921	0.087551	0.73%	0.094054	0.094774	0.77%
T_t	K				365.45	364.81	-0.18%
T_s	K	328.25	328.25	0.00%	364.81	364.15	-0.18%
P_t	Pa				81446.5	80763	-0.84%
P_s	Pa	83083.0	82493.3	-0.71%	80944.2	80258	-0.85%

It can be seen that most of the FM results obtained are consistent with the expected results by hand calculation. Therefore, temperature predictions for this component are reliable but tends to be less accurate as the temperature difference is greater than 100 K.

2.3.3 Fan model

Dimensional analysis

Fans are typically modeled by means of their performance maps made by their manufacturers. However, these maps are generally built for a given set of operating conditions: constant fan diameter or constant rotational speed for instance. Therefore, dimensional analysis is necessary to adjust the performance maps to different operating conditions.

The performance of a family of geometrically similar fans, under the assumptions of low-speed (Mach<0.3) and same representative roughness surface finish length, can be expressed as a function of: [27]

- Flow rate $\dot{Q}$ [m^3/s]
- Rotor speed N [RPM]
- Fluid density ρ [kg/m^3]

- Fluid viscosity μ [kg/m·s]
- Rotor diameter D [m]
- Power developed $\dot{W}$ [J/s]
- Pressure p [Pa]
- Efficiency η

By performing dimensional analysis (Buckingham's π-theorem), four dimensionless groups are obtained: [28]

- $\pi_1 = \frac{\dot{Q}}{ND^3}$ $\quad Flow\ coefficient$
- $\pi_2 = \frac{P}{\rho N^2 D^2}$ $\quad Pressure\ coefficient$
- $\pi_3 = \frac{W}{\rho N^3 D^5}$ $\quad Power\ coefficient$
- $\pi_4 = \frac{\rho N D^2}{\mu}$ $\quad Fan\ Reynolds\ number$

Therefore, if the operating conditions of two geometrically similar fans are dynamically similar, then all the dimensionless groups are the same. Moreover, since the efficiency η does not appear in the dimensionless groups, we must then conclude that two dynamically similar flows have the same efficiency.

We can reduce the number of dimensionless groups by eliminating π_3 since the Power coefficient can be written as being equal to:

$$\frac{W}{\rho N^3 D^5} = \frac{1}{\eta} \times \frac{\dot{Q}}{ND^3} \times \frac{P}{\rho N^2 D^2}$$

Furthermore, in most cases, the Reynolds number is assumed constant (turbulent regime) and only π_1, π_2 are considered. As shown on Figure 10, this simplification holds true for a wide range of Flow coefficient values but deviates to some extent at low speeds because of unsteady Reynolds number (laminar regime). At very high speeds, the unsteadiness is due to cavitation.

The efficiency, defined as the ratio between the shaft power transferred to the fluid and the power to drive the fan, can be introduced with respect to the flow, pressure and power coefficients.

$$\eta = \frac{\dot{Q}P}{W} = \frac{\pi_1 \cdot \pi_2}{\pi_3}$$

As far as dimensional analysis can be taken, $\frac{Q}{ND^3}$, $\frac{P}{\rho N^2 D^2}$ and η are the dimensionless groups to be considered. However, the actual relationship between them must be ascertained experimentally.

$$\eta = f\left(\frac{\dot{Q}}{ND^3}\right)$$

$$\frac{P}{\rho N^2 D^2} = f\left(\frac{\dot{Q}}{ND^3}\right)$$

Finally, the well-known *Fan laws*, which are simply the ratio of the same dimensionless group for two different operating conditions are

$$\dot{Q}_1 = \dot{Q}_2 \left(\frac{N_1}{N_2}\right)\left(\frac{D_1}{D_2}\right)^3$$

$$p_1 = p_2 \left(\frac{\rho_1}{\rho_2}\right)\left(\frac{N_1}{N_2}\right)^2\left(\frac{D_1}{D_2}\right)^2$$

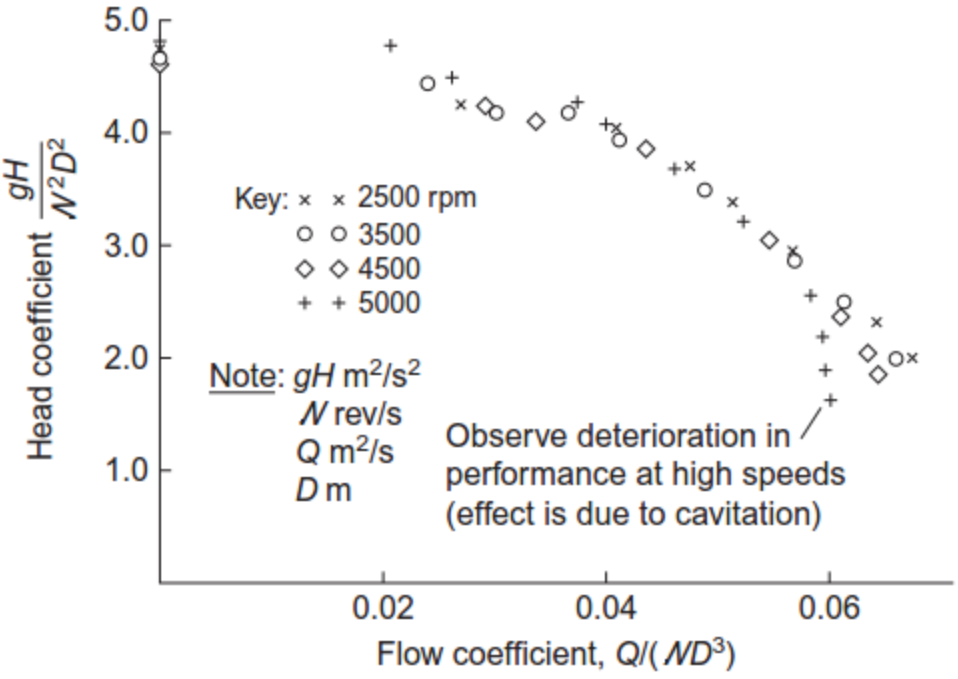

Figure 10 Fan dimensionless groups [29]

Fan model within Flowmaster

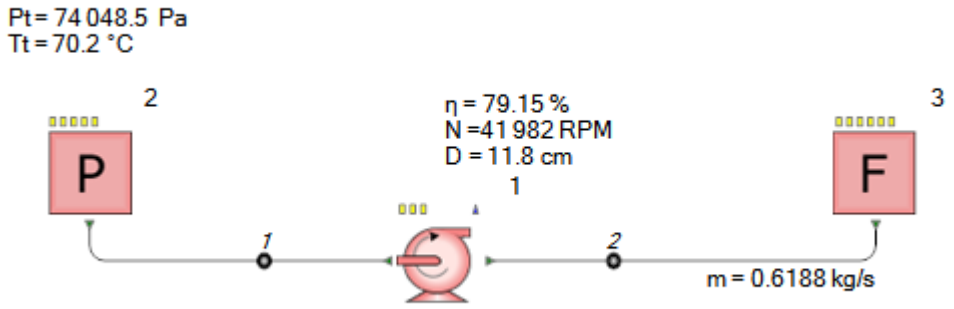

Figure 11 Fan component

Fans in FM are modeled using the fan component shown in Figure 11. In order to function properly, the user must supply two performance maps: static pressure increase vs. flow rate and polytropic efficiency vs. flow rate. Clearly, the maps are only accurate for a specific speed and fan diameter. For other sizes and speeds, the efficiency and pressure rise are approximated using the fan laws. The operating conditions for which the maps were built must be specified in the *Design Point Data* feature in FM.

FM uses a slightly different version of the fan laws adding a correction factor:

$$\dot{\boldsymbol{Q}}_{\boldsymbol{ref}} = \dot{\mathbf{Q}}\left(\frac{\boldsymbol{N_{ref}}}{\boldsymbol{N}}\right)\left(\frac{\boldsymbol{D_{ref}}}{\boldsymbol{D}}\right)^{\mathbf{3}}\boldsymbol{Z} \tag{21}$$

$$\Delta\boldsymbol{P_{s,ref}} = \Delta\boldsymbol{P_s}\left(\frac{\boldsymbol{\rho_{ref}}}{\boldsymbol{\rho}}\right)\left(\frac{\boldsymbol{N_{ref}}}{\boldsymbol{N}}\right)^{\mathbf{2}}\left(\frac{\boldsymbol{D_{ref}}}{\boldsymbol{D}}\right)^{\mathbf{2}}\boldsymbol{Z} \tag{22}$$

The correction factor is defined as [30]

$$\boldsymbol{Z} = \frac{\mathbf{1}}{\mathbf{1}+(\boldsymbol{M}-\mathbf{1})(\mathbf{1}-\boldsymbol{\eta A})} \tag{23}$$

Where $A = \frac{\gamma}{(\gamma-1)}\frac{\left(\left(\frac{P_{0,2}}{P_{0,1}}\right)^{\frac{(\gamma-1)}{\gamma\eta}}-1\right)}{\left(\frac{P_{0,2}}{P_{0,1}}-1\right)}$ and $M = \left(\frac{N}{N_{ref}}\right)^2\left(\frac{D}{D_{ref}}\right)^2\left(\frac{T_s}{T_{s,ref}}\right)$.

Additionally, the total temperature rise is computed using the definition of the polytropic efficiency.

$$\frac{T_{0,2}}{T_{0,1}} = \left(\frac{P_{0,2}}{P_{0,1}}\right)^{\frac{(\gamma-1)}{\gamma\eta_p}} \quad (24)$$

Fan choking and surging are not modeled within this component. However, the choking flow rate at the design conditions can be specified as an upper limit for the performance maps. FM will then use the pressure and efficiency at this point for any flow rate above this limit. The same considerations apply to fan surging. The surging flow rate can be specified as a lower limit and FM will use the pressure increase and efficiency at this point for any flow rate below this limit.

Fan performance maps

The performance maps taken from FM and used for the assessment are showed below. These maps correspond to the reference conditions presented in Table 6, where the flow rate is measured at the fan inlet.

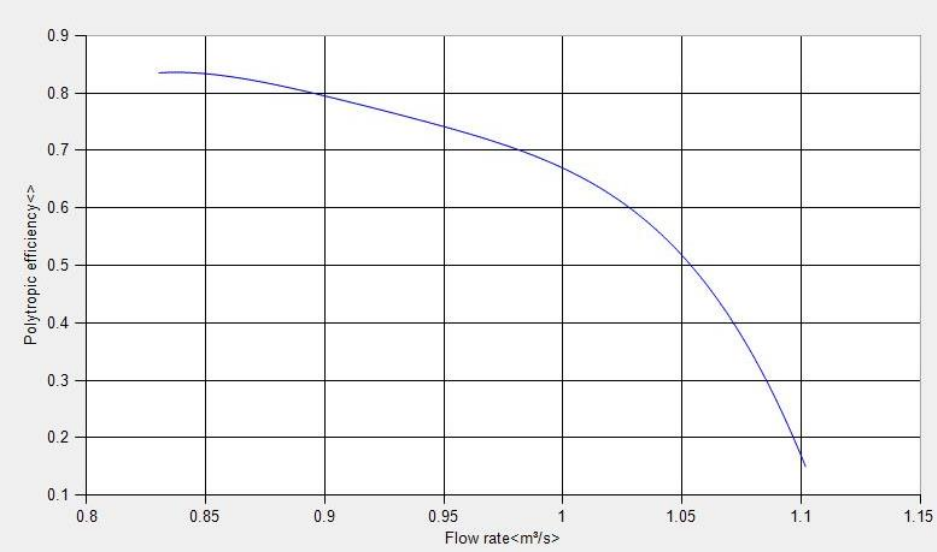

Figure 12 Fan polytropic efficiency plot

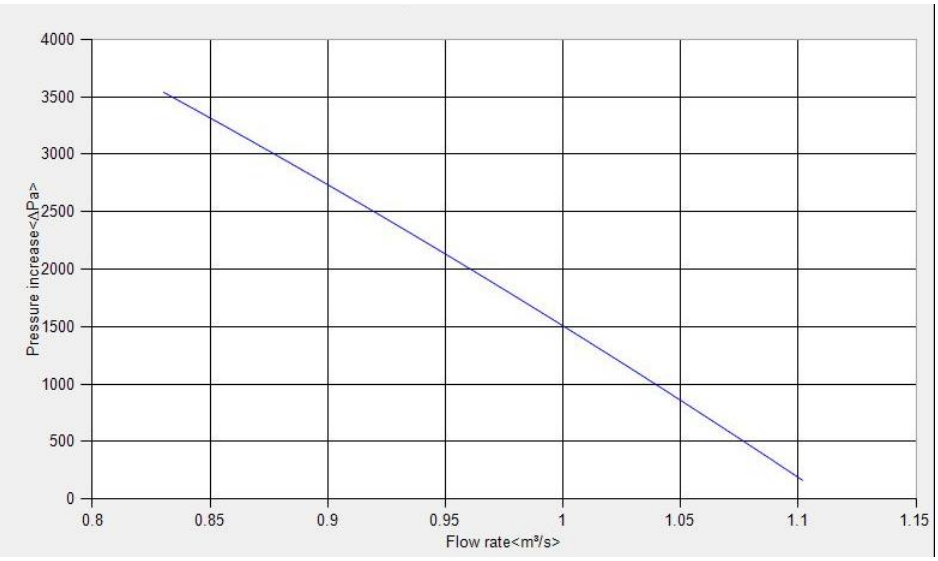

Figure 13 Fan pressure increase plot

If the fan is operated at a different speed or with a different fan diameter than those at the reference, the actual flow rate cannot be used directly to find the efficiency and pressure increase on the maps. The equivalent flow must first be calculated. With the equivalent flow, efficiency and pressure increase can be read from the maps.

Fan assessment

Table 6 Fan Reference data

$T_{s\ inlet}$	K	380.55
ρ	kg/m^3	0.39038
Fan diameter	m	0.118
N	RPM	44962
Choking rate	m^3/s	1.02
Surge flow rate	m^3/s	0.831

Table 7 Fan Inlet conditions

$T_{t\ inlet}$	K	343.35
$P_{t\ inlet}$	Pa	74048.5
$\dot{m}$	kg/s	0.6188
N	RPM	41982
Fan diameter	m	0.118
Pipe diameter	m	0.11938

Since the operating speed is different from the reference, the reference flow rate and the actual pressure increase are calculated and showed in Table 8 among other intermediate results.

Table 8 Fan Efficiency and actual pressure increase

Q_{actual}	m^3/s	0.8405
Q_{ref}	m^3/s	0.9038
η (from map)	%	79.145
$\Delta P_{s,\ ref}$ (from map)	Pa	2691.5
M		0.780
A (pipe cross area)		1.240
Z		1.004
$\Delta P_{s,\ actual}$	Pa	4443.0

Table 9 Fan Output values

		Inlet			**Outlet**		
		FM	Hand calculation	Deviation (%)	FM	Hand calculation	Deviation (%)
Mach		0.20298	0.20299	0.00	0.19331	0.19325	-0.03
T_t	K				350.46	350.52	0.02

T_s	K	340.54	340.54	0.00	347.86	347.92	0.02
P_t	Pa				78 376.4	78 410.3	0.04
P_s	Pa	71 951.8	71 951.6	0.00	76 360.8	76 394.8	0.04

The deviation in outlet pressure is relatively small. Nevertheless, the difference is mainly due to the precision when reading the maps (η and $\Delta P_{s,ref}$).

2.3.4 Compressor model

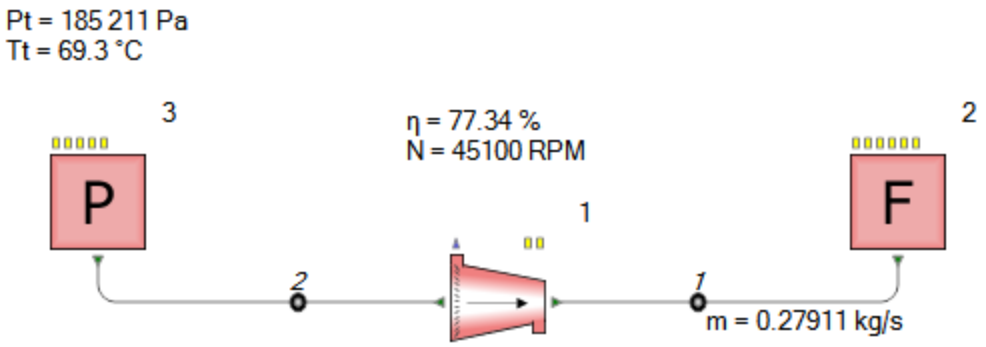

Figure 14 Compressor component

Compressor dimensional analysis

Compressors are used to increase the pressure of a gas. Like fans, compressor modeling requires information on their performance provided by the manufacturer. To derive the performance relations, dimensional analysis of compressors is accomplished. Indeed, compressibility effects must be taken into account by considering additional parameters. In this analysis, the stagnation speed of sound, a_0, at the entry of the compressor and the ratio of specific heats, γ, are chosen for this task. In fact, the Mach number can take values up to one whereas with fans, we assumed Mach<03. Also, instead of considering the pressure as a performance parameter, the isentropic stagnation enthalpy change $\Delta h_{0,ise}$ is selected. Instead of the volume flow rate $\dot{Q}$ and density ρ, the

mass flow rate $\dot{m}$ and total density ρ_0 are employed. By convenience, $\Delta h_{0,ise}$, η_{ise} and W are considered as the dependent variables while the remaining variables $\mu, N, D, \dot{m}, \rho_{0,1}, a_{0,1}$ and γ are the independent variables. Therefore, in light of what has been previously said, the compressor performance can be expressed functionally as

$$\Delta h_{0,ise}, \eta_{ise}, \dot{W} = f\left(\mu, N, D, \dot{m}, \rho_{0,1}, a_{0,1}, \gamma\right)$$

From dimensional analysis, seven dimensionless groups are obtained:[29]

$$\frac{\Delta h_{0,ise}}{a_{0,1}^2}, \eta_c, \frac{\dot{W}}{\rho_{0,1} a_{0,1}^3 D^2} = f\left(\frac{\dot{m}}{\rho_{0,1} a_{0,1} D^2}, \frac{\rho_{0,1} a_{0,1} D}{\mu}, \frac{ND}{a_{0,1}}, \gamma\right)$$

In practice, it is not very convenient to use these groups. In reality, the majority of turbo-compressors manufacturers will deal with a different set of dimensionless groups that will be derived herein by straightforward transformations.

For an isentropic process and assuming constant specific heat, the equation below is always verified. [31]

$$\frac{\boldsymbol{T_{0,2ise}}}{\boldsymbol{T_{0,1}}} = \left(\frac{\boldsymbol{P_{0,2}}}{\boldsymbol{P_{0,1}}}\right)^{(\boldsymbol{\gamma-1})/\boldsymbol{\gamma}} \tag{25}$$

The isentropic specific stagnation enthalpy change, $\Delta h_{0,ise} = C_p\left(T_{0,2ise} - T_{0,1}\right)$, is then

$$\Delta h_{0,ise} = T_{0,1}\left(\left(\frac{P_{0,2}}{P_{0,1}}\right)^{(\gamma-1)/\gamma} - 1\right)$$

Also, $C_p = \gamma R/(\gamma - 1)$ and $a_{0,1}^2 = \gamma R T_{0,1} = (\gamma - 1) C_p T_{0,1}$. Hence,

$$\frac{\Delta h_{0,ise}}{a_{0,1}^2} = \frac{1}{\gamma - 1}\left(\left(\frac{P_{0,2}}{P_{0,1}}\right)^{(\gamma-1)/\gamma} - 1\right)$$

$$\rightarrow \frac{\Delta h_{0,ise}}{a_{0,1}^2} = f\left(\left(\frac{P_{0,2}}{P_{0,1}}\right), \gamma\right)$$

The mass flow coefficient can be rewritten using the equation of state $\rho_0 = P_0/RT_0$ and the definition of stagnation speed of sound.

$$\frac{\dot{m}}{\rho_{0,1} a_{0,1} D^2} = \frac{\dot{m} R T_{0,1}}{\rho_{0,1}\sqrt{\gamma R T_{0,1}} D^2} = \frac{\dot{m}\sqrt{\gamma R T_{0,1}}}{D^2 P_{0,1} \gamma}$$

The power coefficient term can also be transformed.

$$\frac{\dot{W}}{\rho_{0,1}a_{0,1}^3D^2}=\frac{\dot{m}C_p\Delta T_0}{\left(\rho_{0,1}a_{0,1}D^2\right)a_{0,1}^2}=\left(\frac{\dot{m}\sqrt{\gamma RT_{0,1}}}{D^2P_{0,1}\gamma}\right)\frac{C_p\Delta T_0}{a_{0,1}^2}=\left(\frac{\dot{m}\sqrt{\gamma RT_{0,1}}}{D^2P_{0,1}\gamma}\right)\frac{1}{(\gamma-1)}\frac{\Delta T_0}{T_{0,1}}$$

$$\rightarrow\frac{W}{\rho_{0,1}a_{0,1}^3D^2}=f\left(\frac{\dot{m}\sqrt{\gamma RT_{0,1}}}{D^2P_{0,1}\gamma},\frac{\Delta T_0}{T_{0,1}},\gamma\right)$$

After considering the previous transformations, the new dimensionless groups can be functionally expressed as

$$\frac{P_{0,2}}{P_{0,1}},\eta_{ise},\frac{\Delta T_0}{T_{0,1}}=f\left(\frac{\dot{m}\sqrt{\gamma RT_{0,1}}}{D^2P_{0,1}\gamma},\frac{\rho_{0,1}\sqrt{\gamma RT_{0,1}}D}{\mu},\frac{ND}{\sqrt{\gamma RT_{0,1}}},\gamma\right)$$

Further simplification can be accomplished for a compressor of constant diameter handling a single fluid by dropping R, γ and D. Consequently, the resulting variables can only be applied to map a unique compressor of a given size and compressing a specific gas. In addition, the term $\frac{\rho_{0,1}\sqrt{\gamma RT_{0,1}}D}{\mu}$, which is a form of the Reynolds number, can also be dropped assuming turbulent regime. Under these conditions, the previous relation turns out to be

$$\frac{P_{0,2}}{P_{0,1}},\eta_{ise},\frac{\Delta T_0}{T_{0,1}}=f\left(\frac{\dot{m}\sqrt{T_{0,1}}}{P_{0,1}},\frac{N}{\sqrt{T_{0,1}}},\right)$$

The performance variable $\frac{\Delta T_0}{T_{0,1}}$ can also be dropped because it can be back calculated if the efficiency and the pressure ratio are known. In fact,

$$\eta_{ise}\equiv\frac{minimum\ energy\ difference\ possible\ for\ the\ fluid}{actual\ work\ input\ to\ the\ fluid}\ [31]$$

$$\boldsymbol{\eta_{ise}=\frac{\cancel{\dot{m}C_p}(T_{0,2ise}-T_{0,1})}{\cancel{\dot{m}C_p}(T_{0,2}-T_{0,1})}} \tag{26}$$

But $T_{0,2ise}$ is equal to $T_{t,1}\left(\frac{P_{0,2}}{P_{0,1}}\right)^{(\gamma-1)/\gamma}$ from Equation 25.

$$\rightarrow\eta_{ise}=\frac{\left(\left(\frac{P_{0,2}}{P_{0,1}}\right)^{(\gamma-1)/\gamma}-1\right)}{\Delta T_0/T_{0,1}}$$

Furthermore, it is common practice to express the mass flow rate and speed variables in terms of their *corrected* form.

$$\boldsymbol{Corrected\ mass\ flow\ rate}: \frac{\dot{m}\sqrt{T_{0,1}/T_{ref}}}{P_{0,1}/P_{ref}} \tag{27}$$

$$\boldsymbol{Corrected\ speed}: \frac{N}{\sqrt{T_{0,1}/T_{ref}}} \tag{28}$$

The corrected mass flow rate (CMFR) and the corrected speed represent the mass flow and rotational speed that would be measured if the compressor was operating at an arbitrary reference pressure and temperature; standard sea-level conditions for instance.

To conclude, we can finally express the performance relation as

$$\frac{P_{0,2}}{P_{0,1}} = f\left(\frac{\dot{m}\sqrt{T_{0,1}/T_{ref}}}{P_{0,1}/P_{ref}}, \frac{N}{\sqrt{T_{0,1}/T_{ref}}}\right) \tag{29}$$

$$\eta_{ise} = f\left(\frac{\dot{m}\sqrt{T_{0,1}/T_{ref}}}{P_{0,1}/P_{ref}}, \frac{P_{0,2}}{P_{0,1}}\right) \tag{30}$$

Notice that the new variables on the right-hand side are no longer dimensionless.

Humid air effects

Presence of water vapor changes the air properties such as C_p, γ, and R. Of course, the deviation from the dry air state increases as more vapor is present. Yet, the compressor dimensional analysis done previously applies only to perfect gases with constant caloric properties. According to [32], ignoring this deviation can lead to 2-3% efficiency errors. However, under 10% specific humidity, humid gas mixture can be considered as dry [33].

Samuel's and Gales's correction factors [34] can be useful to take into account the effects of humidity on R and γ. By doing so, the new corrected mass flow rate and corrected rotational speed numbers become

- $\frac{\dot{m}\sqrt{T_{0,1}/T_{ref}}}{P_{0,1}/P_{ref}}\sqrt{\frac{R_{mix}}{\gamma_{mix}}}$

- $\frac{N}{\sqrt{T_{0,1}/T_{ref}}} \frac{1}{\sqrt{R_{mix} \cdot \gamma_{mix}}}$

Flowmaster's compressor model

FM's definition of compressor pressure ratio is slightly different than what was presented above. FM uses the outlet *static* pressure instead of the outlet total pressure.

$$Pressure\ ratio = \frac{Outlet\ static\ pressure}{Inlet\ total\ pressure} = \frac{P_{s,2}}{P_{0,1}}$$

Two 3D performance maps represented by the functions below must be supplied prior to running a simulation in order to fully characterize the compressor.

$$\frac{P_{s,2}}{P_{0,1}} = f\left(\frac{\dot{m}\sqrt{T_{0,1}/T_{ref}}}{P_{0,1}/P_{ref}}, \frac{N}{\sqrt{T_{0,1}/T_{ref}}}\right) \tag{31}$$

$$\eta_{ise} = f\left(\frac{\dot{m}\sqrt{T_{0,1}/T_{ref}}}{P_{0,1}/P_{ref}}, \frac{P_{s,2}}{P_{0,1}}\right) \tag{32}$$

Humidity correction is not supported by FM, so R and γ were assumed constant and equal to dry air values in our ECS model.

Compressor performance maps

Figure 15 shows a typical compressor performance map from Garret's [35]. The contour lines represent constant efficiencies whereas the perpendicular lines represent constant corrected speeds. From a map like this, it is possible to extract all the necessary information needed to predict compressor's outlet conditions of temperature, pressure and power consumption.

From the same figure, one can also estimate the surge and choke lines. These are two important lines that show the operating limits of the equipment. The surge limit is the left hand boundary green line. This region is characterized by flow instability where the mass flow is too small for the generated boost and spinning. Operating at this limit may cause reversal of airflow through the unit. On the other hand, the choke line in red is characterized by a low backpressure and high

compressor output at a given speed. The gas velocity and gas flow rate cannot go beyond the value at the choke point.

Finally, the dashed line represents the *operating line*. Its exact position is not a property of the compressor, but rather of the rest of the system. [36] For the ECS pack, the operating line is contingent upon many factors such as the flow area downstream of the compressor, the turbine's throat area and the amount of heat removed by the heat-exchangers. Nevertheless, the system designer will try to locate the compressor's operating line so as to allow for operating in the higher efficiency range.

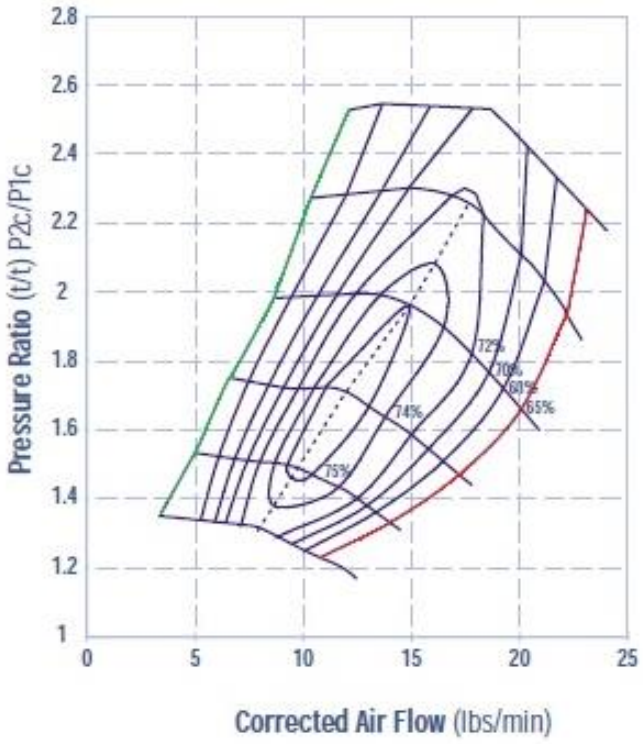

Figure 15 Typical compressor performance map [35]

Figures 16 and 17 are examples of performance maps used in FM simulation. Though, surge and choke flow rates are specified elsewhere in the component's option screen. They can be specified as constants values or as functions of rotational speed.

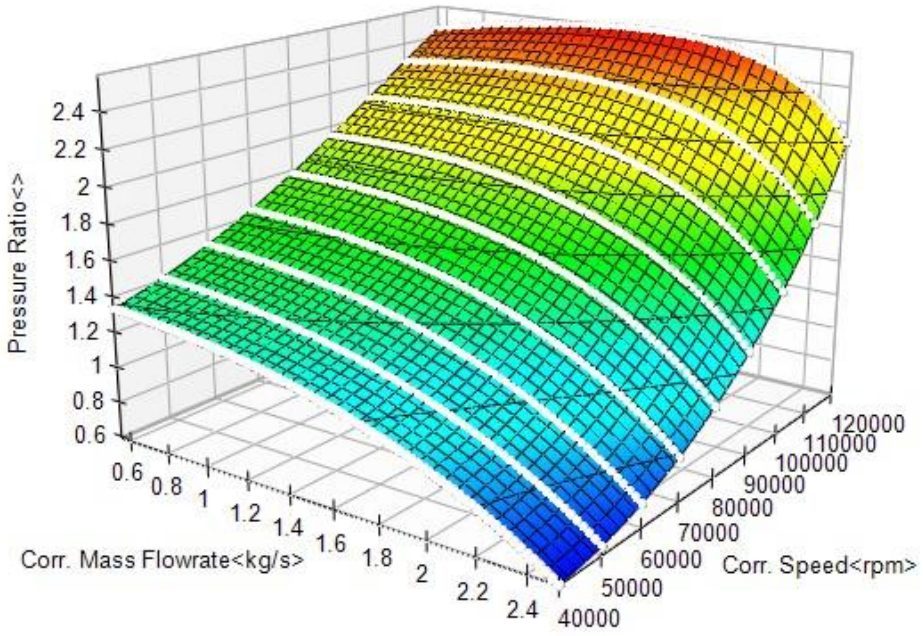

Figure 16 Compressor pressure ratio surface

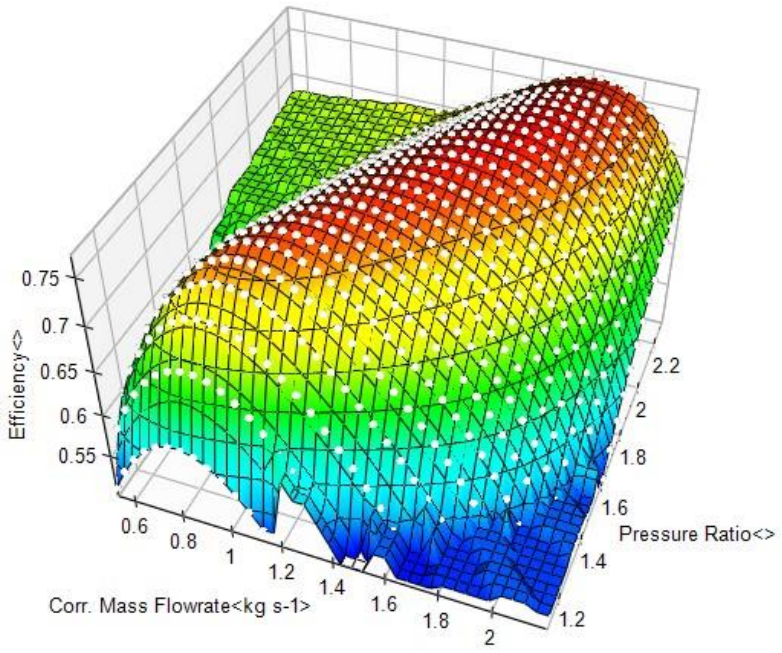

Figure 17 Compressor efficiency surface

Compressor assessment

Table 10 Compressor Input values

$T_{t\ inlet}$	K	342,45
$P_{t\ inlet}$	Pa	185211
$\dot{m}$	kg/s	0.27911
N	RPM	45100
Pipe diameter	m	0.0889
T_{ref}	K	298.15
P_{ref}	Pa	100000
$\dot{m}_{corr}$	kg/s	0.1615
N_{corr}	RPM	42081
P.R (from map)		1.332
η (from map)	%	77.344

Table 11 Compressor Output values

		Inlet			**Outlet**		
		FM	Hand calculation	Deviation (%)	FM	Hand calculation	Deviation (%)
Mach		0.06448	0.06449	0.01	0.05087	0.05088	0.01
T_t	K				380.54	380.54	0.00
T_s	K	342.17	342.17	0.00	380.35	380.35	0.02
P_t	Pa				247128	247243	0.05
P_s	Pa	184 673	184 673	0.00	246796	246796	0.04

2.3.5 Turbine model

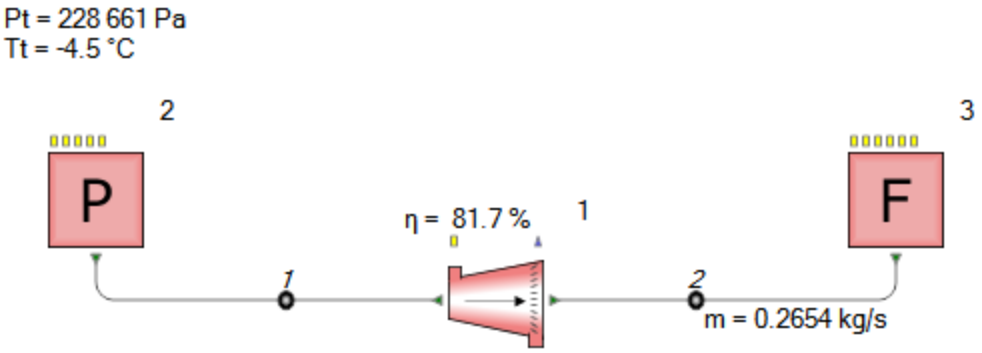

Figure 18 Turbine component

Turbines transform fluid pressure into useful work by the action of the moving fluid on the blades so that they move and impart rotational energy to the rotor assembly. The dimensional analysis of the expansion process in turbines is similar to the compression process. This means that the performance is determined by the same dimensionless groups.

$$\frac{P_{0,2}}{P_{0,1}}, \eta_{ise}, \frac{\Delta T_0}{T_{0,1}} = f\left(\frac{\dot{m}\sqrt{T_{0,1}/T_{ref}}}{P_{0,1}/P_{ref}}, \frac{N}{\sqrt{T_{0,1}/T_{ref}}}, \right)$$

However, since expansion involves decreasing the pressure of the entering fluid and extracting energy, the isentropic efficiency is defined differently.

$$\eta_{ise} \equiv \frac{Actual\ work\ done\ by\ the\ fluid}{Maximum\ energy\ difference\ possible\ for\ the\ fluid} \approx \frac{\cancel{\dot{m}C_p}(T_{0,1} - T_{0,2})}{\cancel{\dot{m}C_p}(T_{0,1} - T_{0,2ise})}$$

$$\boldsymbol{\eta_{ise}} = \frac{(\boldsymbol{T_{0,1} - T_{0,2}})/\boldsymbol{T_{0,1}}}{\left(\mathbf{1} - \left(\frac{\boldsymbol{P_{0,2}}}{\boldsymbol{P_{0,1}}}\right)^{(\gamma-1)/\gamma}\right)} \tag{33}$$

Flowmaster's turbine model

In FM, the turbine pressure ratio is defined in terms of total pressure.

$$Pressure\ ratio = \frac{Inlet\ total\ pressure}{Outlet\ total\ pressure} = \frac{P_{0,1}}{P_{0,2}}$$

As a result, the two required maps for turbine characterization are:[29]

$$\frac{P_{0,1}}{P_{0,2}} = f\left(\frac{\dot{m}\sqrt{T_{0,1}/T_{ref}}}{P_{0,1}/P_{ref}}, \frac{N}{\sqrt{T_{0,1}/T_{ref}}}\right) \tag{34}$$

$$\eta_{ise} = f\left(\frac{\dot{m}\sqrt{T_{0,1}/T_{ref}}}{P_{0,1}/P_{ref}}, \frac{P_{0,1}}{P_{0,2}}\right) \tag{35}$$

Differing from the compressor component, FM's turbine component allows specifying a constant efficiency (not as a function of corrected mass flow rate and corrected rotational speed). This option makes the component to be more flexible to work with. For instance, when only data of PR vs. corrected mass flow rate is available for a constant efficiency, a simulation can still be solved. The corresponding rotational speed will be unknown, but sometimes one might be only interested in finding the outlet fluid conditions. For the assessment, only a PR vs. corrected mass flow rate map is supplied. The efficiency and corrected speed are chosen arbitrarily.

The power output from the turbine (actual work done by the fluid) is a very important information for simulation of the ACM as we will see later. To calculate the isentropic efficiency, we've approximated the power output by assuming a constant specific heat. In fact, this reasonable approximation has lead us to develop simple relations to predict outlet temperature. Now, to calculate the power output from the turbine we should write

$$Actual\ work\ done\ by\ the\ fluid = \dot{m}\int_{T_{t,1}}^{T_{t,2}} C_p(T)dT$$

However, FM approximates the power output by using the average specific heat.

$$\boldsymbol{Power\ output} = \dot{\boldsymbol{m}} \cdot \boldsymbol{C_{p\,avg}} \cdot \Delta \boldsymbol{T_0} = \dot{\boldsymbol{m}}\left(\frac{C_p(T_{0,1}) + C_p(T_{0,2})}{2}\right)(T_{0,1} - T_{0,2}) \tag{36}$$

Turbine performance maps

Turbines perform quite differently than compressors. In fact, it can be shown that the rotational speed has little effect on pressure ratio. Moreover, turbines are designed to work with high-pressure ratios ultimately leading to choked flow. These considerations are well reflected on their performance maps as in Figure 19. Figure 20 illustrates the performance map used for the assessment.

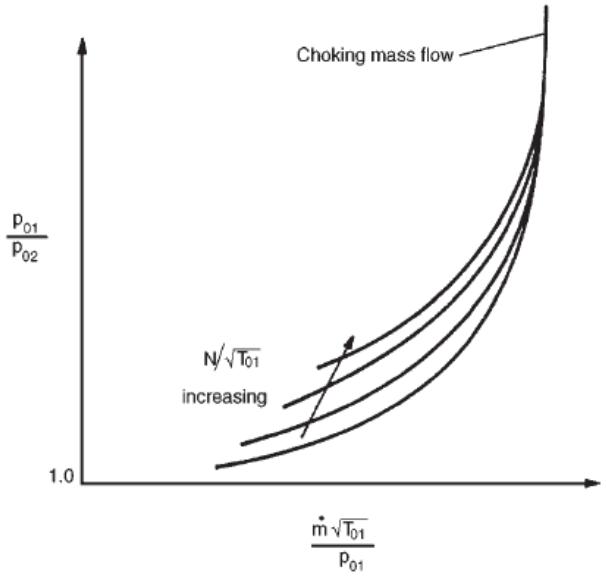

Figure 19 Typical Turbine map

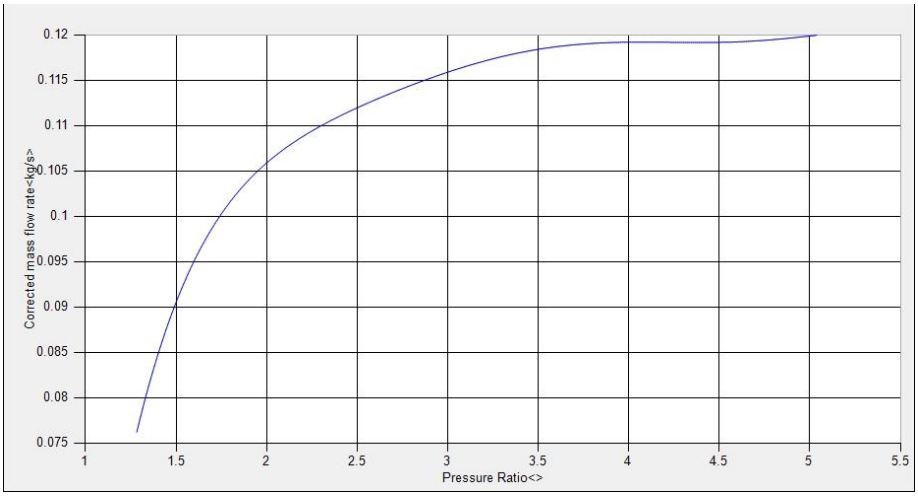

Figure 20 Turbine cmfr vs pr

Turbine assessment

Table 12 Turbine Input values

$T_{t\ inlet}$	K	268.55
$P_{t\ inlet}$	Pa	228 661
$\dot{m}$	kg/s	0.26541
N	RPM	44962
Pipe diameter	m	0.1016
T_{ref}	K	298.15
P_{ref}	Pa	100 000
$\dot{m}_{corr}$	kg/s	0.11015
N_{corr}	RPM	47 375
P.R (from map)		2.32
η (from map)	%	81.7

Table 13 Turbine Output values

		Inlet			**Outlet**		
		FM	Hand calculation	Deviation (%)	FM	Hand calculation	Deviation (%)
Mach		0.03362	0.03361	-0.01	0.07105	0.07105	0.01
T_t	K				221.63	221.66	0.01
T_s	K	268.49	268.49	0.00	221.41	221.43	0.02
P_t	Pa				98 556.1	98 556.1	0.00
P_s	Pa	228 480.2	228 480.2	0.00	98 160.1	98 208.6	0.05
Power	W				12517	12 521	-0.05

2.3.6 Cd valve model

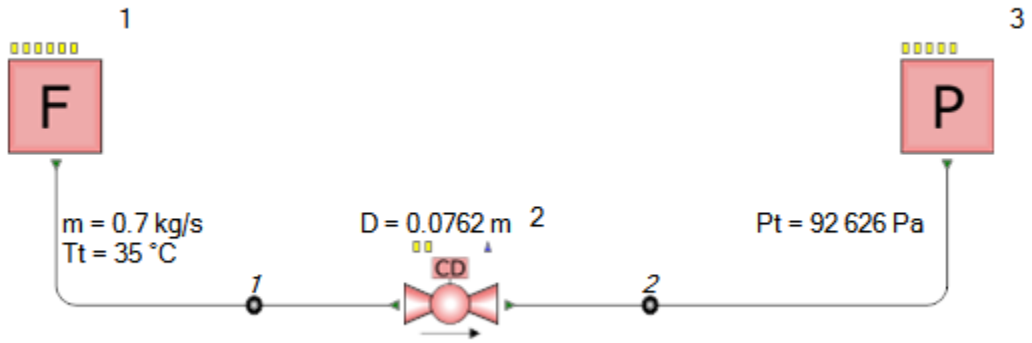

Figure 21 Cd valve component

The Cd valve component uses the coefficient of discharge value to compute the pressure drop. The process within the valve is assumed to be adiabatic where all the pressure drop is converted to kinetic energy. To derive the modeling equation, we start from the fact that for an adiabatic process, the total enthalpy is conserved.

$$h + \frac{v^2}{2} = h_0$$

$$\frac{v^2}{2} = h_0 - h$$

$$v = \sqrt{2(h_0 - h)}$$

$$v = \sqrt{2C_{P0}(T_0 - T)}$$

$$v = \sqrt{2C_{P0}T_0\left(1 - \frac{T}{T_0}\right)}$$

Since for an isentropic process $\frac{T}{T_0} = \left(\frac{P}{P_0}\right)^{(\gamma-1)/\gamma}$ and $C_{P0} = \frac{\gamma R}{\gamma - 1}$, the velocity can be written as

$$v = \sqrt{\frac{2\gamma R}{\gamma - 1}T_0\left(1 - \left(\frac{P}{P_0}\right)^{(\gamma-1)/\gamma}\right)}$$

The mass flow rate at any point in the valve is

$$\dot{m} = Av\rho$$

$$\dot{m} = A\sqrt{\frac{2\gamma R}{\gamma - 1}T_0\left(1 - \left(\frac{P}{P_0}\right)^{(\gamma-1)/\gamma}\right)}\rho_0\frac{\rho}{\rho_0}$$

From the idea gas law, $\rho_0 = \frac{P_0}{RT_o}$. Also, $\frac{\rho}{\rho_0} = \left(\frac{P}{P_0}\right)^{1/\gamma}$ for an isentropic process. Thus,

$$\boldsymbol{\dot{m} = AP_0\sqrt{\frac{2\gamma}{(\gamma-1)RT_0}}\sqrt{\left(\frac{P}{P_0}\right)^{2/\gamma} - \left(\frac{P}{P_0}\right)^{(\gamma+1)/\gamma}}} \quad (37)$$

This equation provides the ideal mass floor rate through a device undergoing an isentropic process.

The isentropic process is an ideal path where the net change in entropy is zero. In contrast, a real process is irreversible and its path can be defined by comparing it to an ideal one. The coefficient of discharge is the parameter to quantify the deviation from the ideal process and it is defined as the ratio between actual and ideal mass flow rates.[21]

$$Cd \equiv \frac{actual\ mass\ flow\ rate}{mass\ flow\ rate\ with\ isentropic\ flow}$$

The isentropic mass flow rate is determined using the backpressure if the nozzle is not choked. If the flow is choked, the isentropic mass flow is based on the sonic velocity at the throat.

Cd valve assessment

For this example, the three diameters (entrance, throat, and exit) lengths were assumed identical.

Table 14 Cd valve Inputs values

T_t	K	308.15
$P_{t\ outlet}$	Pa	92 626
$\dot{m}$	kg/s	0.7
D_{throat}	m	0.0762

D_1	m	0.0762
D_2	m	0.0762
Cd		0.9

Table 15 Cd valve Output values

		Inlet			Outlet		
		FM	Hand calculation	Deviation (%)	FM	Hand calculation	Deviation (%)
Mach		0.45370	0.45484	0.25	0.47565	0.47564	0.00
T_s	K	295.97	295.91	-0.02	294.81	294.81	0.00
P_t	Pa	95964.0	95790.2	-0.18			
P_s	Pa	83334.6	83118.1	-0.26	79335.2	79335.3	0.00
Cd	W	0.9003222	0.9	-0.04	0.899995372	0.9	0.00

Our outlet values are almost identical to FM's, whereas the inlet pressures (static and total) are around 200 Pa off. Nevertheless, this error is acceptable as it represents less than 0.3%. We calculated the coefficient of discharge with FM's results and, as it can be seen, it is not exactly 0.9. Hence, the offset can be due to convergence precision.

CHAPTER 3 ECS MODEL

In this chapter, the ECS model is presented in three parts. First, the architecture within the FM environment is portrayed. Then, the core of the model is described by explaining the internal inputs. At last, the external inputs needed by the model are enumerated.

3.1 Model Architecture

In this section, important comments are made with regard to the model. The goal is to review key modeling decisions with regard to the architecture and convergence workarounds.

3.1.1 ECS pack

The environmental control system model comprises two parts: the ECS packs and cabin distribution. The former consists of two identical packs, right and left. An illustration of the right pack and a screen capture of the equivalent FM model are shown in Figure 22 and Figure 23, respectively.

There are many signals used by the different components in the model. In most cases, a signal will interact with one of the three signal components that are summarized in Table 16.

Table 16 Controller components

Symbol	Name and function
	*Gauge*: The gauge component can only accept one measurement input signal taken from a node or a component branch. Exemples of measurements are pressure, temperature, density, flow rate, etc. The output signal is the measurement selected in the gauge.

	*Controller Template*: Used to create a custom output signal based on a custom script and/or plots (2-D lines or 3-D surfaces). The template can accept up to five input signals from gauges or tabular components.
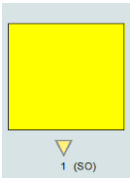	*Tabular Controller*: Whenever a value is needed to compute a calculation with the controller template that is not a measurement, the value is entered in the Tabular controller and connected to one of the controller template's inputs. Tabular controllers has no input ports.

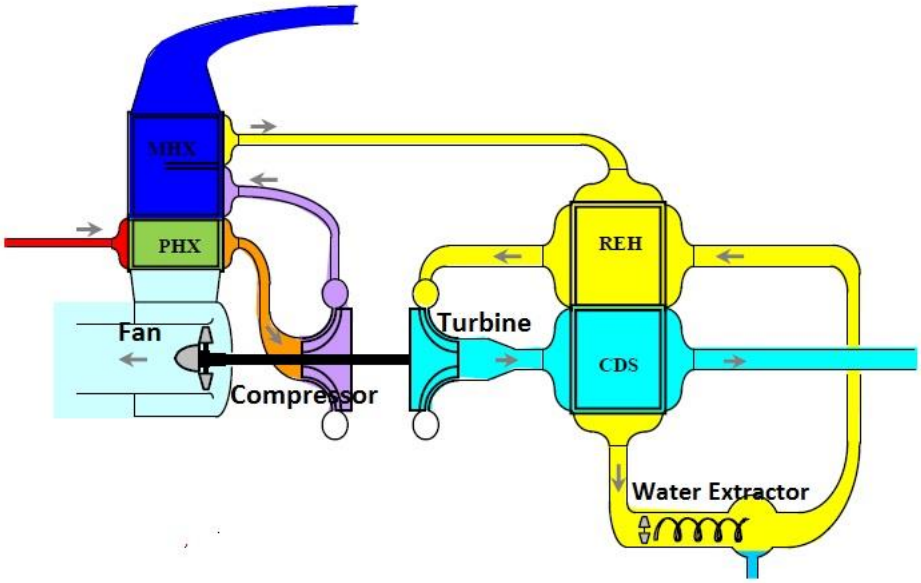

Figure 22 ESC pack illustration

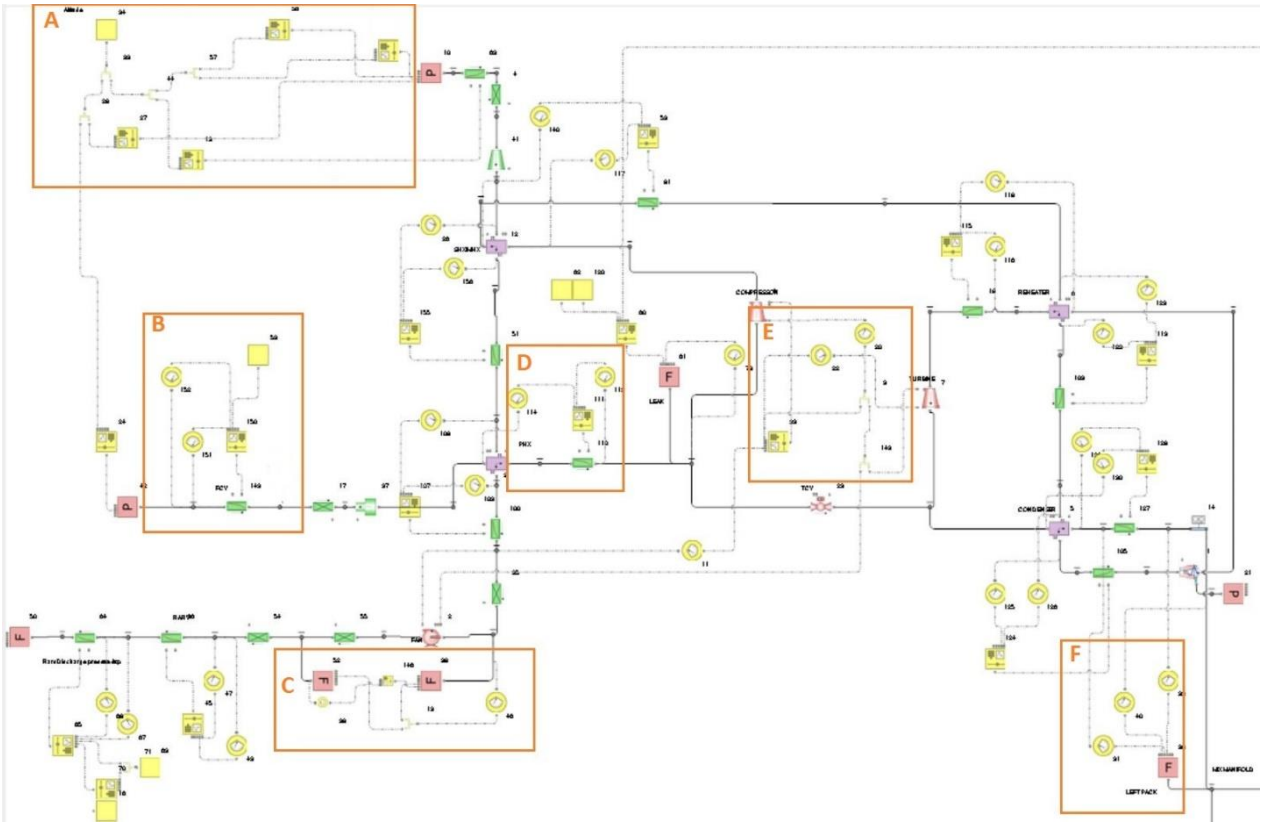

Figure 23 Flowmaster ECS pack model schematic

Ram air channel inlet signals

Rectangle A, in Figure 23, consists of four controller templates that compute the total temperature, total pressure and humidity at the ram inlet according to the altitude and A/C speed set by the user.

Flow control valve (FCV)

The FCV is located inside rectangle B. Two gauges measure the density and mass flow and the loss coefficient is set in the tabular controller. The signals are sent to a controller template in which a script computes the pressure loss.

Ram air by pass

In rectangle C, two flow sources with flow rates defined by the user in the input screen are linked to each other. What the controller template does is simply to inverse the sign of the mass flow rate set for the flow sources at the left.

Heat-exchangers pressure loss

Pressure loss in the PHX is located inside rectangle D. Pressure loss in heat-exchangers have been mapped as a function of density and mass flow rate. The surface is added to the controller template, which computes the pressure loss by means of a script.

ACM matching

A script that reads the different signals from the compressor, turbine and fan carries out speed and power matching of the ACM (rectangle E).

Second pack

Modeling two packs can be achieved by copying the architecture showed in Figure 23 and joining the two at one node. However, convergence time to solve such system was found to be lengthy as the pack is solved twice. A workaround to reduce computing time consists on solving for one pack. Knowing the pack discharge conditions, and by means of gauges that reads flow, temperature and humidity, a flow source with the same pack discharge conditions can be added. The gauges and flow source component for this purpose are inside rectangle F. This workaround is acceptable because we know the two packs are identical and should converge to the same conditions.

There are two versions of the ECS model, one with two packs, and one with a single pack. Besides the additional flow source explained above, the difference between both versions resides in the flow schedule. The flow schedule in the double pack and single pack versions are set according to

Table 22 and Table 23, respectively. The recirculation flow script is also different to take into account the difference in flow schedule.

3.1.2 Cabin Distribution

The main purpose of modeling the cabins and cockpit is to predict cabin temperature by taking into consideration the heat loads, thermal losses and TAVs heating. To accomplish this, the model shall split the flow coming from the packs adequately.

Distribution starts at the mix manifold (Figure 24, rectangle A) which is represented by a simple node. In fact, it is unnecessary to model the mix manifold by a volume component since we are not interested on its dynamic behaviour (the outlet temperature for a given a residence time), but rather the stead-state temperature.

The TAPRV is located inside rectangle B. It can be seen that the flow is directed to the three TAVs, the one at the bottom inside rectangle C being the aft cabin TAV.

Flow from mix manifold and recirculation fan are split into three streams in order to reach the cockpit, fwd cabin and aft cabin. Since LPDS pressure lost data was unavailable, the split was modeled by inserting three Cd pressure loss components, one at each stream. The three coefficient of discharges are normally set to one, thus no pressure loss through the components is assumed. However, the cross section areas are such as the flow splits according to Table 22. The controller template output inside rectangle J was inserted to display the cockpit percentage split which should be around 12.5%. Although, it is possible to change this value by reducing the cockpit's TAV coefficient of discharge.

Thermal losses in cockpit ducting discussed in Section 3.2.7 are carried out by the heater-cooler component inside rectangle E. The same applies for fwd and aft cabins. After the thermal loss, heat loads are added also by a heater-cooler component (rectangle F).

A script in the controller template shown inside rectangle H computes the flow schedule and the signal is directed to a flow source just below. Performance data on the recirculation fan was found insufficient to build an appropriate model. Consequently, the recirculation flow is defined with respect to the recirculation percentage input. Moreover, a temperature increase of 4°C has been

assumed. Recirculation flow sources and controller templates are showed inside rectangles G and I.

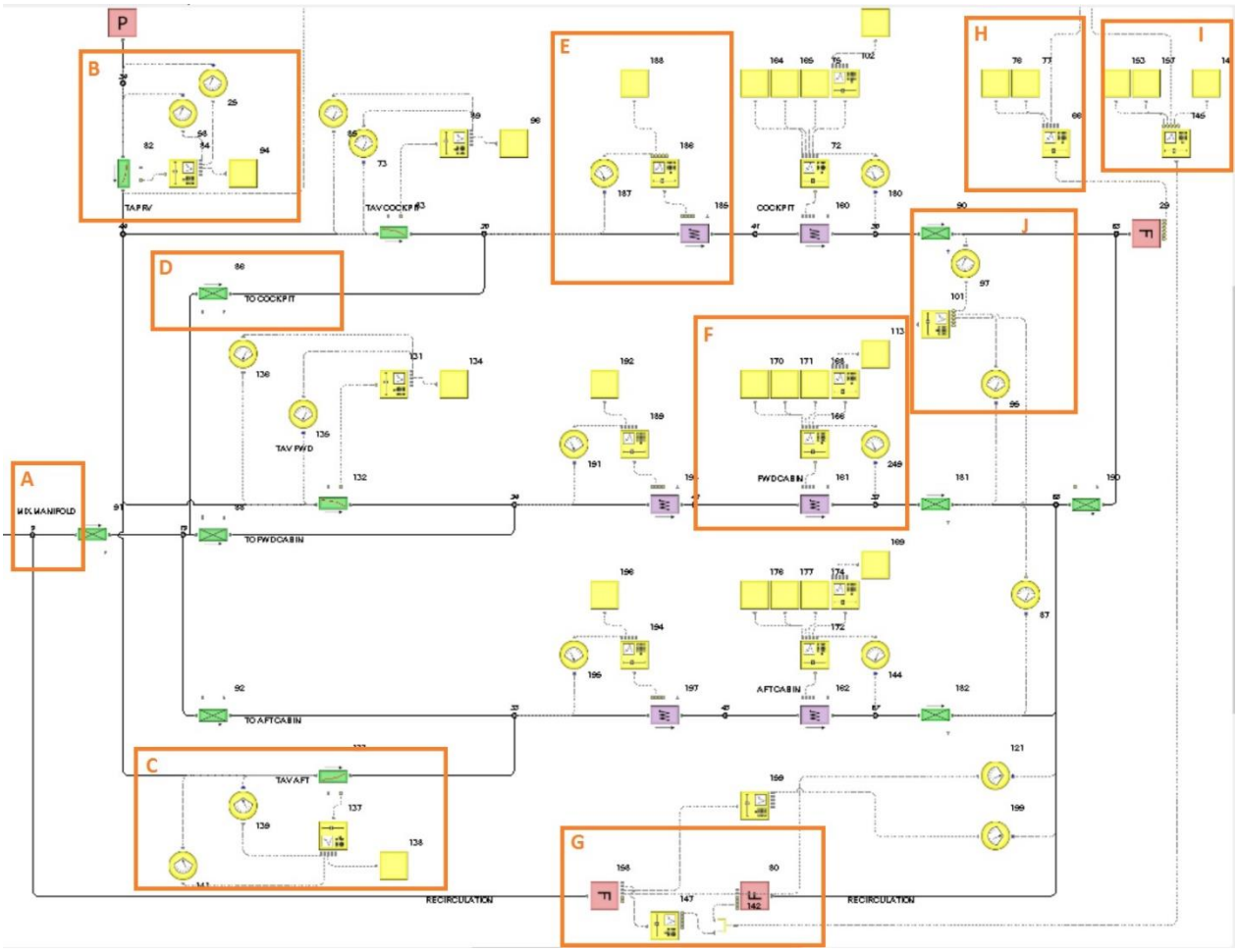

Figure 24 Flowmaster distribution model schematic

3.2 Internal inputs

The internal inputs are defined as all the information required to build the ECS model (modeling equations, ambient pressure model, ambient temperature model, etc.). All this data is already stocked in the model or computed by the model. Therefore, it is not required to be given by the user. On the other hand, all information required to define the flight conditions prior to running a simulation case is called external input. That said, the purpose of this section is to present the main

internal inputs that make the ECS model. Equipment maps (compressor maps, turbine maps, etc.) are also internal inputs, but because of their particular importance, they are presented distinctly in Section 4.

3.2.1 Ambient Conditions

The ECS model computes the ambient temperature and humidity based on aircraft altitude according to Table 17. The ambient pressure is also computed as a function of altitude according to Table 18. Values that are not listed are interpolated linearly.

Table 17 Ambient temperature and humidity [6]

A/C	Outside Ambient Temperature (OAT)										Outside Ambient Humidity									
Altitude	XCD		CD		ISA		HD		XHD		XCD		CD		ISA		HD		XHD	
ft	°C	°F	°C	°F	°C	°F	°C	°F	°C	°F	g/kg	gr/lb	g/kg	gr/lb	g/kg	gr/lb	g/kg	gr/lb	g/kg	gr/lb
-2000	-54.0	-65.2	-40.0	-40.0	19.0	66.1	44.0	111.1	52.5	126.5	0.0	0.0	0.0	0.0	10.7	74.9	19.0	133.0	10.0	70.0
-1000	-54.0	-65.2	-40.0	-40.0	17.0	62.6	42.0	107.6	52.5	126.5	0.0	0.0	0.0	0.0	10.7	74.9	19.0	133.0	10.0	70.0
0	-54.0	-65.2	-40.0	-40.0	15.0	59.0	40.0	104.0	52.5	126.5	0.0	0.0	0.0	0.0	10.7	75.0	19.0	133.0	10.0	70.0
1 000	-54.0	-65.2	-40.0	-40.0	13.0	55.4	38.0	100.4	52.5	126.5	0.0	0.0	0.0	0.0	9.8	68.3	19.0	133.0	10.0	70.0
2 000	-54.0	-65.2	-40.0	-40.0	11.0	51.9	36.0	96.9	51.0	123.9	0.0	0.0	0.0	0.0	8.9	62.0	19.0	133.0	10.0	70.0
3 000	-54.0	-65.2	-40.0	-40.0	9.1	48.3	34.1	93.3	49.1	120.3	0.0	0.0	0.0	0.0	8.0	56.3	19.0	133.0	10.0	70.0
4 000	-54.0	-65.2	-40.0	-40.0	7.1	44.7	32.1	89.7	47.1	116.7	0.0	0.0	0.0	0.0	7.3	50.9	19.0	133.0	10.0	70.0
5 000	-54.0	-65.2	-40.0	-40.0	5.1	41.2	30.1	86.2	45.1	113.2	0.0	0.0	0.0	0.0	6.6	46.0	19.0	133.0	10.0	70.0
6 000	-54.0	-65.2	-40.0	-40.0	3.1	37.6	28.1	82.6	43.1	109.6	0.0	0.0	0.0	0.0	5.9	41.5	19.0	133.0	10.0	70.0
7 000	-54.0	-65.2	-40.0	-40.0	1.1	34.1	26.1	79.1	41.1	106.1	0.0	0.0	0.0	0.0	5.3	37.4	19.0	133.0	10.0	70.0
8 000	-54.0	-65.2	-40.0	-40.0	-0.8	30.5	24.2	75.5	39.2	102.5	0.0	0.0	0.0	0.0	4.8	33.6	19.0	133.0	10.0	70.0
9 000	-54.0	-65.2	-40.0	-40.0	-2.8	26.9	22.2	71.9	37.2	98.9	0.0	0.0	0.0	0.0	4.3	30.1	19.0	133.0	10.0	70.0
10 000	-54.0	-65.2	-40.0	-40.0	-4.8	23.4	20.2	68.4	35.2	95.4	0.0	0.0	0.0	0.0	3.9	27.0	19.0	133.0	10.0	70.0
11 000	-54.0	-65.2	-40.0	-40.0	-6.8	19.8	18.2	64.8	33.2	91.8	0.0	0.0	0.0	0.0	3.4	24.1	19.0	133.0	10.0	70.0
12 000	-54.0	-65.2	-40.0	-40.0	-8.8	16.2	16.2	61.2	31.2	88.2	0.0	0.0	0.0	0.0	3.1	21.5	18.5	129.2	10.0	70.0
13 000	-54.0	-65.2	-40.0	-40.0	-10.7	12.7	14.3	57.7	29.3	84.7	0.0	0.0	0.0	0.0	2.7	19.1	16.9	118.0	10.0	70.0
14 000	-54.0	-65.2	-40.0	-40.0	-12.7	9.1	12.3	54.1	27.3	81.1	0.0	0.0	0.0	0.0	2.4	16.9	15.4	107.6	10.0	70.0
14 500	-54.0	-65.2	-40.0	-40.0	-13.7	7.3	11.3	52.3	26.3	79.3	0.0	0.0	0.0	0.0	2.1	15.0	14.0	97.9	10.0	70.0
14 501	-54.0	-65.2	-40.0	-40.0	-13.7	7.3	11.3	52.3	21.3	70.3	0.0	0.0	0.0	0.0	1.9	13.2	12.7	89.0	10.0	70.0
16 000	-54.0	-65.2	-41.7	-43.0	-16.7	2.0	8.3	47.0	18.3	65.0	0.0	0.0	0.0	0.0	1.7	11.6	11.5	80.8	10.0	70.0
17 000	-54.0	-65.2	-42.8	-45.0	-18.7	-1.6	6.3	43.4	16.3	61.4	0.0	0.0	0.0	0.0	1.5	10.2	10.5	73.2	10.0	70.0
18 000	-54.0	-65.2	-43.9	-47.1	-20.6	-5.2	4.4	39.8	14.4	57.8	0.0	0.0	0.0	0.0	1.3	8.9	9.5	66.2	9.5	66.2
19 000	-54.0	-65.2	-45.0	-49.1	-22.6	-8.7	2.4	36.3	12.4	54.3	0.0	0.0	0.0	0.0	1.1	7.8	8.5	59.8	8.5	59.8
20 000	-54.0	-65.2	-46.2	-51.1	-24.6	-12.3	0.4	32.7	10.4	50.7	0.0	0.0	0.0	0.0	1.0	6.8	7.7	53.8	7.7	53.8
21 000	-54.0	-65.2	-47.3	-53.1	-26.6	-15.8	-1.6	29.2	8.4	47.2	0.0	0.0	0.0	0.0	0.8	5.9	6.9	48.4	6.9	48.4
22 000	-54.0	-65.2	-48.4	-55.1	-28.6	-19.4	-3.6	25.6	6.4	43.6	0.0	0.0	0.0	0.0	0.7	5.1	6.2	43.4	6.2	43.4
23 000	-54.0	-65.2	-49.5	-57.1	-30.5	-23.0	-5.5	22.0	4.5	40.0	0.0	0.0	0.0	0.0	0.6	4.4	5.6	38.9	5.6	38.9
24 000	-54.0	-65.2	-50.6	-59.2	-32.5	-26.5	-7.5	18.5	2.5	36.5	0.0	0.0	0.0	0.0	0.5	3.8	5.0	34.7	5.0	34.7
25 000	-54.0	-65.2	-51.8	-61.2	-34.5	-30.1	-9.5	14.9	0.5	32.9	0.0	0.0	0.0	0.0	0.5	3.2	4.4	31.0	4.4	31.0
26 000	-54.0	-65.2	-52.9	-63.2	-36.5	-33.7	-11.5	11.3	-1.5	29.3	0.0	0.0	0.0	0.0	0.4	2.8	3.9	27.6	3.9	27.6
27 000	-54.0	-65.2	-54.0	-65.2	-38.5	-37.2	-13.5	7.8	-3.5	25.8	0.0	0.0	0.0	0.0	0.3	2.3	3.5	24.4	3.5	24.4
28 000	-54.4	-66.0	-54.4	-66.0	-40.4	-40.8	-15.4	4.2	-5.4	22.2	0.0	0.0	0.0	0.0	0.3	2.0	3.1	21.6	3.1	21.6
29 000	-56.4	-69.6	-56.4	-69.6	-42.4	-44.4	-17.4	0.6	-7.4	18.6	0.0	0.0	0.0	0.0	0.2	1.7	2.7	19.1	2.7	19.1
30 000	-58.4	-73.1	-58.4	-73.1	-44.4	-47.9	-19.4	-2.9	-9.4	15.1	0.0	0.0	0.0	0.0	0.2	1.4	2.4	16.8	2.4	16.8
31 000	-60.4	-76.7	-60.4	-76.7	-46.4	-51.5	-21.4	-6.5	-11.4	11.5	0.0	0.0	0.0	0.0	0.2	1.2	2.1	14.8	2.1	14.8
32 000	-62.4	-80.2	-62.4	-80.2	-48.4	-55.0	-23.4	-10.0	-13.4	8.0	0.0	0.0	0.0	0.0	0.1	1.0	1.8	12.9	1.8	12.9
33 000	-64.3	-83.8	-64.3	-83.8	-50.3	-58.6	-25.3	-13.6	-15.3	4.4	0.0	0.0	0.0	0.0	0.1	0.8	1.6	11.3	1.6	11.3
34 000	-66.3	-87.4	-66.3	-87.4	-52.3	-62.2	-27.3	-17.2	-17.3	0.8	0.0	0.0	0.0	0.0	0.1	0.7	1.4	9.8	1.4	9.8
35 000	-68.3	-90.9	-68.3	-90.9	-54.3	-65.7	-29.3	-20.7	-19.3	-2.7	0.0	0.0	0.0	0.0	0.1	0.6	1.2	8.5	1.2	8.5
36 000	-70.5	-94.9	-70.5	-94.9	-56.5	-69.7	-31.5	-24.7	-21.3	-6.3	0.0	0.0	0.0	0.0	0.1	0.6	1.3	8.8	1.3	8.8
37 000	-70.5	-94.9	-70.5	-94.9	-56.5	-69.7	-31.5	-24.7	-23.3	-9.9	0.0	0.0	0.0	0.0	0.1	0.6	1.3	9.3	1.3	9.3
38 000	-70.5	-94.9	-70.5	-94.9	-56.5	-69.7	-31.5	-24.7	-25.2	-13.4	0.0	0.0	0.0	0.0	0.1	0.6	1.4	9.7	1.4	9.7
39 000	-70.5	-94.9	-70.5	-94.9	-56.5	-69.7	-31.5	-24.7	-27.2	-17.0	0.0	0.0	0.0	0.0	0.1	0.7	1.5	10.2	1.5	10.2
40 000	-70.5	-94.9	-70.5	-94.9	-56.5	-69.7	-31.5	-24.7	-29.2	-20.6	0.0	0.0	0.0	0.0	0.1	0.7	1.5	10.7	1.5	10.7
41 000	-70.5	-94.9	-70.5	-94.9	-56.5	-69.7	-31.5	-24.7	-31.2	-24.1	0.0	0.0	0.0	0.0	0.1	0.7	1.5	10.7	1.5	10.7

Table 18 Atmospheric pressure law [37]

Altitude [ft]	Press. [mbar]	Press. [psi]	Altitude [ft]	Press. [mbar]	Press. [psi]	Altitude [ft]	Press. [mbar]	Press. [psi]
-3546	1150.000	16.691	12500	631.816	9.170	29000	314.848	4.570
-3500	1148.144	16.664	13000	619.426	8.990	29500	307.807	4.468
-3000	1128.030	16.372	13500	607.234	8.813	30000	300.894	4.367
-2500	1108.202	16.084	14000	595.237	8.639	30500	294.107	4.269
-2000	1088.658	15.801	14500	583.432	8.468	31000	287.445	4.172
-1500	1069.394	15.521	15000	571.817	8.299	31500	280.906	4.077
-1000	1050.406	15.246	15500	560.391	8.134	32000	274.487	3.984
-500	1031.693	14.974	16000	549.150	7.970	32500	268.188	3.892
0	1013.250	14.706	16500	538.092	7.810	33000	262.006	3.803
500	995.075	14.443	17000	527.216	7.652	33500	255.940	3.715
1000	977.165	14.183	17500	516.518	7.497	34000	249.989	3.628
1500	959.517	13.926	18000	505.996	7.344	34500	244.150	3.544
2000	942.128	13.674	18500	495.649	7.194	35000	238.422	3.460
2500	924.996	13.425	19000	485.474	7.046	35500	232.803	3.379
3000	908.116	13.180	19500	475.468	6.901	36000	227.292	3.299
3500	891.486	12.939	20000	465.630	6.758	36500	221.837	3.220
4000	875.104	12.701	20500	455.958	6.618	37000	216.569	3.143
4500	858.967	12.467	21000	446.449	6.480	37500	211.427	3.069
5000	843.071	12.236	21500	437.101	6.344	38000	206.406	2.996
5500	827.415	12.009	22000	427.913	6.211	38500	201.505	2.925
6000	811.995	11.785	22500	418.881	6.080	39000	196.720	2.855
6500	796.808	11.565	23000	410.004	5.951	39500	192.049	2.787
7000	781.852	11.348	23500	401.281	5.824	40000	187.489	2.721
7500	767.124	11.134	24000	392.708	5.700	40500	183.037	2.657
8000	752.622	10.924	24500	384.284	5.577	41000	178.691	2.594
8500	738.342	10.716	25000	376.007	5.457	41500	174.448	2.532
9000	724.283	10.512	25500	367.875	5.339	42000	170.305	2.472
9500	710.441	10.311	26000	359.886	5.223	42500	166.261	2.413
10000	696.815	10.114	26500	352.038	5.109	43000	162.314	2.356
10500	683.400	9.919	27000	344.329	4.998	43500	158.459	2.300
11000	670.196	9.727	27500	336.758	4.888	44000	154.697	2.245
11500	657.199	9.539	28000	329.322	4.780	44500	151.023	2.192
12000	644.406	9.353	28500	322.019	4.674	44641	150.000	2.177

At 41 000 feet, the ambient pressure reaches 2.59 psia, which is undoubtedly too thin for passenger oxygenation. Consequently, in flight cases, the cabin pressure is always greater the ambient and the overpressure increases with altitude. For ground cases, the cabin and ambient pressure are the same. The correspondence between aircraft altitude and cabin pressure is showed in Table 19.

Table 19 Cabin pressure law [6]

A/C Altitude	Cabin pressure
feet	**psia**
0	14.7
5 000	[…]*
10 000	[…]
15 000	[…]
20 000	[…]
25 000	[…]
30 000	[…]
35 000	[…]
40 000	[…]
41 000	[…]

*Values have been removed for confidential reasons as in agreement with Bombardier.

3.2.2 Flow schedule

The flow schedule is the fresh air mass flow rate calculated so as to reach cabin temperature performance and ventilation requirements. It is function of the cabin pressure, but also of whether one or two packs are functioning. Additionally, when the cargo heat and recirculation are set to *ON*, the flow schedule is increased. Table 20 and 21 indicate the flow schedule for the CSeries 300. Currently, the ECS model only supports CS300 flight and ground cases with the flow schedule set for the maximum number of passengers. Values that are not listed are interpolated linearly.

Table 20 Dual pack fcv flow schedule [6]

		DUAL PACK FLOW @ FCV		
		S1	**S2 =S1 +** […] **lb/min**	**S3 = S1** […] **lb/min**
CS300		Dual Pack - Cargo Heat OFF	Dual Pack - Recirc ON - Cargo Heat ON	Dual Pack - Recirc OFF - Cargo Heat ON
A/C Altitude	Cabin Pressure	Flow schedule	Flow schedule	Flow schedule
ft	psia	lb/min	lb/min	lb/min
-2 000	[…]	[…]	[…]	[…]
0	[…]	[…]	[…]	[…]
5 000	[…]	[…]	[…]	[…]
10 000	[…]	[…]	[…]	[…]
15 000	[…]	[…]	[…]	[…]
20 000	[…]	[…]	[…]	[…]
25 000	[…]	[…]	[…]	[…]
30 000	[…]	[…]	[…]	[…]
35 000	[…]	[…]	[…]	[…]
40 000	[…]	[…]	[…]	[…]
41 000	[…]	[…]	[…]	[…]
14500	[…]	[…]	[…]	[…]

Table 21 Single pack fcv flow schedule [6]

		SINGLE PACK FLOW @ FCV		
		S4	**S5 = S4 +** […]**lb/min**	**S6 = S4 +** […]**lb/min**
CS300		Single PACK - Cargo Heat OFF	Single PACK - Recirc ON - Cargo Heat ON	Single PACK - Recirc OFF - Cargo Heat ON
A/C Altitude	Cabin Pressure	Flow schedule	Flow schedule	Ventilation flow
ft	psia	lb/min	lb/min	lb/min
-2 000	[…]	[…]	[…]	[…]
0	[…]	[…]	[…]	[…]
5 000	[…]	[…]	[…]	[…]
10 000	[…]	[…]	[…]	[…]
15 000	[…]	[…]	[…]	[…]
20 000	[…]	[…]	[…]	[…]
25 000	[…]	[…]	[…]	[…]
30 000	[…]	[…]	[…]	[…]
35 000	[…]	[…]	[…]	[…]
40 000	[…]	[…]	[…]	[…]
41 000	[…]	[…]	[…]	[…]
14500	[…]	[…]	[…]	[…]

3.2.3 Ram air outlet pressure drop

Pressure drop due to the flow exhaust into the free stream is calculated with Equation 38.

$$\Delta \boldsymbol{P} = \frac{\dot{\boldsymbol{m}}^{\boldsymbol{2}}\boldsymbol{T}}{[\boldsymbol{6{,}87KD^2}]^{\boldsymbol{2}}\boldsymbol{P_{static\_\infty}}} \tag{38}$$

- ΔP: Discharge loss [in. H_2O];
- $\dot{m}$: Discharge flow rate [lb/min];
- T: Ram air outlet temperature [°R];
- K: Outlet coefficient of discharge;
- D: Outlet diameter [in];
- P_{static_∞}: Free stream static pressure [in. Hg abs.].

The outlet coefficient of discharge is an empirical parameter defined as the ratio of the measured mass flow to the ideal outlet mass flow. The value of K is computed by interpolation using the chart presented in Figure 25, which has been digitalized [38]. The independent variable is the discharge flow ratio defined as the ratio of the outlet mass flow to the free stream mass flow that would go through the same outlet area. The chart is valid for aircraft speed of Mach=0.7. As a consequence, for different speeds, K is an approximation.

$$\boldsymbol{Discharge\ ratio} = \frac{\dot{\boldsymbol{m}}}{\boldsymbol{\rho g U A}} \tag{39}$$

- $\dot{m}$: Discharge mass flow rate [lb/s];
- ρg: Free stream density [lb/ft^3];
- U: Free stream velocity [ft/s], $U = M\sqrt{\gamma RT}$;
- A: Outlet cross sectional area [ft^2] based on a rounded section with an outlet diameter of 10.2 in.

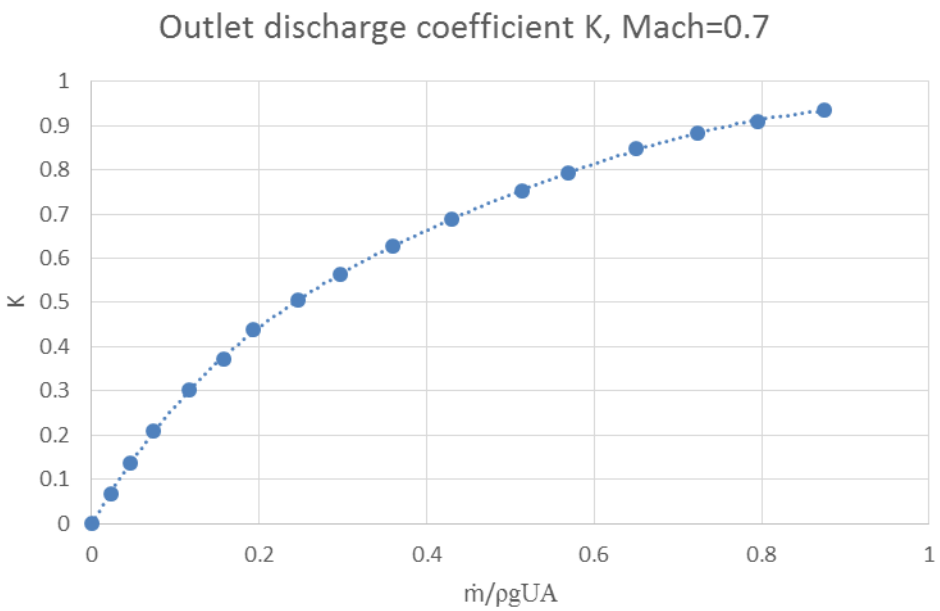

Figure 25 Outlet coefficient of discharge plot

3.2.4 Cabin flow split

The total mass flow from the mix manifold including and the TAVs is split to the cabins as indicated in Table 22.

Table 22 Cabin flow split [6]

	Cockpit	**Fwd cabin**	**Aft cabin**
Dual and singe pack	[…] %	[…] %	[…] %

The flow split is not subject to control, rather it is expected based on the LPDS design. However, the ECS model doesn't take into consideration the ducting pressure losses in the LPDS by lack of data. Therefore, the flow split is modeled by setting the three ducts, from the mix manifold to the cabins, with a cross section area so as to meet the split constraint.

$$\frac{A_{cockpit}}{[\dots]} = \frac{A_{fwd}}{[\dots]} = \frac{A_{aft}}{[\dots]}$$

3.2.5 Three-wheel ACM

The rotational speed of the three components (turbine, compressor and fan) of the ACM are matched; i.e. they rotate at the same speed. [2]

$$\boldsymbol{N_{compressor} = N_{fan} = N_{turbine}} \quad (40)$$

The turbine power output drives the fan and the compressor. Considering the mechanical loss (friction), the total ACM power is balanced according to the following equation:

$$\boldsymbol{\dot{W}_{turbine} + \dot{W}_{compressor} + \dot{W}_{fan} + Mechanical\ loss = 0} \quad (41)$$

This is done in the ECS model by means of a script that ensures that Equation 41 is verified. FM tries to solve the system iteratively by computing the rotational speed and power based on the performance maps. [10] The process is illustrated of Figure 26.

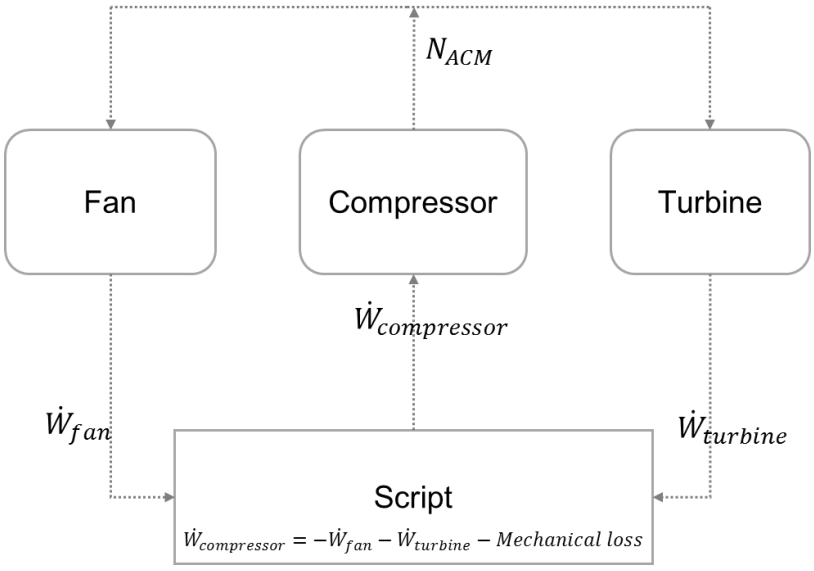

Figure 26 ACM matching algorithm

The mechanical loss was found to be a function of the rotational speed. As a matter of fact, the faster the rotation, the greater the friction force. The relationship extracted from data is illustrated on Figure 27, where unlisted rotational speeds are linearly interpolated by FM.

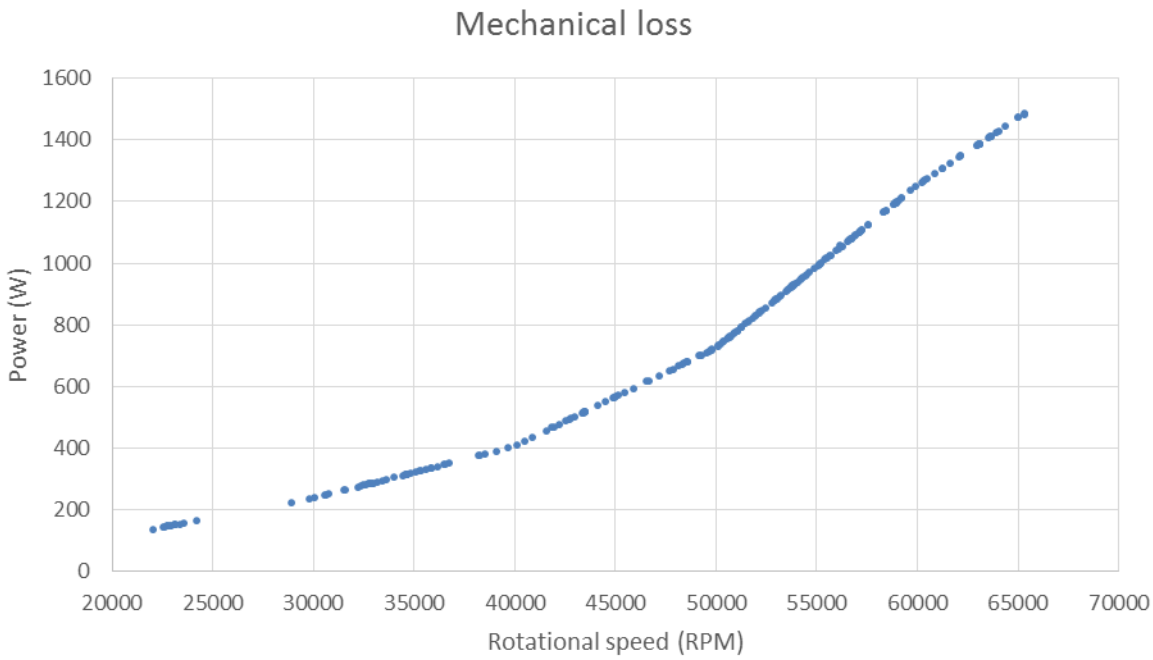

Figure 27 Mechanical loss vs rotational speed plot

3.2.6 Heat Loads

The cabin heat loads have been estimated by BA. They are divided in four different categories:

- Fixed: the sum of electrical heat loads, IFE and floor heat flow.
- Metabolic: the heat dissipated from passengers and crew.
- Solar: the heat carried by solar radiation through the windows.
- External: the heat transferred between the inside cabin and the outside fuselage skin.

Only the metabolic, solar and external heat loads are set as internal inputs. They are given for two versions of the CS300:

- CS300 SHD: Super high density, 160 maximum passenger, without IFE.
- CS300 HD: High density, 150 maximum passengers, with IFE.

Furthermore, heat loads are given distinctly for cockpit, fwd cabin and aft cabin.

Metabolic heat loads

Clearly, the heat dissipated by the crew and the passengers to the cabin must be considered. The values are computed using the following relations. [39]

$$\dot{W}_{metabolic} = \dot{W}_{passengers} + \dot{W}_{crew} \quad (42)$$

$$\dot{W}_{passengers} = N_{passengers}\left(188 - 4.7 \cdot T_{cabin\,[℃]}\right) \quad (43)$$

$$\dot{W}_{crew} = 2 \cdot N_{crew}\left(188 - 4.7 \cdot T_{cabin\,[℃]}\right) \quad (44)$$

The number of passengers per cabin is stated in Table 23. The numbers are chosen so as to be conservative. That is why during cooling mode, the number of passengers is set to the maximum (including a margin of 4 passengers). Inversely, during heating mode, the number of passengers is set to a minimum.

Table 23 Number of pilots in cockpit

	CS300 SHD Cockpit	**CS300 HD cockpit**
	Pilots	
Cooling Cruise	3	3
Heating Cruise	2	2

Table 24 Number of cabin passengers

	CS300 SHD Cabin		**CS300 HD Cabin**	
	Fwd cabin	**Aft cabin**	**Fwd cabin**	**Aft cabin**
	Passengers			
Cooling Cruise	84	84	74	84
Heating Cruise	8	8	7	8
	Crew			
Cooling Cruise	2	3	2	3
Heating Cruise	1	1	1	1

Solar heat loads

The solar radiation is computed using the following equation:

$$\dot{W}_{solar} = A_{effective} \cdot \phi(z) \quad (45)$$

$$A_{effective} = A_{window} \cdot \cos(l) \cdot 0.5 \cdot \tau \quad (46)$$

The window area, A_{window}, is the total area covered by windows in the cabin, and l is the incidence angle (estimated to 27°) between the sun rays and windows. The solar heat flux, $\phi(z)$, is a function of the altitude and is computed by linear interpolation from the digitalized data taken from [40] and showed in Figure 28.

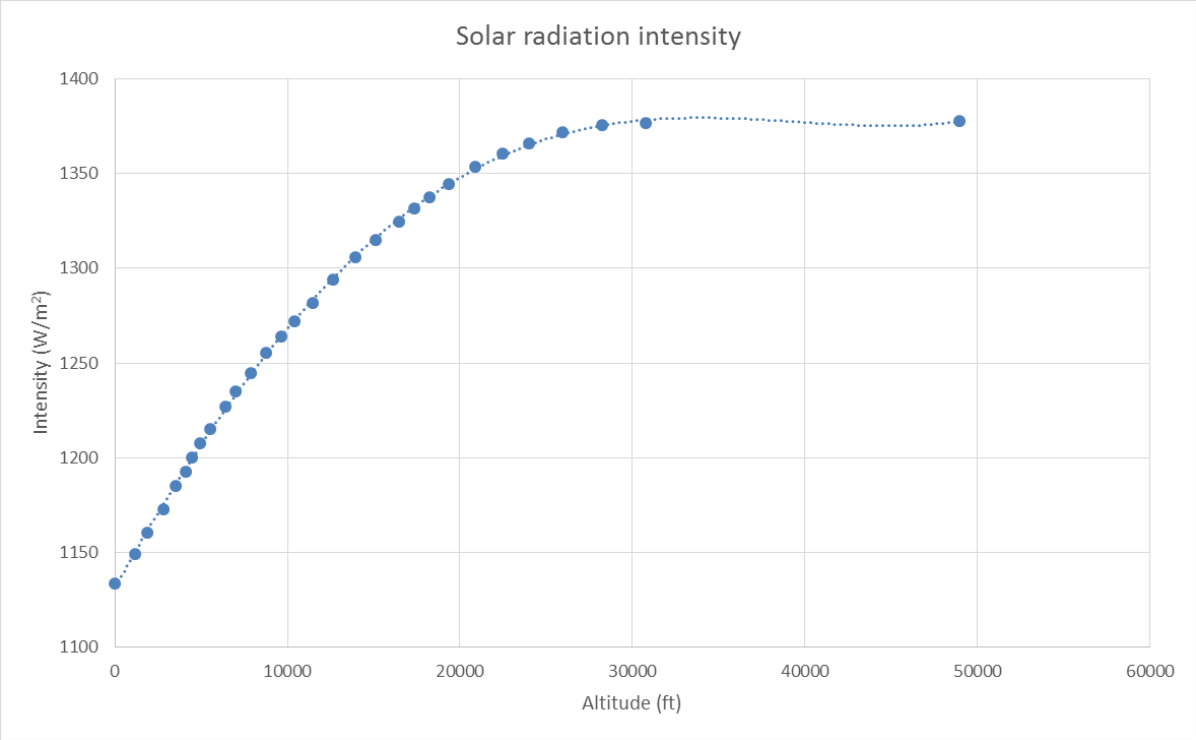

Figure 28 Solar radiation intensity plot

The solar heat load is computed internally based on the solar radiation intensity. Nevertheless, the effective area was set as internal inputs to the ECS model, thereby they are presented in this section in Table 25 and Table 26. For heating cases, the area has been assumed to zero to be conservative.

Table 25 Cockpit effective area

	CS300 SHD Cockpit	CS300 HD Cockpit
	Windows Effective Area (m^2) transmissivity = […]	
Cooling	[…]	[…]
Heating	[…]	[…]

Table 26 Aft cabin effective area

	CS300 SHD Cabin		CS300 HD Cabin	
	Fwd cabin	**Aft cabin**	**Fwd cabin**	**Aft cabin**
	Windows Effective Area (m^2) transmissivity = […]			
Cooling	[…]	[…]	[…]	[…]
Heating	[…]	[…]	[…]	[…]

External heat loads

The external heat loads relate to the heat transferred between the inside cabin and the outside fuselage skin:

$$\dot{W}_{external} = UA(T_{skin} - T_{cabin}) \quad (47)$$

The overall heat transfer coefficient, UA, takes into account the fuselage conduction and convection between the cabin air and the fuselage interior wall. The fuselage external skin temperature, T_{skin}, is determined by the equilibrium between thermal conductivity, radiation and convection. However, good estimations can be achieved by empirical relations:

For Mach > 0 :

$$T_{skin} = T_{ambient\,(K)} \cdot \left(1 + 0.18 \cdot Mach^2\right) \quad (48)$$

For Mach = 0:

$$T_{skin\,(℃)} = 1.238 \cdot T_{ambient(℃)},\ if\ T_{ambient} > 0℃ \quad (49)$$

$$T_{skin\,(°C)} = T_{ambient(°C)},\ if\ T_{ambient} < 0°C, T_{skin\,(°C)} \quad (50)$$

The default overall heat transfer coefficients used by the ECS model are presented in Table 27.

Table 27 CS300 UA factors

CS300 SHD			CS300 HD		
UA factor (W/m^2)			UA factor (W/m^2)		
Cockpit	**Fwd cabin**	**Aft cabin**	**Cockpit**	**Fwd cabin**	**Aft cabin**
[…]	[…]	[…]	[…]	[…]	[…]

3.2.7 Thermal losses

Thermal losses from pack discharge to cabins and cockpit are due to heat transfer from the LPDS ducting to the surroundings. The losses have been modeled with the following equation:

$$Q_{loss} = h\left(T_{compartment,total} - T_{ambien,t}\right) \quad (51)$$

The driving force being the difference in compartment and ambient total temperatures. The heat transfer coefficients, *h*, for the two cabins and the cockpit are given in the table below. Thermal losses in the recirculation piping have been modeled by a temperature decrease of […]°C. [6]

Table 28 Thermal loss coefficients

Compartment	Heat transfer coefficient (W/K)
Fwd cabin supply duct	[…]
Aft cabin supply duct	[…]
Cockpit supply duct	[…]

3.2.8 Geometry data

Data on heat-exchanger geometry was necessary to complete the model. For example, in order to predict choked flow if any, the inlet and outlet cross section pipe area of the heat exchangers must

be specified. For the PHX and SHX, the required area was estimated based on CS300 Catia 3D drawings, whereas for the REH and COND, the information was found in [41] . Figure 29 shows an example of the digital drawings used to calculate PHX and SHX pipe areas.

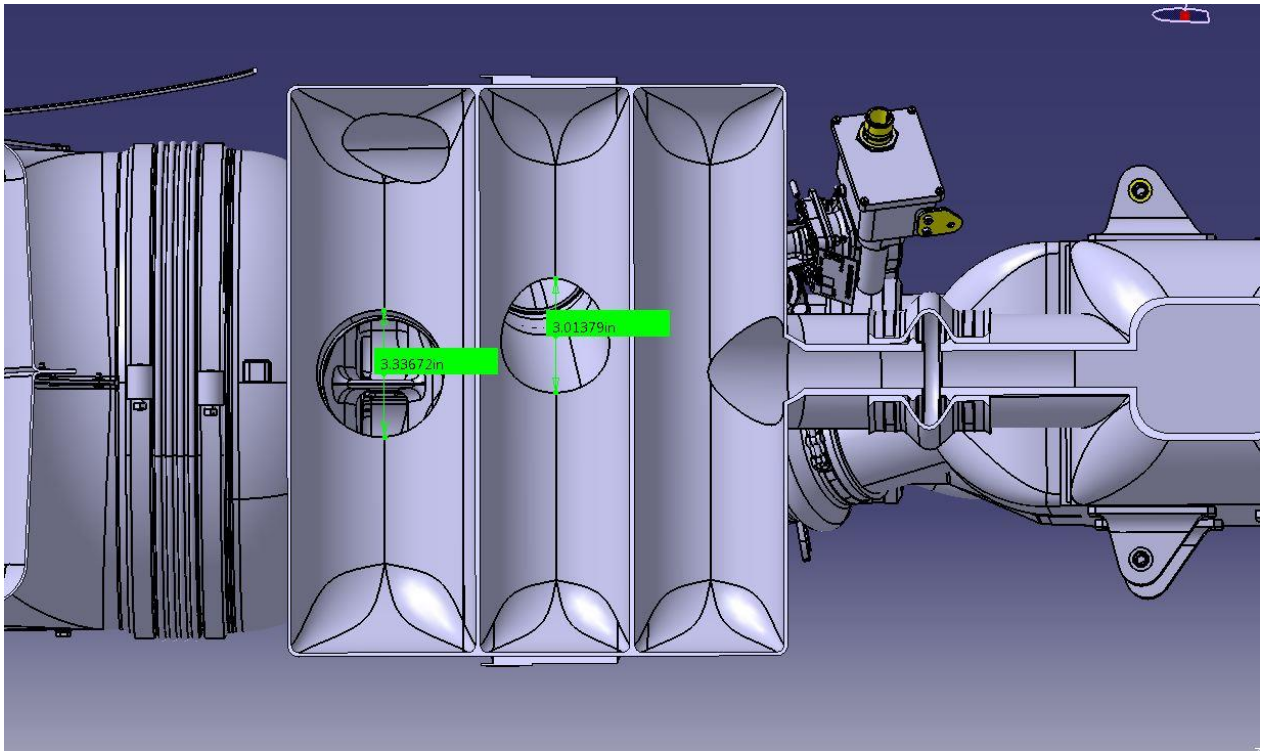

Figure 29 Inside view of shx and phx

The ram air duct cross section area changes throughout the channel. The values were also estimated based on the Catia drawings. For instance, the figure on the next page shows the measures taken to model the gradual transition at the SHX entry.

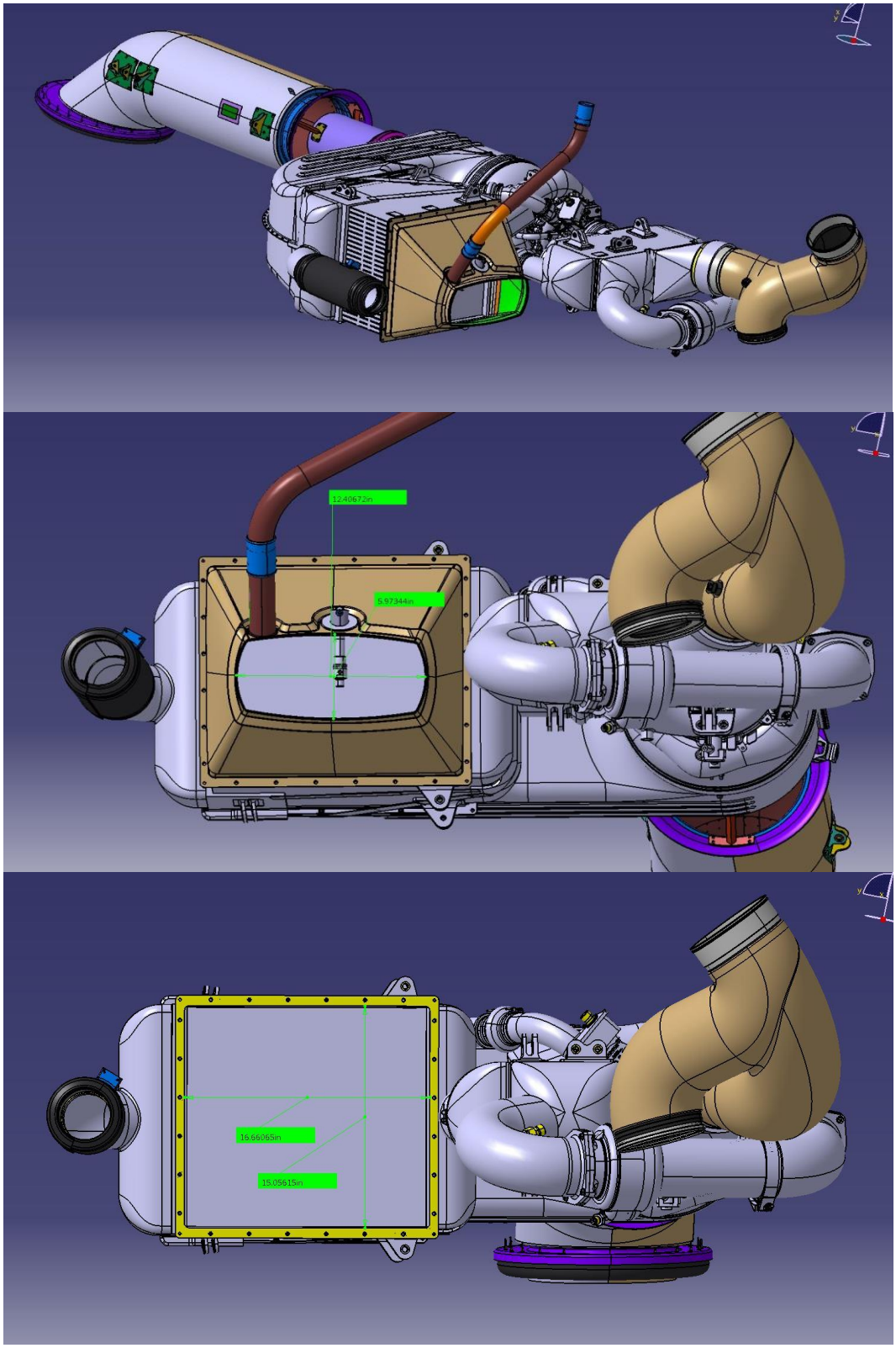

Figure 30 SHX inlet dimensions (ram air side)

3.3 External inputs

External inputs are parameters that must be specified by the user to the model prior to running a simulation. These parameters are entered under the *Experiment* tab in the Network View window. They are set as external because their value might change considerably depending on the flight conditions. As mentioned previously, internal inputs are computed by the model, but some of them require parameters to be specified to complete the calculation. This is the case for the metabolic heat loads (an internal input), where the number of passengers is set as an external input.

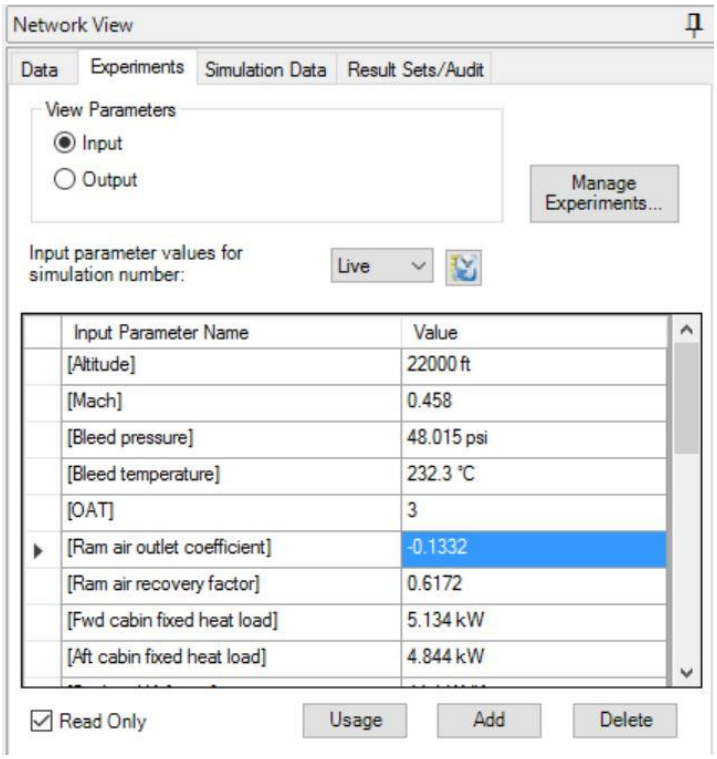

Figure 31 FM's external inputs tab

3.3.1 Ram air factors

Ram air inlet pressure recovery factor

The ram air inlet pressure recovery factor, η_{inlet}, is defined as

$$\eta_{inlet} = \frac{(P_{inlet\_ram} - P_{static\_\infty})}{(P_{total\_\infty} - P_{static\_\infty})} \quad (52)$$

The infinity subscript represents the ambient conditions. The inlet recovery factor is a function of the ram air mass flow rate, altitude and aircraft speed. The next table indicates a limited range of inlet recovery factors for the CS300. For this reason, the ECS model requires the user to specify the factor.

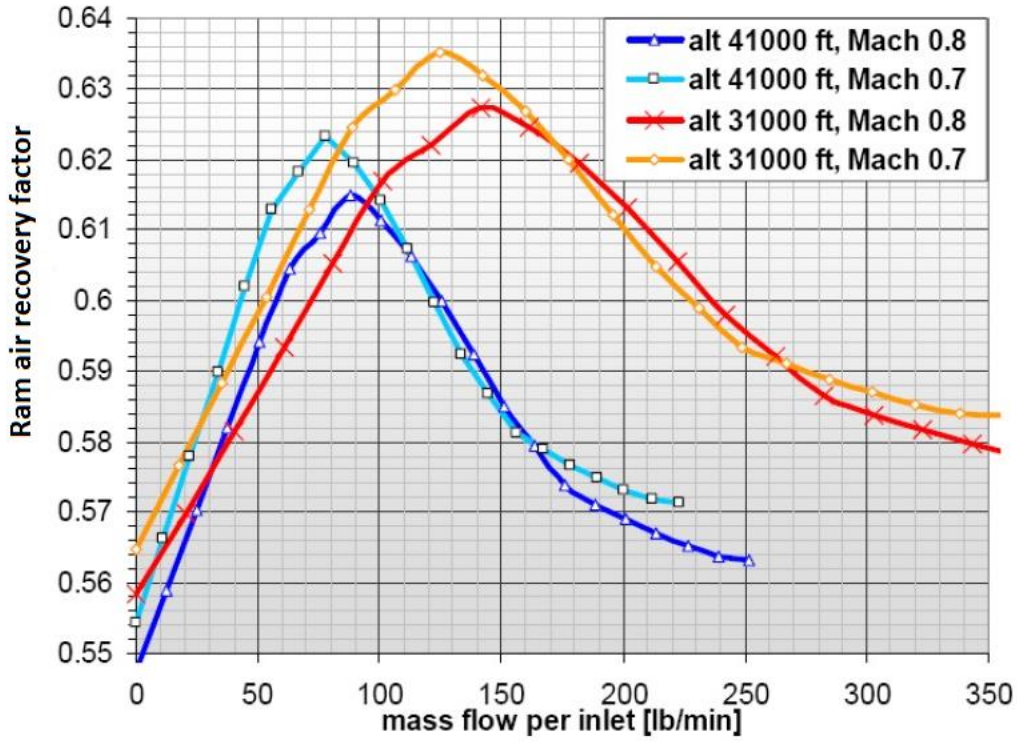

Figure 32 Ram air recovery factor for different altitudes and speeds [6]

Ram air inlet outlet pressure coefficient

The total pressure at the ram outlet is computed by means of the pressure coefficient, C_p :

$$C_p = \frac{(P_{outlet\_ram} - P_{static\_\infty})}{(P_{total\_\infty} - P_{static\_\infty})} \quad (53)$$

The value of the pressure coefficient has been calculated for two different speeds stated in Table 29.

Table 29 Ram outlet pressure coefficients

	Ram air Outlet C_p	
A/C Mach	**0.7**	**0.8**
CS300	-0.19	-0.228

3.3.2 Pack leakage

The pack leakage is defined as the mass percentage that has leaked between the FCV and the mix manifold. It can be set by the user.

$$\boldsymbol{Dual\ Pack\ leakge\ flow} = \frac{(\boldsymbol{2 \times Flow\ schedule - TAVs\ flow})}{\boldsymbol{2}} \times \boldsymbol{Leak\ Percentage} \quad (3.17)$$

$$\boldsymbol{One\ Pack\ leakge\ flow} = (\boldsymbol{Flow\ schedule - TAVs\ flow}) \times \boldsymbol{Leak\ Percentage} \quad (3.18)$$

3.3.3 Cabin flow recirculation

Air is recirculated to the cabins in order to decrease the amount of fresh air demand, which in return decreases the engines energy demand. How much air is recirculated is determined by the recirculation fan, which have been designed to recirculate approximately 50% of the fresh air brought to the cabins.

In reality, the recirculation fan drives also air to the cargo compartment. However, because the LPDS pressure loss data was not readily available, the cargo compartment ventilation has not been modeled. Performance data on the recirculation fan was also unavailable. Hence, the recirculation is set by the user by specifying a recirculation percentage (mass flow recirculated out of the total fresh air mass flow) in the input screen. A temperature increase of 4°C through the fan have been assumed as stated in [6].

3.3.4 Valve pressure loss coefficients

Valves are modelled according to the following equation:

$$\boldsymbol{\sigma \Delta P = K Q^{\alpha}} \quad (54)$$

ΔP is the pressure drop $[bar]$, K is the pressure loss coefficient $[bar/(kg/min)^{\alpha}]$, Q is the mass flow rate $[kg/min]$, $\sigma = \frac{\rho}{\rho_0}$ is the density ratio where $\rho_0 = \frac{P_0}{RT_0}$, the density at standard conditions ($T_0 = 28815\ K, P_0 = 1.013 \cdot 10^5\ Pa$).

The table below summarizes the pressure loss coefficients for fully opened and fully closed valve positions, the pressure loss exponents and the valve diameters. The valve opening is then defined by setting the value of the pressure loss coefficient between the fully opened and fully closed values. The TCV is the only valve that have been modeled as a Cd valve component (section 2.3.6) for control purposes. The TCV opening is therefore defined by setting a Cd (coefficient of discharge) value.

Table 30 Valve pressure loss coefficients

	Fully opened		**Fully closed**		**Area**
	Pressure loss coefficient (bar/(kg/min)$^{\alpha}$)	**Pressure loss exponent α**	**Pressure loss coefficient (bar/(kg/min)$^{\alpha}$)**	**Pressure loss exponent α**	**Diameter (in)**
TCV	--	--	--	--	2
FCV	$2.4 \cdot 10^{-5}$	2.14	$1 \cdot 10^{5}$	2.14	3
RARV	$4.42 \cdot 10^{-7}$	1.92	$4 \cdot 10^{-4}$	1.06	7
TAPRV	$1.92 \cdot 10^{-3}$	1.92	$1 \cdot 10^{5}$	1.92	1.5
TAV	$1.92 \cdot 10^{-3}$	1.92	$1 \cdot 10^{5}$	1.92	1.5

3.3.5 Fixed heat loads

Fixed heat loads are assigned as external inputs. In fact, floor heat flows have been estimated for a limited number of flight cases (Table 33). Unlisted cases in Table 33 must be interpolated. For this reason, setting this parameter as external was judged to be a better choice so it can be easily changed for each simulation by a prior assessment by the user. Otherwise, the user is summoned to look up on the table for a quick approximation.

The fixed heat loads for each compartment are given by

$$\dot{W}_{fixed} = \dot{W}_{electrical} + \dot{W}_{IFE} + \dot{W}_{floor} \quad (55)$$

The exception being the cockpit as it is only subject to electrical heat loads. The tables below show the fixed heat loads for the cockpit, fwd and aft cabin.

Table 31 Cockpit fixed heat loads

	CS300 SHD Cockpit (W)	**CS300 HD Cockpit (W)**
Pull Down	500	500
Pull Up	452	452
Cooling steady state	571	571
Heating steady state	492	492

Table 32 Electrical + IFE heat loads

	CS300 SHD Cabin		**CS300 HD Cabin**	
	Fwd cabin (W)	**Aft cabin (W)**	**Fwd cabin (W)**	**Aft cabin (W)**
Pull Down	689	569	633	554
Pull Up	623	515	573	502
Cooling steady state, IFE ON, ground	996	835	3 233	3 091
Cooling steady state, IFE OFF, ground	996	835	938	797
Cooling steady state, IFE ON, Flight	1 111	921	5 068	4 899
Cooling steady state, IFE OFF, Flight	1 111	921	1 052	883
Cooling, ram air operation	746	666	705	625

Heating steady state ground	1 417	1 297	1 401	1 281
Heating steady state Flight	1 485	1 349	1 431	1 333

Table 33 Floor heat flow

	CS300 SHD Cabin		**CS300 HD Cabin**	
	Fwd cabin (W)	**Aft cabin (W)**	**Fwd cabin (W)**	**Aft cabin (W)**
Ground, XHD, OAT of 52.5°C, 2 Packs (APU0XHD2P)	526	809	526	809
Ground, HD, OAT of 40°C, 2 Packs (APU0HD2P)	462	707	462	707
Ground, HD, OAT of 40°C, 1 Pack (APU0HD1P)	489	788	489	788
Ground, ISA, OAT of 15°C, 2 Packs (APU0ISA2P)	285	351	285	351
Ground, CD, OAT of -40°C, 2 Packs (APU0C2P)	-149	-292	-149	-292
Ground, CD, OAT of -40°C, 1 Pack (APU0CD1P)	-239	-352	-239	-352
In-flight, Cruise, 41000ft, HD, OAT of -31.5°C, 2 Packs (CR41HD2P)	120	-29	120	-29
In-flight, Cruise, 31000ft, HD, OAT of -21.4°C, 1 Pack (CR31HD1P)	66	-55	66	-55

in-flight, Descent, 20000ft, HD, OAT of 0.4°C, 1 Pack (DE20HD1P)	390	401	390	401
In-flight, Cruise, 41000ft, ISA, OAT of -56.5°C, 2 Packs (CR41ISA2P)	-209	-515	-209	-515
In-flight, Cruise, 31000ft, ISA, OAT of -46.4°C, 2 Packs (CR31ISA2P)	-404	-614	-404	-614
In-flight, Cruise, 41000ft, CD, OAT of -70.5°C, 2 Packs (CR41CD2P)	-1 204	-1 614	-1 204	-1 614
In-flight, Cruise, 37000ft, CD, OAT of -70.5°C, 2 Packs (CR37CD2P)	-602	-1 037	-602	-1 037
In-flight, Cruise, 31000ft, CD, OAT of -60.4°C, 2 Packs (CR31CD2P)	-1 033	-1 385	-1 033	-1 385
in-flight, Descent, 20000ft, XCD, OAT of -65.2°C, 1 Pack (DE20XCD1P)	-652	-972	-652	-972

3.3.6 External input summary

Table 34 summarizes all the external inputs that must be specified prior to running a steady-state simulation. As an example, values are given for a holding (HO) cooling case, high density, ISA, 22 000 ft. and with two packs.

Table 34 External input summary

#	Parameter	Description	Value	Units
1	**[Altitude]**	A/C altitude	22000	ft
2	**[Mach]**	A/C speed	0.458	
3	**[Bleed pressure]**	Pressure at the FCV inlet	48.015	psia
4	**[Bleed temperature]**	Total temperature at the FCV inlet	232.3	°C
5	**[OAT]**	The outside ambient temperature category	3	
6	**[Ram air recovery factor]**	The ram air inlet recovery factor	0.6172	
7	**[Fwd cabin fixed heat load]**	Fixed heat load for fwd cabin	4859	W
8	**[Aft cabin fixed heat load]**	Fixed heat load for the aft cabin	4385	W
9	**[Npax_fwd]**	The number of passengers in the fwd cabin to compute the heat load	74	passengers
10	**[Ncrew_fwd]**	The number of crew members in the fwd cabin to compute the metabolic heat load	2	crew members
11	**[Npilots]**	Number of pilots in the cockpit to compute the metabolic heat load	3	pilots
12	**[Npax_aft]**	The number of passengers in the aft cabin to compute the metabolic heat load	84	passengers
13	**[Ncrew_aft]**	The number of crew members in the aft cabin to compute the metabolic heat load.	3	crew members
14	**[Effective cockpit area]**	Cockpit effective area to compute solar heat loads	1798	in^2

15	**[Effective fwd area]**	Fwd effective area to compute solar heat loads	1829	in^2
16	**[Effective aft area]**	Aft cabin effective area to compute solar heat loads	2092.5	in^2
17	**[Cockpit fixed heat load]**	Fixed heat load for cockpit	571	W
18	**[PackLeakage]**	The percentage of flow leaked through the pack	1.85817	%
19	**[Recirculation percentage]**	The percentage of flow recirculated to the cabins	45.83	%
20	**[Ground/Flight]**	A/C on ground: 0 A/C in flight: 1	1	
21	**[TAPRV]**	Trim air pressure regulating valve pressure loss coefficient	12.9	$bar/(kg/min)^{\alpha}$
22	**[TAV cockpit]**	Cockpit trim air valve pressure loss coefficient	0.47	$bar/(kg/min)^{\alpha}$
23	**[TAV fwd]**	Fwd cabin trim air valve pressure loss coefficient	1.00E+07	$bar/(kg/min)^{\alpha}$
24	**[TAV aft]**	Aft cabin trim air valve pressure loss coefficient	1.00E+07	$bar/(kg/min)^{\alpha}$
25	**[TCV]**	Temperature control valve opening, modelled as a coefficient of discharge	20.9	%
26	**[RARV]**	Ram air regulating valve pressure loss coefficient	4.42E-07	$bar/(kg/min)^{\alpha}$
27	**[Ram flow rate]**	The total mass flow rate through the ram channel. Must be a negative value.	-115.88	lb/min
28	**[Ram bypass flow]**	The flow bypassing the ram air fan. Negative value if reverse flow.	63.55	lb/min
29	**[Packs]**	The number of packs in function	2	

30	**[FCV]**	Flow control valve pressure loss coefficient	0.00206	bar/(kg/min)$^{\alpha}$
31	**[Fan power]**	Power consumed by the fan	2027	W
32	**[Distribution split]**	Cockpit stream coefficient of discharge	0.99803	

The ECS model does not predict conditions upstream of the FCV. Therefore, the absolute pressure and total temperature at the FCV inlet must be specified by the user (parameter #3 and #4).

The aircraft flight mode must be set to compute the flow schedule. Indeed, the flow schedule is set according to the cabin pressure. Yet, the functional relation of the cabin pressure with altitude differs whether the aircraft is on ground or in-flight. For ground cases, the user must enter the value 0 in the external input tab (parameter #20), whereas for a flight case, the appropriate value is 1.

The number of working packs must also be specified. This parameter also affects the flow schedule. The user must select 1 for one pack, and 2 for two packs (parameter #29).

Flight data shows inconsistent fan behaviour (Section 5.2). Thus, in some cases the fan power was forced to match the data. Otherwise, in normal conditions the fan power is found by the solver iteratively.

When the cockpit TAV is opened, it might be necessary to adjust the cockpit coefficient of discharge value, normally set to 1, so as to keep the cockpit flow split to around 12.5%.

3.3.7 Ambient conditions

Prior to computing the ambient temperature and humidity as a function of the altitude, the OAT category (Section 3.2.1) must be selected by setting a value between 1 and 5 (parameter #5).

Table 35 OAT input values

		Input value
XCD	**Extreme cold day**	1
CD	**Cold day**	2
ISA	**International Standard Atmosphere**	3
HD	**Hot day**	4
XHD	**Extreme hot day**	5

CHAPTER 4 PERFORMANCE MAPS AND SIMULATION RESULTS

4.1 Performance maps

In Section 2.3, it was shown that performance maps were critical for running simulations involving fans, compressors, turbines and heat-exchangers. Without them, it would be impossible to predict the unknown conditions of the flow going through such component. Therefore, in this section we present the performance maps for all the components in the ECS model and show how they were obtained.

4.1.1 Data source

The data used to reverse engineer the performance maps were obtained from Liebherr's (LTS) flight simulations. The data consists of exhaustive calculation cases identified as follows:

Flight Condition_Altitude_Ambient_Number of packs

Table 36 flight case identification

Flight Condition	Altitude	Ambient	Number of packs
APU GI = Ground Idle TO = Take Off CL - Climb CR = Cruise HO = Holding DE = Descent AI = Anti-Ice	Altitude in kft	CD = Cold Day ISA = International Standard Day HD = Hot Day XHD = Extreme Hot Day	2P = 2 Packs (normal operation) 1P = 1 Pack (failure case)

Each item in the calculation case identification is described in Table 36. Moreover, for each case, data on mass flow rate, total temperature, total pressure and humidity at the inlet and outlet of every component was available. More information such as ACM rotational speed, HX effectiveness, efficiencies, power consumptions, heat loads and mechanical losses were also available.

4.1.2 Ram air fan performance maps

Our objective here is to obtain the two maps as required by FM, i.e. build a first map relating the static pressure difference with respect to volumetric flow, $\Delta P_s = f(Q)$, and a second one relating the fan efficiency with respect to volumetric flow rate, $\eta = f(Q)$.

Prior to building the maps, we examined our data in order to assess its reliability. As discussed in Section 2.3.3, the general fan performance can be visualized by plotting the dimensionless groups: Pressure coefficient vs. Flow Coefficient and Efficiency vs. Flow coefficient. As shown in Figure 33, data in blue represents operating cases where fan performed as anticipated, i.e. an intrinsic pattern can be drawn and corresponds to a decreases in ΔP_s as the flow coefficient increases. However, at high Flow Coefficient values, the fan acts as a resistance and even shows some turbine effects. That is, fan exhibits pressure loss and also produces work. We named *Resistance*, cases where fan exhibited pressure loss but did not produced work. Vortex phenomena is thought to be the reason of this behaviour.

For our modeling purposes, it would be ideal to incorporate all three patterns in our fan model. Nevertheless, turbine and resistance effects cannot be accurately predicted by only the Flow Coefficient number, making this task unsuitable. Prediction was attempted by considering the Reynolds number but no correlation was found (data not showed).

From Section 2.3.3, we recall that an efficiency map is also required to complete flow prediction. Yet the map obtained showed highly disseminated data for turbine and resistance effects with values ranging from -107% to 265% efficiency. Therefore, we limited our modeling to the normal fan operation (blue data). When turbine and resistance effects cases is discarded, the efficiency map in Figure 34 is obtained.

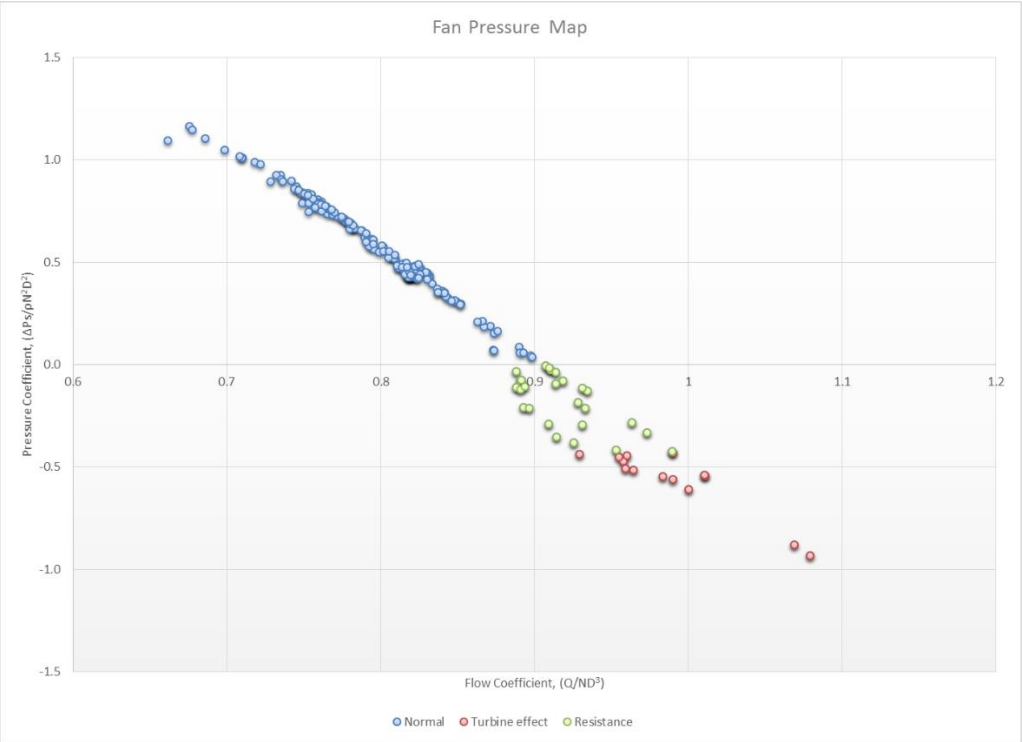

Figure 33 Pressure coefficient vs. flow coefficient

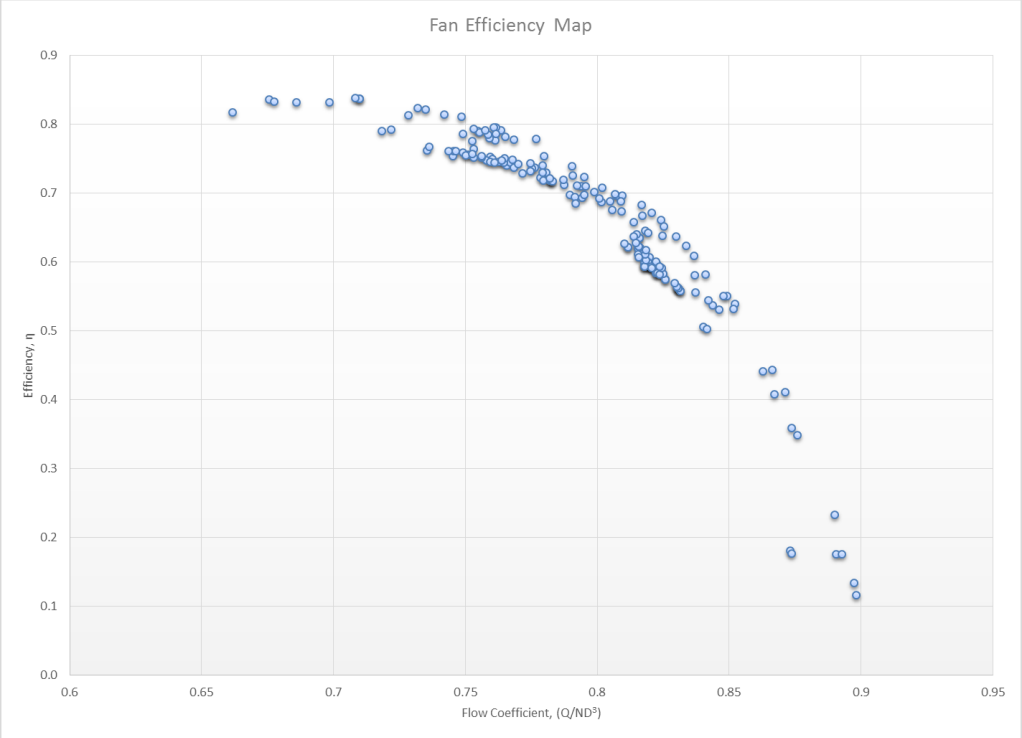

Figure 34 Efficiency vs. flow coefficient

Intermediate calculations

Our data indicated isentropic efficiencies whereas the FM fan component is modeled with polytropic efficiencies. Hence, data was manipulated to retrieve the polytropic efficiency η_p from the relationship between the polytropic and isentropic efficiency, η_{ise}. [31]

$$\boldsymbol{\eta_{ise}} = \frac{\left(\frac{P_{0,2}}{P_{0,1}}\right)^{(\gamma-1)/\gamma} - 1}{\left(\left(\frac{P_{0,2}}{P_{0,1}}\right)^{(\gamma-1)/\gamma\eta_p} - 1\right)} \tag{56}$$

FM's fan model only accepts static values to map the component whereas our data only indicates total values. Thus, retrieving the static values was undertaken by solving for the Mach number in Equation 12 and using the stagnation relations. To solve Equation 12, the cross section area A was required. This area was calculated with the fan diameter, 11.8 cm as indicated in our data sheets.

FM fan maps

In FM, the data required to build the pressure difference and efficiency map must come from a fan rotating at a constant speed, of constant diameter, inlet density and inlet static temperature. In practise, this is very inconvenient to obtain, because, despite the exhaustive simulation flight cases, not even two operating points were found to turn at the same rotational speed or be at the same inlet temperature and inlet density (in contrast, all cases had obviously the same fan diameter). To overcome this problem, we chose an arbitrary case among our data and we defined it as a reference case ($N_{ref}, T_{in\,ref}, \rho_{ref}$). Then, with the remaining data, we computed the equivalent ΔP_{eq} and Q_{eq} as if the fan was operated at the reference conditions. This is easily done using the fan laws seen in Section 2.3.3. The two new maps could then be imported to FM and be considered as operating at the constant reference conditions.

The maps obtained are showed in Figure 35 and Figure 36. The flight case H022_ISA_2P2BAI was chosen as the reference, rotating at a speed of 44 962 RPM, 0.3898 kg/m^3 density and 103.1°C inlet temperature. The blue data represents the calculated equivalent points while the red point is the reference and is taken directly from flight data.

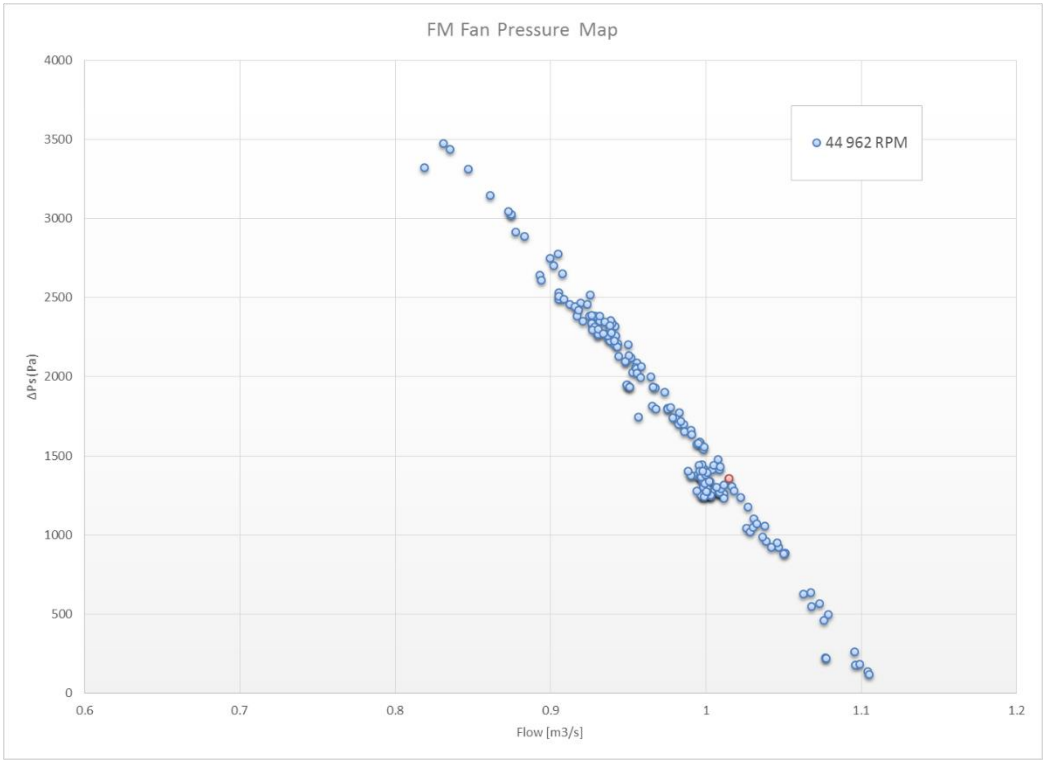

Figure 35 Fan pressure increase vs. flow chart

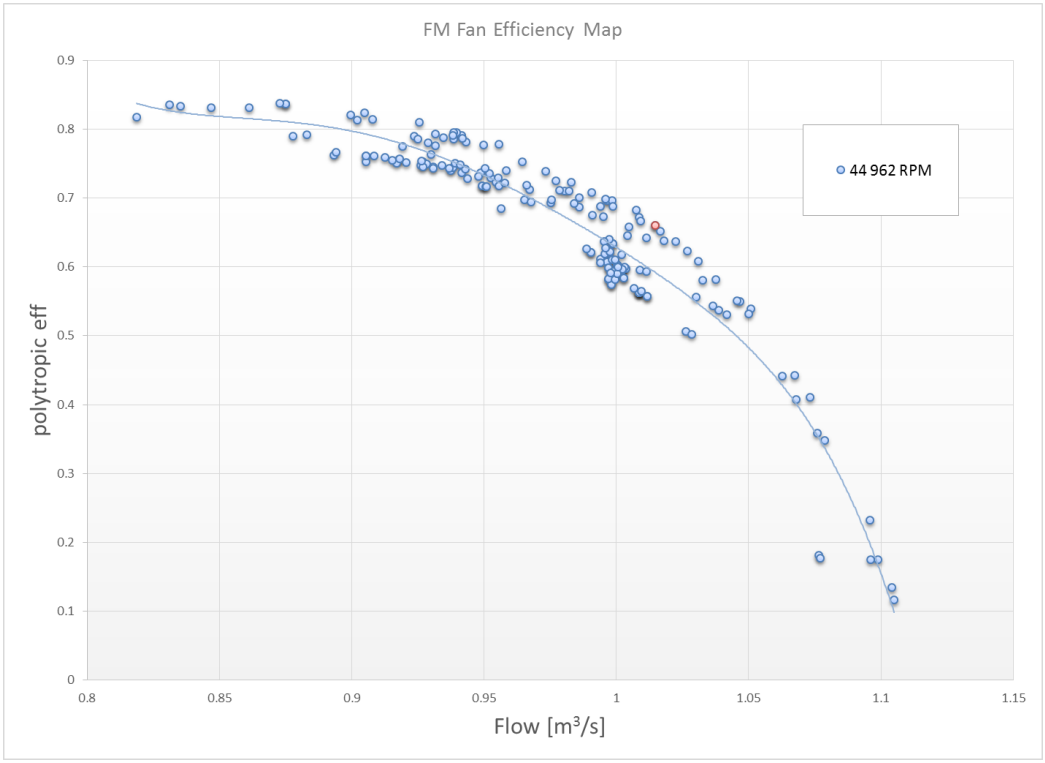

Figure 36 Fan polytropic efficiency vs. flow chart

4.1.3 3D mapping from scattered data

To create the performance maps of the remaining components, we needed to build continuous surfaces in the form of z=f(x,y) without any prior knowledge of the exact form of this function. To achieve this, data points were first examined by plotting them and an example of the result for the compressor is showed on Figure 37. It can be seen that the points are contained around what seems to be the compressor operating line. Beyond that region, there is insufficient data to build a reliable map. Therefore, using an interpolant algorithm that would estimate the surface based on our limited data points was attempted, but unfortunately without much success. In fact, interpolation turned out to be an unwise decision as the output resulted on a very bumpy surface (result not showed) due to the inherent data noise and absence of data points. The best solution was found to be a surface smoothing algorithm. John D'Errico's Matlab code *Gridfit* was used for this purpose. [42] as it produces a surface based on scattered data by balancing fidelity (interpolation) and smoothness.

Fidelity equations

First, the rectangular x-y plane over which the input data points are positioned is discretized into n number of nodes where each unknown z value is to be found. The fidelity equations correspond to the equations that originates from bilinear interpolation. Thus, if there are m input data points, there can only be m fidelity equations. The equations are converted to the matrix form

$$[A_{fidelity}] \cdot \boldsymbol{Z} = \boldsymbol{B}$$

The vector **Z** contains all the z values at every node that are to be found, $A_{fidelity}$ is the matrix that contains the weights derived from bilinear interpolation and where each row denotes one equation. **B** is the data input vector.

Commonly, the total number of nodes (variables) is greater than the number of input points (equations). Therefore, the problem is ill-posed and cannot be solved as such.

Smoothness

Additional information is introduced by assuming a given smoothness of the 3D surface. Thereby regularizing the problem. For the surface to be smooth, we can try to set the two second partial derivatives at every node point to be equal to zero. That is, at every node j

$$\left.\frac{\partial^2 z}{\partial x^2}\right|_j = 0 \text{ and } \left.\frac{\partial^2 z}{\partial y^2}\right|_j = 0$$

The second derivative is computed using a finite difference formula and the equations are converted to the matrix form

$$[A_{smoothness}] \cdot \boldsymbol{Z} = \boldsymbol{0}$$

Matrix $A_{smoothness}$ contains the second partial derivatives information at every node based on finite difference where each row represents one equation. For n nodes, there are 2n equations (rows) inside $A_{smoothness}$.

Regularization

The fidelity and smoothness equations are coupled:

$$\begin{bmatrix} A_{fidelity} \\ \lambda \cdot A_{smoothness} \end{bmatrix} \cdot \boldsymbol{Z} = \begin{bmatrix} \boldsymbol{B} \\ \boldsymbol{0} \end{bmatrix}$$

$$\Rightarrow [A] \cdot \boldsymbol{Z} = \boldsymbol{B'}$$

The user can define the balance between fidelity and smoothness by setting the *smoothing parameter* λ. When this parameter approaches zero, D'Errico's algorithm works as a pure interpolant whereas the result of a large value will approach a planar surface.

At this point, the problem is still ill-posed, that is the system is now likely to have more equations than variables. However, if $\hat{\mathbf{Z}}$ is the optimal estimator of $\mathbf{Z}$ and we define the scalar function S($\hat{\mathbf{Z}}$) as the sum of the squared residuals, we can solve $\hat{\mathbf{Z}}$ by trying to minimize S($\hat{\mathbf{Z}}$).

$$S(\widehat{\boldsymbol{Z}}) = \left\| \boldsymbol{B'} - [A] \cdot \widehat{\boldsymbol{Z}} \right\|^2$$

$$\Rightarrow \min_{\widehat{\boldsymbol{Z}}} \quad S(\widehat{\boldsymbol{Z}})$$

We do this by differentiating S($\hat{\mathbf{Z}}$) with respect to $\hat{\mathbf{Z}}$ and equating to zero.

$$\frac{\partial S(\widehat{\boldsymbol{Z}})}{\partial \widehat{\boldsymbol{Z}}} = \mathbf{0}$$

$$\Rightarrow -[A]^T \boldsymbol{B}' + ([A]^T[A])\widehat{\boldsymbol{Z}} = \mathbf{0}$$

The solution to this system is then

$$\widehat{\boldsymbol{Z}} = ([A]^T[A])^{-1}[A]^T \boldsymbol{B}'$$

An alternative to Gridfit is *RegularizeData3D* [43], which is a modified version of *Gridfit* and achieves similar results. To build maps in the future, it is advised to test both codes and chose the one that fits the data better. This is what has been done in this report.

4.1.4 Compressor performance map

Two 3D maps are required to map the compressor because PR and efficiency depend on two variables as discussed in Section 2.3.4:

- Map 1: $\frac{P_{s,2}}{P_{0,1}} = f\left(\frac{\dot{m}\sqrt{T_{0,1}/T_{ref}}}{P_{0,1}/P_{ref}}, \frac{N}{\sqrt{T_{0,1}/T_{ref}}}\right)$
- Map 2: $\eta_{ise} = f\left(\frac{\dot{m}\sqrt{T_{0,1}/T_{ref}}}{P_{0,1}/P_{ref}}, \frac{P_{s,2}}{P_{0,1}}\right)$

The reference conditions have been arbitrarily chosen so as to be $P_{ref} = 100\ kPa$, and $T_{ref} = 25℃$. Temperature and pressure were taken directly from our data source, except $P_{s,2}$ that has been calculated by solving Equation 8 for each data point. The cross sectional area used corresponds to a diameter of 9.9 cm as stated in our data sheets.

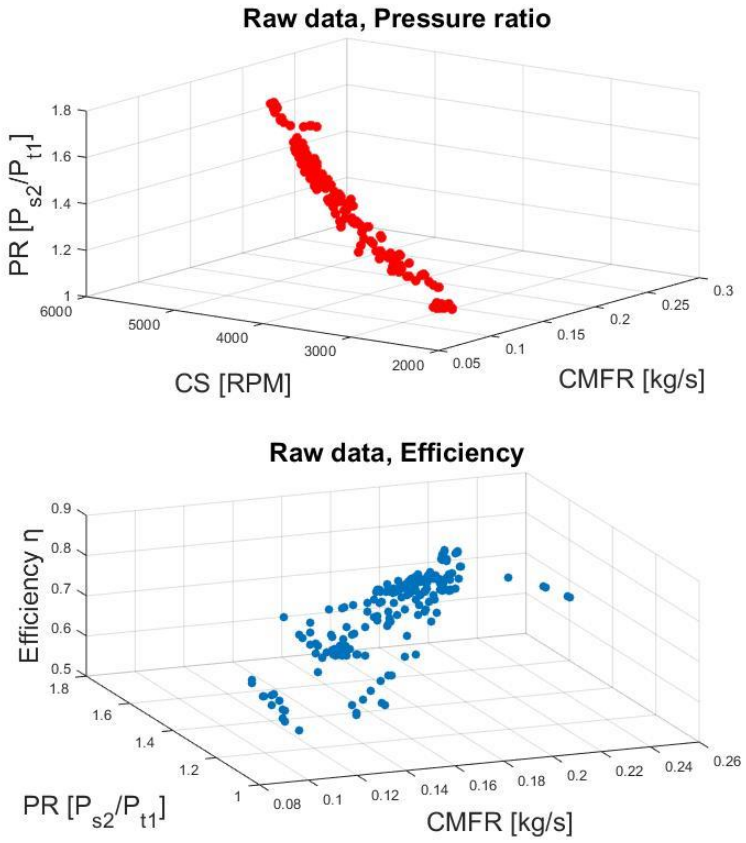

Figure 37 Pressure ratio and efficiency data points

Figure 38 shows the resulting surfaces compatible with FM. Indeed, one simply needs to export the Gridfit data output to FM's performance surface building tool. When running an ECS simulation, the compressor should be operated close to the operating line. Regions far from this line (bright yellow and dark blue area) are subject to major uncertainty as no data was was available to corroborate the surface approximation.

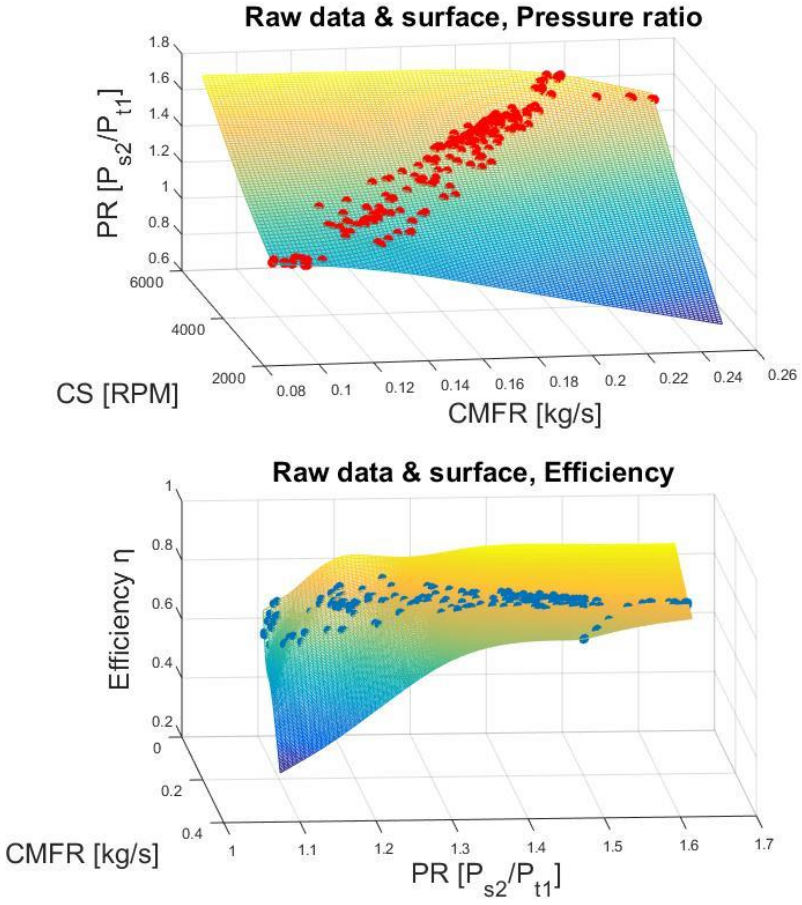

Figure 38 Compressor performance surfaces

4.1.5 Turbine performance maps

Turbine performance maps are generated from data in a similar way the compressor maps were obtained. Because the compressor and turbine are coupled together by the main shaft, their rotational speed are matched. Consequently, the corrected rotational speed is considered regardless of the weak dependence on pressure ratio as stated in Section 2.3.5.

- Map 1: $\frac{P_{t,1}}{P_{t,2}} = f\left(\frac{\dot{m}\sqrt{T_{t.1}/T_{ref}}}{P_{t,1}/P_{ref}}, \frac{N}{\sqrt{T_{t.1}/T_{ref}}}\right)$

- Map 2: $\eta_{ise} = f\left(\frac{\dot{m}\sqrt{T_{t.1}/T_{ref}}}{P_{t,1}/P_{ref}}, \frac{N}{\sqrt{T_{t.1}/T_{ref}}}\right)$

Some data points were excluded as they were situated past the choking mass flow limit. The excluded points are illustrated in red in Figure 39. These points correspond to the cases stated in the table below, all HD and XHD cases. The resulting maps are shown on Figure 40.

Table 37 Turbine data excluded

CS300 - Engine Cooling performance (Single Pack)	CS300 150 PAX with IFE	Ground HAAO	GI15HD1P
			GI15XHD1P
	CS300 160 PAX without IFE		GI15HD1P
			GI15XHD1P
CS100 (125pax) - Engine Cooling performance (Single Pack)		Ground HAAO	GI15XHD1P

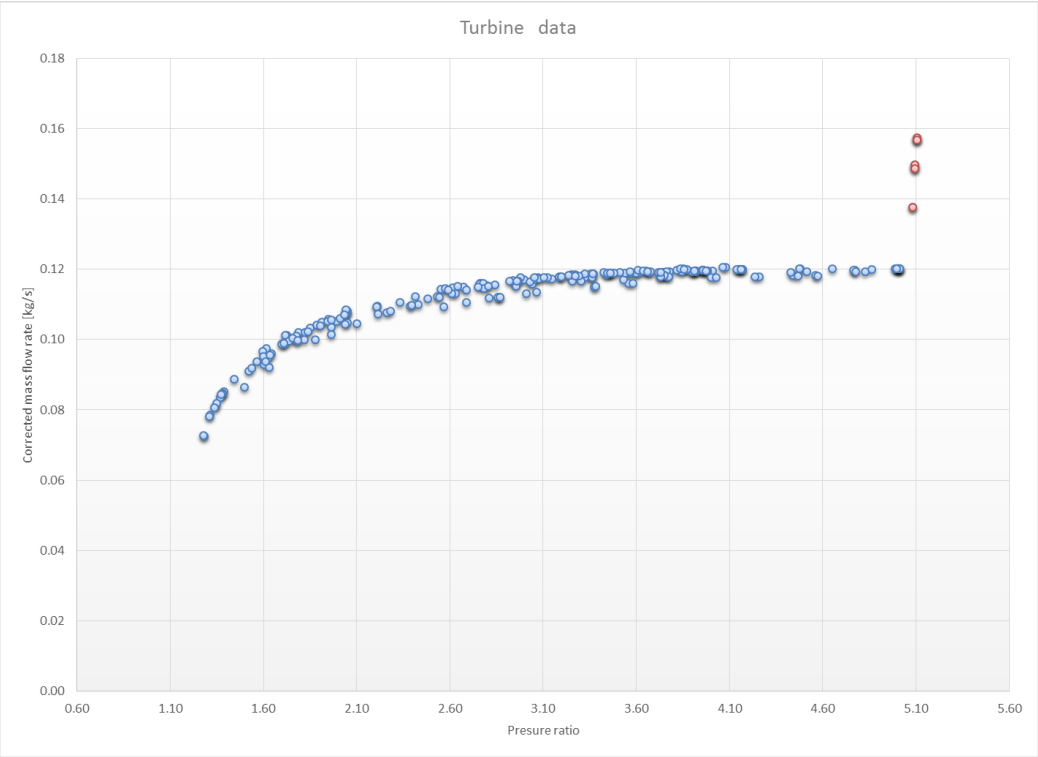

Figure 39 Turbine cmfr vs. pr plot

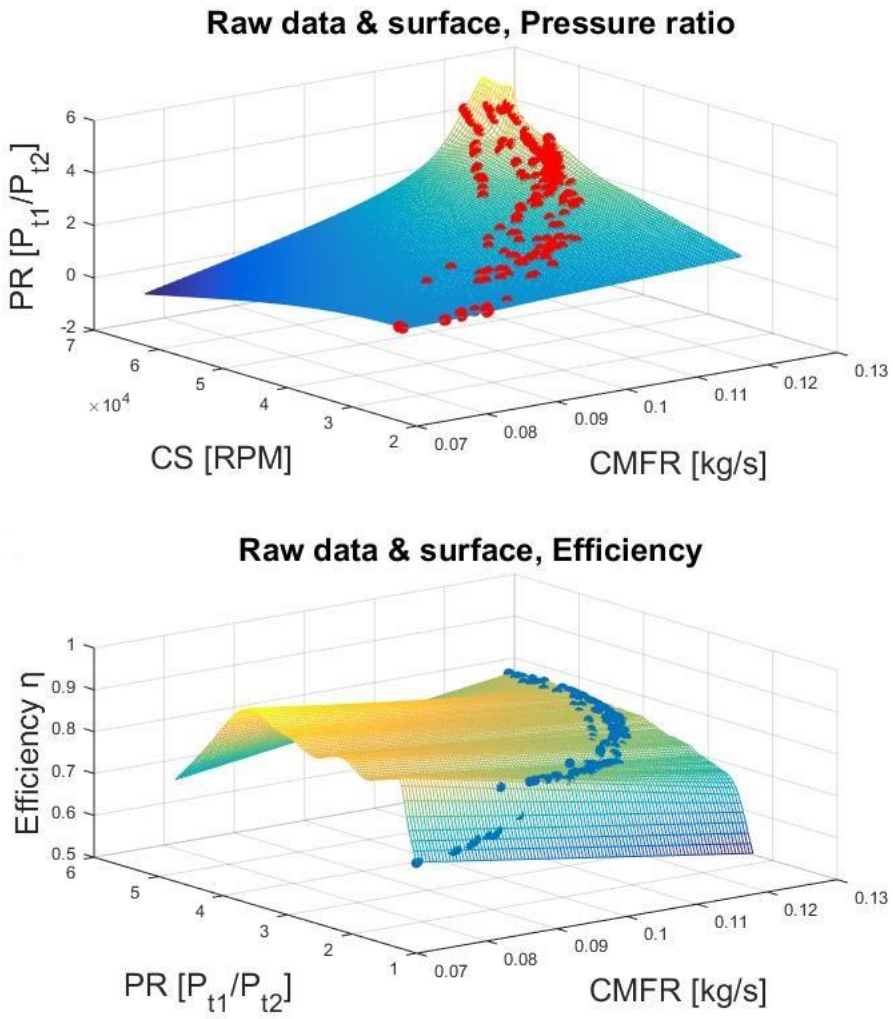

Figure 40 Turbine performance surfaces

4.1.6 Heat exchanger performance maps

To model heat-exchangers, three maps are needed. The first is the thermal performance map, while the two others are pressure drop maps, one for each stream.

Thermal performance map

The performance of the thermal heat-exchanger component can be mapped in several ways. Two of them are particularly interesting for us because data at our disposition contains all the necessary information to construct them and both methods are available in FM:

- $Effectiveness = f(hot\ stream\ mass\ flow\ rate, cold\ stream\ mass\ flow\ rate)$
- $\frac{Q}{(ITD \cdot A)} = f(hot\ stream\ mass\ flow\ rate, cold\ stream\ mass\ flow\ rate)$

The first method consists on mapping the effectiveness as a function of the mass flow rate of the hot and cold streams. The second one uses the performance capability. These relations are explained more thoroughly in Section 2.3.2.

To map the PHX, the performance capability is chosen so as to minimise the deviation (offset) between data and FM's results. In fact, if the effectiveness is chosen, the heat exchanged is computed as $Q = \varepsilon \cdot \left(\dot{m}C_p\right)_{min} \cdot ITD$. However, the exact relation used by FM model to compute C_p is unknown and might be slightly different from LTS'. Thus, results from both platforms might also differ to some extent.

To compute $\frac{Q}{(ITD \cdot A)}$, for every flight case, the heat load is divided by the exchange area A and the inlet temperature difference (ITD). The same area must also be specified in the heat-exchanger component so FM can compute Q. However, the internal geometry for all the HXs are unknown. Yet, one can simply assume any exchange area value when computing $\frac{Q}{(ITD \cdot A)}$ as long as the same area is specified in FM. Ultimately, both values will cancel.

Pressure drop maps

To map the pressure drop, we looked at the pressure drop equation for an incompressible fluid in a cylindrical pipe: $\Delta P = \frac{f_D L}{D} \frac{\dot{m}^2}{2\rho A}$. The Darcy friction factor, *f*, multiplied by L/D is the pressure loss coefficient that characterises the pipe and is constant for a single pipe when the flow is turbulent. The cross section area A (uniform pipe) and the density are constant (incompressible). Therefore, the pressure drop increases as the mass flor rate increases. As a result, pressure drop could be mapped plotting ΔP vs. the mass flow rate.

The pressure drop in ECS heat-exchangers can be mapped similarly except that density must also be considered in order to take into account compressibility effects. Consequently, the pressure drop can be written a function of the mass flow rate and the inlet density.

$$\Delta P = f(\dot{m}, \rho)$$

Surfaces were built based on data and it were imported to the ECS model.

4.1.7 Primary heat-exchanger maps

The PHX maps were built as explained and only the results are showed here. Nevertheless, it should be noted that some data points were omitted when building the performance capability map. These points had effectiveness above 100% and thus violated the second law. Also, the surface was built using RegularizeData3d and is illustrated in Figure 41.

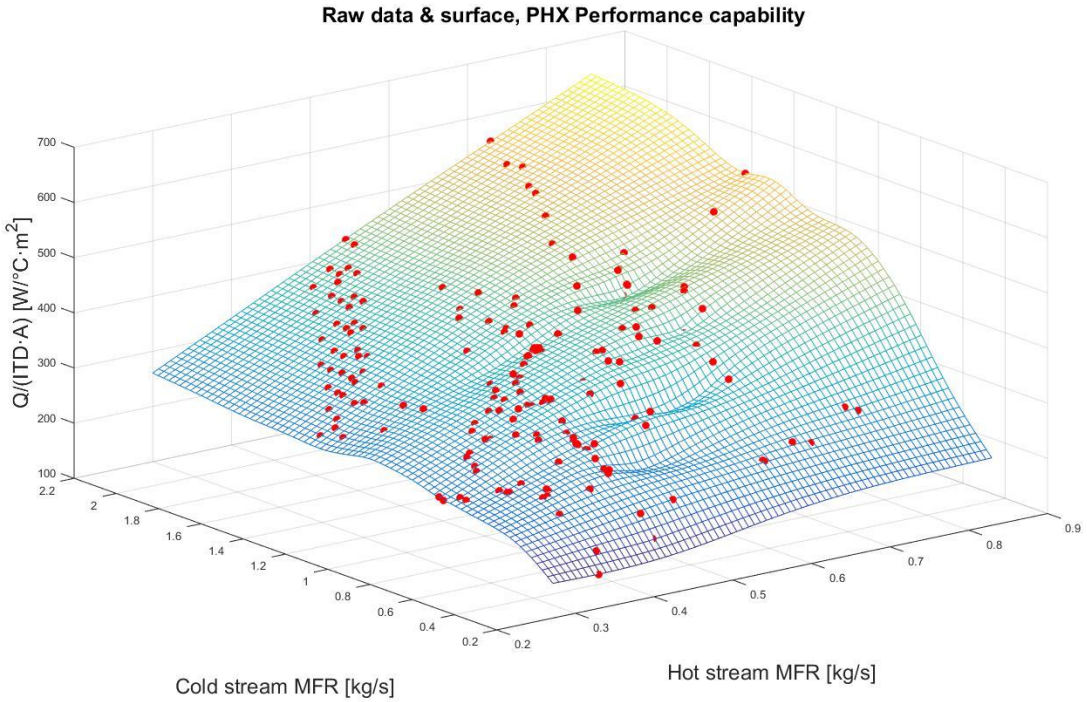

Figure 41 PHX performance map

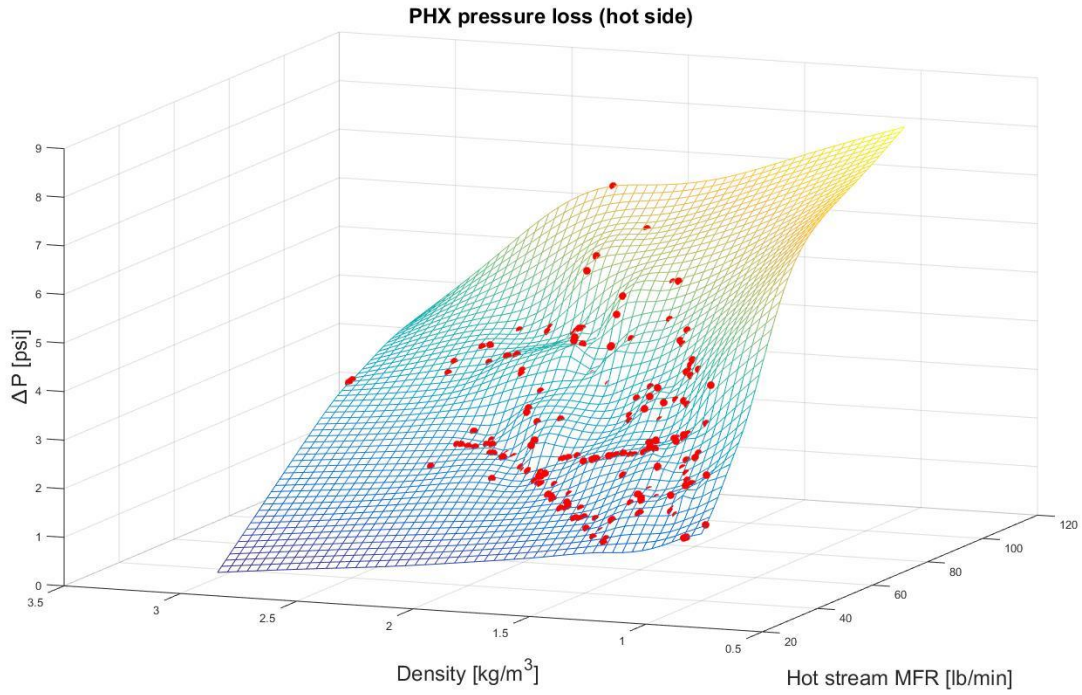

Figure 42 PHX pressure loss map (hot stream)

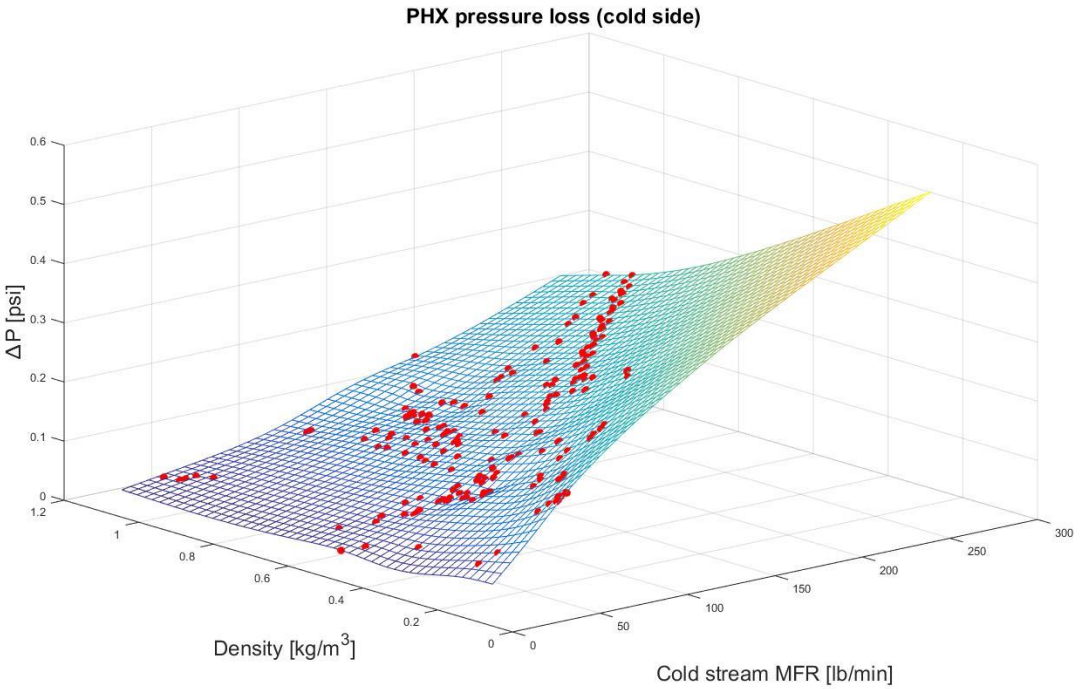

Figure 43 PHX pressure drop map (cold stream)

4.1.8 Secondary heat-exchanger maps

The bumps on the surface showed in Figure 44 are due to the presence of liquid water either at the SHX ram inlet or SHX bleed outlet. The ram air sprayer (not modeled) injects water droplets to ram air before the SHX to improve cooling and can result in liquid water if air is already saturated. On the other hand, bleed humid air might condense after cooling resulting in liquid water at the outlet. In consequence, the performance capability is larger when liquid water is present compared to unsaturated cases.

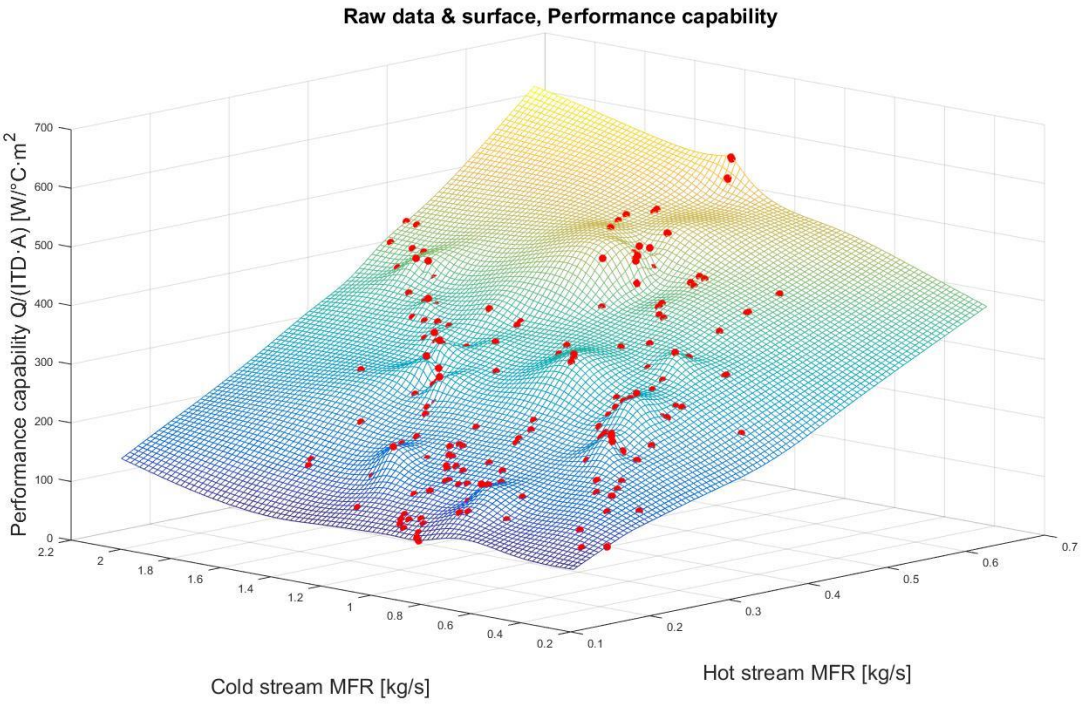

Figure 44 SHX performance map

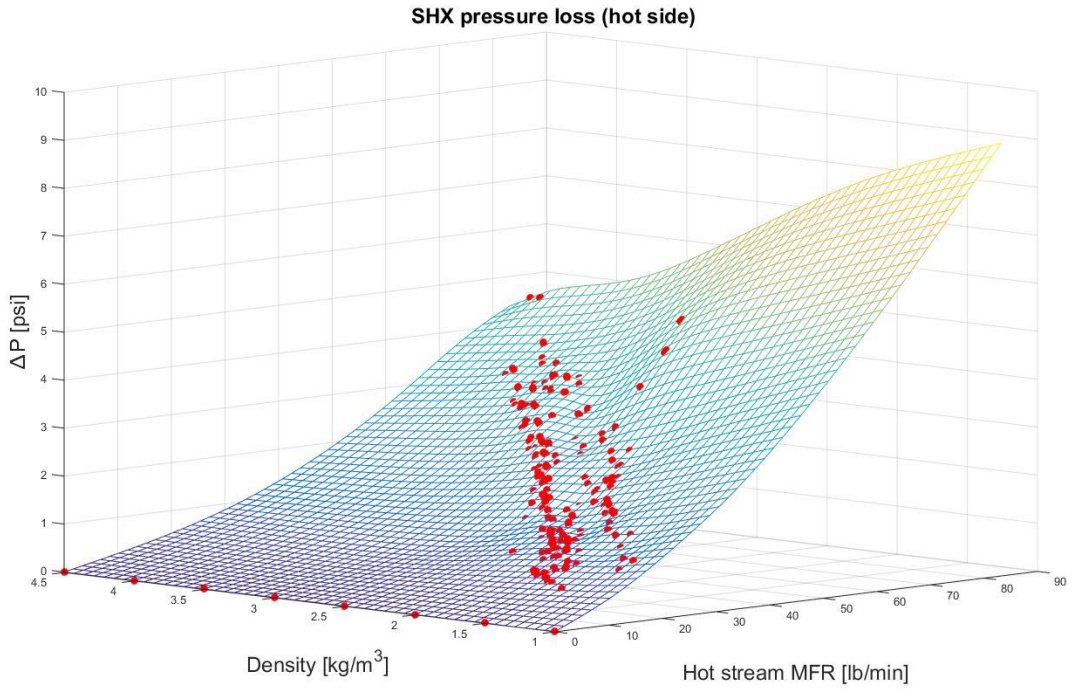

Figure 45 SHX pressure loss map (hot stream)

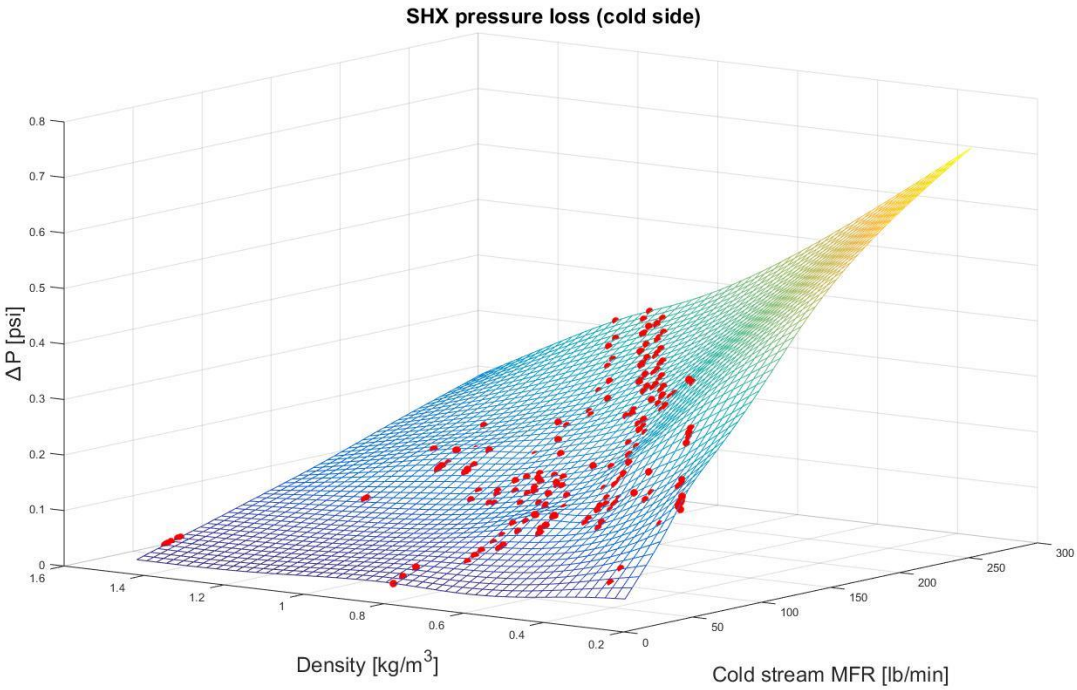

Figure 46 SHX pressure loss map (cold stream)

4.1.9 Reheater performance maps

The reheater is a heat-exchanger where liquid water is often present at the two inlets because of very low air temperatures. Figure 47 below illustrates the REH performance capability vs. the hot stream mass flow rate (hot stream MFR≈cold MFR). As can be seen, the points do not necessarily lie on a straight line, once again, because of condensation. Appropriate mapping of heat-exchangers containing liquid water would require a more complete and accurate approach. This could be as simple as considering adding a third variable on the performance map giving information on water content. Unfortunately, such pathway was not attempted because it would require requesting a new FM feature as this is not currently available on any type of HX.

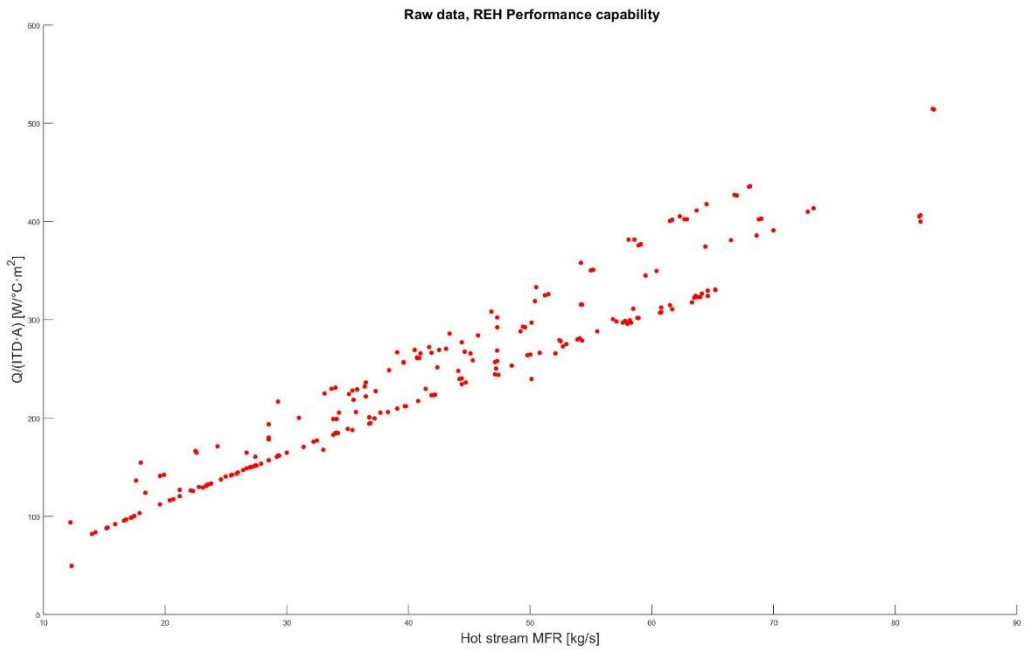

Figure 47 REH performance capability chart

Instead, a typical performance capability surface was built even though this method is more convenient for unsaturated air. The result is a tridimensional surface in Figure 48.

Since overlapping data points are present, the performance capability is roughly approximated to be an average value for a give set of hot and cold mass flow rates. What is more, it is not an obvious

task to build a 3D surface, z=f(x,y), for the particular case where the x and y values are equal and z overlaps. Therefore, the surface is forced to reach zero heat transferred whenever one of the fluid stream has no mass flow. This is done to improve the surface shape.

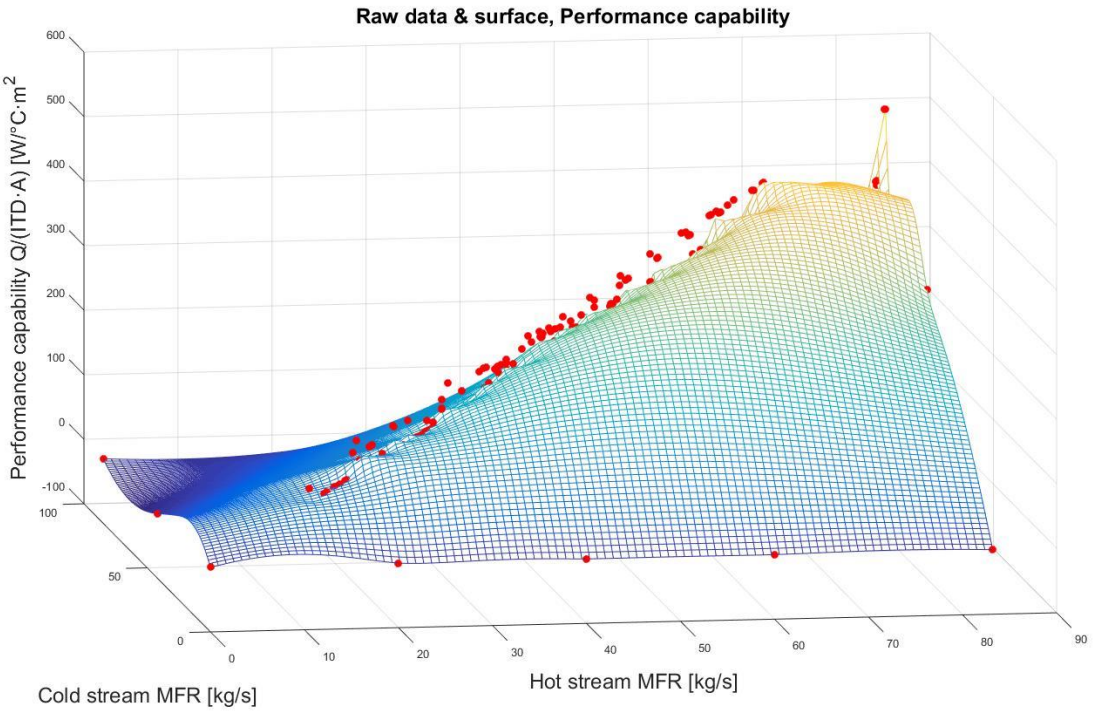

Figure 48 REH performance map

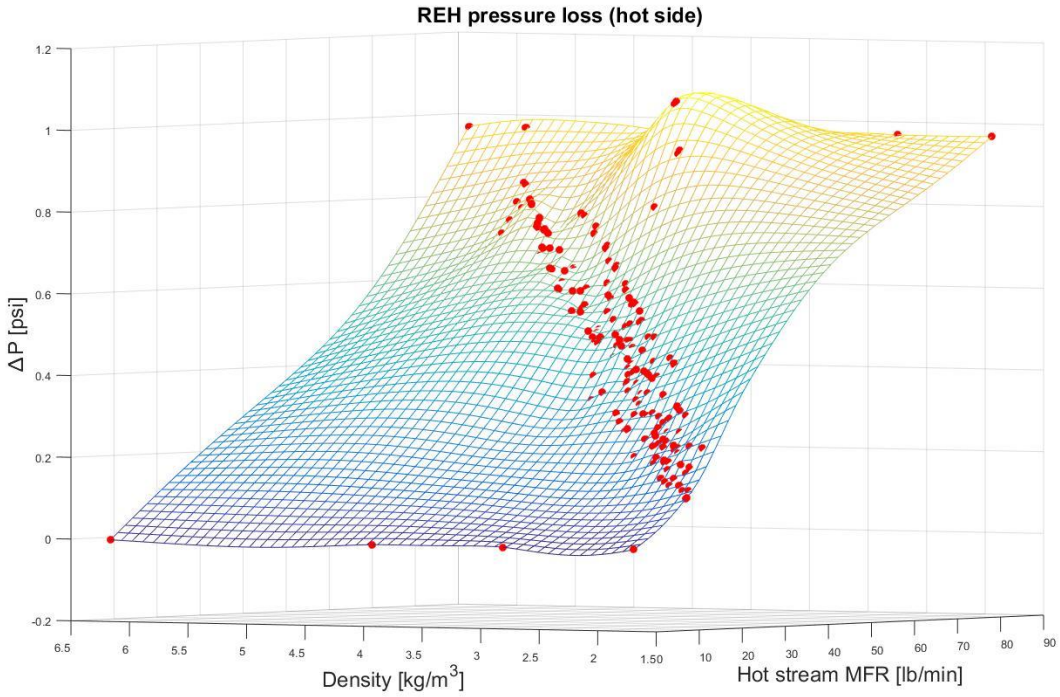

Figure 49 REH pressure loss map (hot stream)

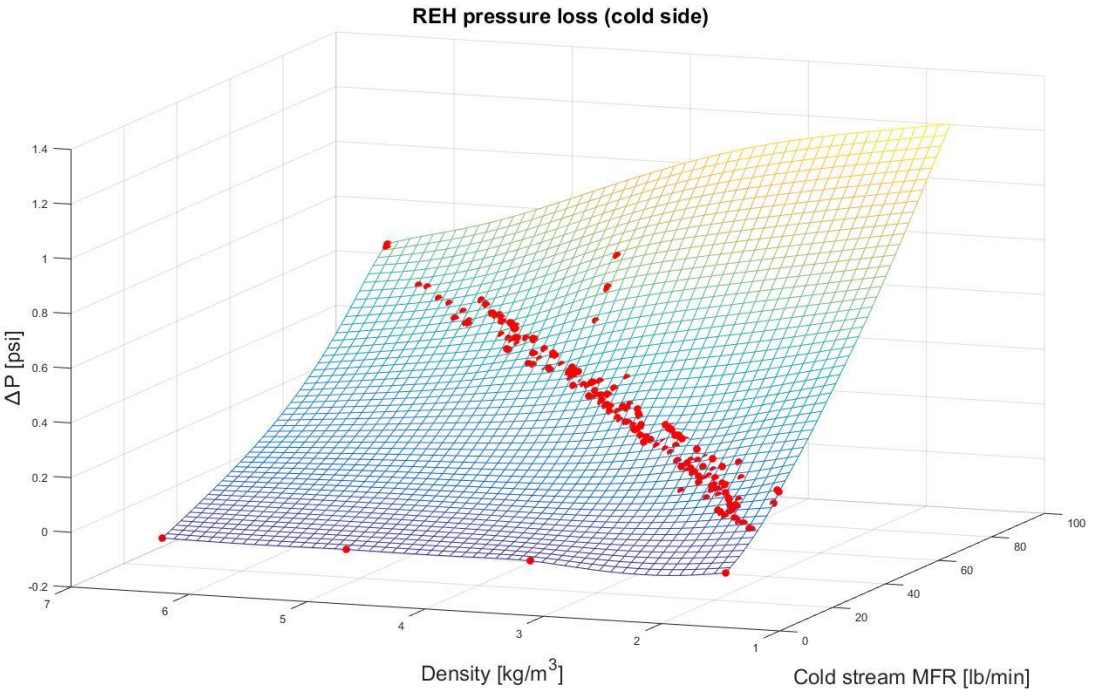

Figure 50 REH pressure loss map (cold stream)

4.1.10 Condenser performance maps

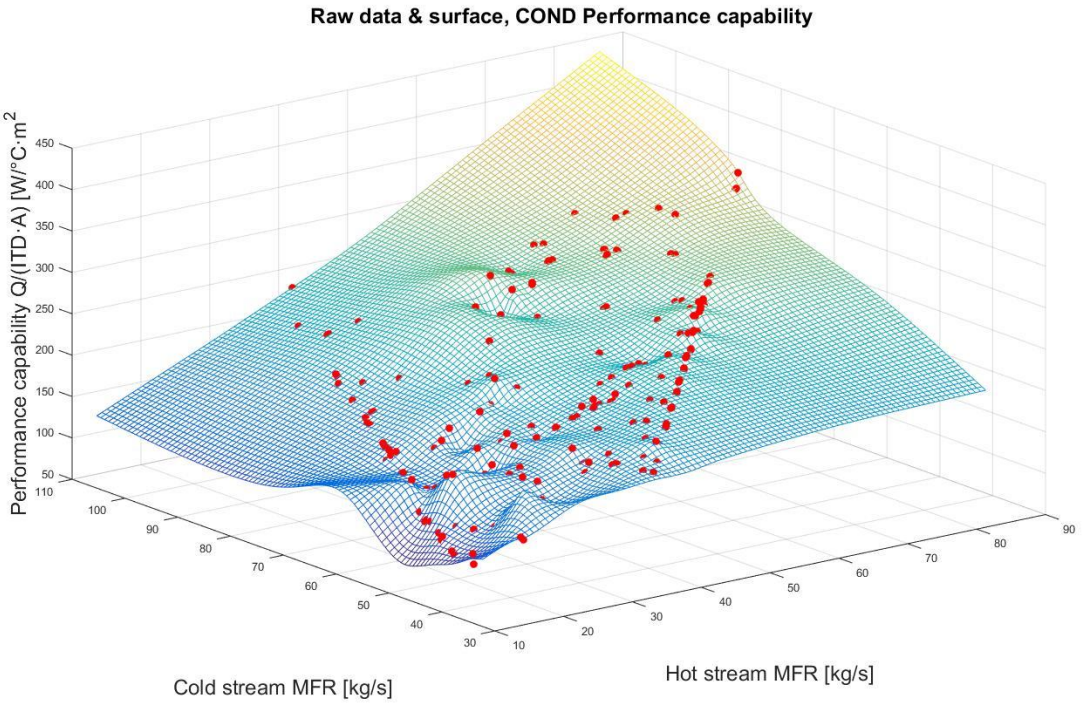

Figure 51 COND performance map

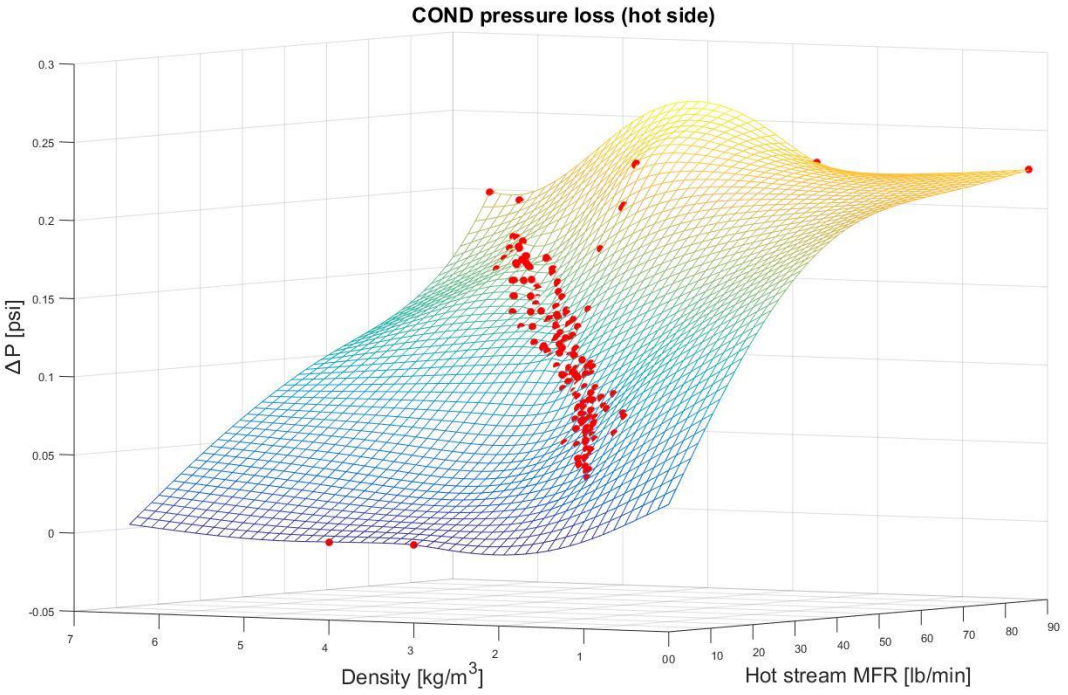

Figure 52 COND pressure loss map (hot stream)

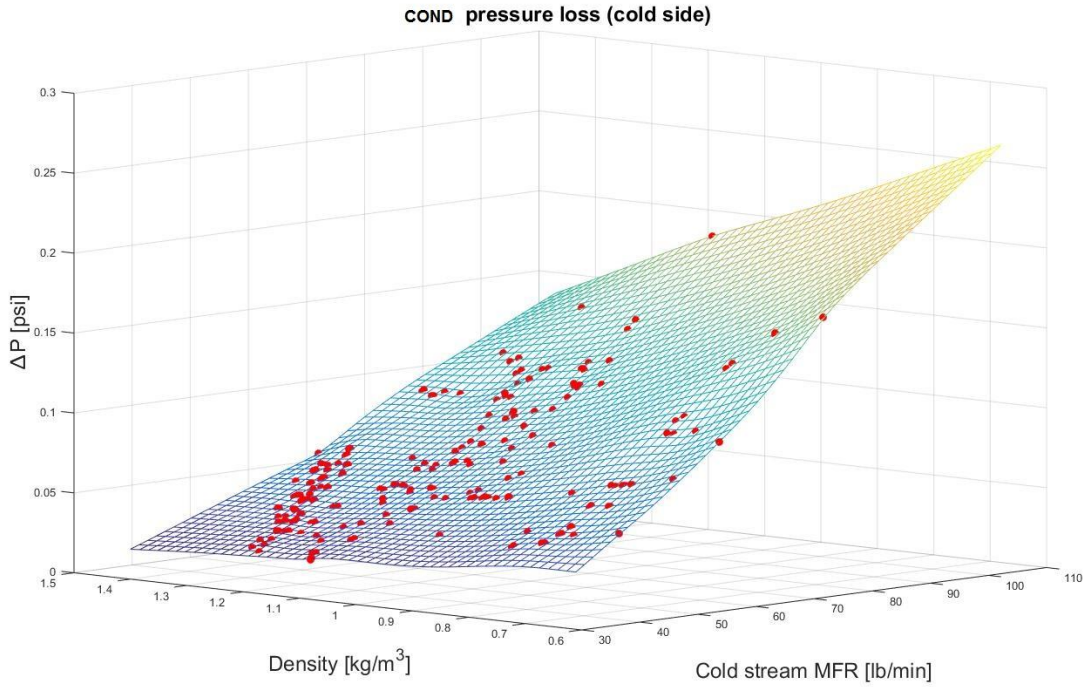

Figure 53 COND pressure loss map (cold stream)

4.2 Simulation results

An assessment on the physics and modelling of each component of the ECS model was accomplished in section 2. The main conclusion was the derivation of the performance maps that could be used to successfully model the different components. In Section 4.1, the performance maps were constructed based on data from LTS. Those performance maps provided very reliable information in the vicinity of the data points and a good estimation far from them. However, since the data is taken from exhaustive flight cases (APU, engine, one pack, two packs, etc.) at different altitudes, speed, ambient conditions, etc., and based on conservative assumptions, it is very unlikely that a simulation solution with the ECS model will be found far from data points. That said, the FM model must be tested and its results on flow, pressure and temperature be compared against LTS data.

4.2.1 Flight cases tested and output parameters

Even though CS100 data was used to map the model components, only results from CS300 HD and CS300 SHD aircraft versions are presented here to avoid redundancy. In fact, the general conclusions presented in the discussion (Section 5) also applies to the CS100. The simulation cases for comparison were chosen as follows: two flight cases among each simulation flight set. The total number of flight cases cover ground, cruise, APU modes; zero altitude, 10 000 feet, 15 000 feet, 16 000 feet, 17 000, 22 000 feet, 38 000 feet, 41 000 feet; and all OAT sets. Table 38 summarizes all the cases tested.

Table 38 Flight cases tested

Flight set	Flight case
HD_COOLING_2PACKS	HO22ISA2P2BAI
	CR38HD2P
HD_HEATING_1PACK	APU0CD1P
	GI10CD1P
HD_HEATING_2PACK	GI15CD2P

	CR41CD2P
SHD_APU_COOLING_2PACK	APU0HD2P
	APU15ISA2P
SHD_COOLING_1PACK	GI0XHD1B1P
	H022ISA1P2BAI
SHD_FLIGHT_APU_ENVELOPE_2PACK	APU16XHD2P
	APU17XCD2P

The model output parameters chosen for comparison are presented in Table 39. These parameters not only include the cabin temperature but also ACM key parameters to be able to compare how well the ACM performance maps can match our data. Total heat loads are also compared because they are computed internally by the model, the exception being the fixed heat loads. The MIXTS measures the temperature at the mix manifold outlet, giving a good indication on how much the air flow from the packs has been heated by being mixed with the recirculation flow. DTS temperature are also reported since by comparing them to the MIXTS, one can assess how much heat was lost (or gained) through the LPDS ducts. Outlet mix manifold pressure is also indicated. However, one can expect the results to show a slight overpressure at this location because mix manifold pressure drop has been ignored. In fact, minimal pressure drop through the whole distribution has been assumed (0.01 psi).

Table 39 Output parameters compared

Output Parameter
ACM Rotational Speed <rpm>
Aft Cabin Flow <lb/min>
Aft Cabin TAV flow <lb/min>
Cockpit Flow <lb/min>
Cockpit TAV flow <lb/min>
DTS Aft Cabin <°C>
DTS Cockpit <°C>
DTS Fwd Cabin <°C>
Fwd Cabin Flow <lb/min>

Fwd Cabin TAV flow <lb/min>
MIXM Pressure <psia>
MIXTS <°C>
PDTS <°C>
TCV flow <lb/min>
Total Aft Cabin Heat loads <kW>
Total Cockpit Heat loads <kW>
Total Fwd Cabin Heat loads <kW>
Turbine Power <W>
VTS Aft Cabin <°C>
VTS Cockpit <°C>
VTS Fwd Cabin <°C>

4.2.2 Input values

The input values are given in Table 40 on the next page. Mach number values of zero were entered as 0.0001. In fact, bugs within FM have been reported when using zero inputs. This bug was found when running the model but can be easily avoided by entering values approaching zero.

Valve pressure loss coefficients were found by tuning (trial and error), by hand calculation using Equation 38 or by PID controllers (more details on this in Section 5). These values are required to compute the pressure loss through the valves.

Ram air flow through the ram air fan and bypass were not meant to be considered as inputs. Ideally, the model should predict the flow based on the ram inlet and outlet pressures and fan driving force. However, LTS ram air data was found dubious, hence it was not possible to match it. A thoroughly discussion on this limitation is presented in Section 5.

Table 40 Simulation input values

Input Parameter	HO22ISA2P2BAI	CR38HD2P	GI15CD2P	CR41CD2P	APU0HD2P	APU15ISA2P	APU17XCD2P	APU16XHD2P	APU0CD1P	GI10CD1P	GI0XHD1B1P	H022ISA1P2BAI
[Altitude] <ft>	22000	37500	14500	41000	0	14500	17000	15500	0	0	0	22000
[Mach] <>	0.458	0.78	0.0001	0.78	0.0001	0.0001	0.57	0.54	0.0001	0.0001	0.0001	0.458
[Bleed pressure] <psia>	48.015	44.852	48.043	44.372	45.165	24.865	20.677	29.094	36.533	56.735	56.657	48.375
[Bleed temperature] <°C>	232.3	200	161.9	200	220	168.2	138.8	221.5	129.5	141.7	170	232
[OAT] <>	3	4	2	2	4	3	1	5	2	2	5	3
[Ram air recovery factor] <>	0.6172	0.65	0.7	0.62	0.66	0.63	0.637	0.6	0.63	0.63	0.65	0.618
[Fwd cabin fixed heat load] <W>	4859	5188	880	829	1486	1294	1358	1116	880	880	1486	902
[Aft cabin fixed heat load] <W>	4385	4870	730	295	1622	1323	1117	812	730	730	1622	406
[Npax_fwd] <>	74	74	7	7	84	84	8	84	7	7	84	84
[Ncrew_fwd] <>	2	2	1	1	2	2	1	2	1	1	2	2
[Npilots] <>	3	3	2	2	3	3	2	3	2	2	3	3
[Npax_aft] <>	84	84	8	8	84	84	8	84	8	8	84	84
[Ncrew_aft] <>	3	3	1	1	3	3	1	3	1	1	3	3
[Effective cockpit area] <in2>	1798	1798	0	0	1798	1798	0	1798	0	0	1798	1798
[Effective fwd area] <in2>	1829	1829	0	0	1829	1829	0	1829	0	0	1829	1829
[Effective aft area] <in2>	2092.5	2092.5	0	0	2092.5	2092.5	0	2092.5	0	0	2092.5	2092.5
[Cockpit fixed heat load] <W>	571	571	492	492	571	571	492	571	492	492	571	571
[PackLeakage] <%>	1.85817	2.1	1.55	1.35	5.8185	9.65548	8.24254	39.6491	0	1.21587	1.85	2.10748
[Recirculation percentage] <%>	45.83	40.93	20.9	37.42	49.23	28.9187	55.8755	80.2306	65.6495	66.6388	67.43	66.2184
[Ground/Flight] <>	1	1	0	1	0	0	1	1	0	0	0	1
[TAPRV] <>	12.9	14	3.07	2.47	7.5	1.47	0.0895	1000	0.42	2.86	9000	42
[TAV cockpit] <>	0.47	0.73	0.39	0.224	1.00E+07	2.8	0.00192	1.00E+07	1	0.79	100000	15
[TAV fwd] <>	1.00E+07	1.00E+07	1.00E+08	1.00E+08	5.7	1.00E+07	0.001919	1.00E+07	1.00E+07	1.00E+07	100000	1.00E+07
[TAV aft] <>	1.00E+07	1.00E+07	1.15	0.38	13	1.00E+07	0.002128	1.00E+07	3	2.3	100000	1.00E+07
[TCV] <%>	20.9	14.95	32.78	36.52	0.324	25.65	45.22	0.01	51.34	45.85	0.006	18.77
[RARV] <>	4.42E-07	4.42E-07	0.000442	0.0003156	4.42E-07	0.0003	0.0004	4.42E-07	0.0004	0.0004	4.42E-07	4.42E-07
[Ram flow rate] <lb/min>	-115.88	-85.46	-34.63	-42.99	-145.66	-60.83	-125.15	-180.02	-57.21	-59.29	-161.74	-122.44
[Ram bypass flow] <lb/min>	63.55	47	-24.38	23.64	10.2	4.11	68.75	98.82	-39.92	-41.5	11.29	67.18
[Packs] <>	2	2	2	2	2	2	2	2	1	1	1	1
[FCV] <>	0.00206	0.00191	0.0034735	0.0024915	2.14E-05	2.48E-05	2.43E-05	2.36E-05	2.47E-05	0.001067	2.35E-05	0.0002173
[Fan power] <W>	2027	-167	2953	818	8410	3598	-1	3179	2780	3204	12468	4476
[Distribution split] <>	0.99803	0.9979	0.99713	0.99767	1	0.9978	0.99711	1	0.99745	0.99769	0.99985	0.9988

4.2.3 Steady-state results

ECS model results are reported in two different tables. Table 41 indicates the output parameters from the model while Table 46 shows the absolute deviation from the expected LTS values (Table 42).

Table 41 Steady-state simulation results

Output Parameter	HO22ISA2P2BAI	CR38HD2P	GI15CD2P	CR41CD2P	APU0HD2P	APU15ISA2P	APU17XCD2P	APU16XHD2P	APU0CD1P	GI10CD1P	GI0XHD1B1P	H022ISA1P2BAI
ACM Rotational Speed <rpm>	45134	56183	43809	39529	56078	42415	23173	47383	34639	38704	61163	57158
Aft Cabin Flow <lb/min>	75.77	69.53	60.707	68.16	82.73	58.64	78.82	59.32	71.67	71.19	64.76	63.36
Aft Cabin TAV flow <lb/min>	0.00	0.00	1.02	1.18	0.48	0.00	4.74	0.00	1.29	1.18	0.010	0.000
Cockpit Flow <lb/min>	20.79	18.93	15.92	18.8728	23.2112	16.2038	21.1147	16.6756	19.7916	19.7303	18.2419	17.6313
Cockpit TAV flow <lb/min>	1.19	1.09	1.79	1.55	0.00	1.04759	5.14188	0.00076909	2.29858	2.06002	0.0103592	0.53323
DTS Aft Cabin <°C>	4.36	1.43	30.51	32.19	-12.17	7.71028	-8.04104	2.94547	29.3819	29.8506	6.67818	8.9043
DTS Cockpit <°C>	16.52	12.02	41.01	42.00	-13.52	16.9842	18.0434	2.92028	38.0081	38.5453	6.701	15.0676
DTS Fwd Cabin <°C>	4.58	1.50	29.92	30.97	-12.15	8.17855	-5.99424	2.22928	28.9628	29.4074	5.7807	9.26592
Fwd Cabin Flow <lb/min>	73.14	67.19	57.68	65.93	79.94	56.67	75.94	57.2149	69.2107	68.8231	62.5796	61.1583
Fwd Cabin TAV flow <lb/min>	0.00	0.00	0.00	0.00	0.75	0.00	5.37	0.00	0.00	0.00	0.01	0.00
MIXM Pressure <psia>	13.80	12.29	9.58	11.99	14.2071	9.37165	13.9779	14.0405	16.138	15.5099	15.3903	13.3415
MIXTS <°C>	5.45	1.75	35.59	36.36	-17.4119	9.98505	-14.8823	-0.560594	33.5589	34.0611	2.28571	10.669
PDTS <°C>	-3.94	-7.71	37.30	39.51	-30.2925	5.01535	-22.8774	-18.1788	37.758	38.3592	-17.3347	0.377293
TCV flow <lb/min>	22.52	15.33	27.07	29.90	0.506113	22.2281	33.0529	0.0111911	60.3444	55.7319	0.0117263	27.2841
Total Aft Cabin Heat loads <W>	10906	11060	-2487	-343	11557	7466.35	1112.42	7255.96	-2487.88	-2487.88	9074.65	6926.96
Total Cockpit Heat loads <W>	1095	1346	-2023	-2389	3470.41	886.73	-1232.65	2398.85	-2023.31	-2023.31	3263.56	1095.42
Total Fwd Cabin Heat loads <W>	10404	10503	-2106	-2634	10953.9	7105.29	1281.22	7215.34	-2106.83	-2106.83	8780.7	6874.84
Turbine Power <W>	12835	18451	10943	6889	37271.1	11343.7	1654.41	15872.8	8995.73	11832.7	57378.4	32618.7
VTS Aft Cabin <°C>	23.22	22.28	25.13	25.58	6.13	24.38	-6.18	18.97	24.83	25.27	25.03	23.23
VTS Cockpit <°C>	23.42	21.33	24.3	25.41	6.06	24.14	10.39	21.77	24.61	25.11	30.14	23.20
VTS Fwd Cabin <°C>	23.22	21.99	25.13	25.73	5.790	24.59	-3.78	18.75	24.97	25.39	24.16	23.99

Table 42 Expected Simulation results (reference)

Output Parameter	HO22ISA2P2BAI	CR38HD2P	GI15CD2P	CR41CD2P	APU0HD2P	APU15ISA2P	APU17XCD2P	APU16XHD2P	APU0CD1P	GI10CD1P	GI0XHD1B1P	H022ISA1P2BAI
ACM Rotational Speed <rpm>	44962	55961	44528	39660	56226	43457	23102	48400	36552	39083	63076	55961
Aft Cabin Flow <lb/min>	75.7	69.4	59.9	68.2	82.8	58.7	78.9	59.3	71.9	71.2	64.8	63.4
Aft Cabin TAV flow <lb/min>	0	0	1.0	1.2	0.5	0	4.8	0.0	1.3	1.2	0.0	0
Cockpit Flow <lb/min>	20.8	19.2	16.5	18.8	23.3	16.2	21.1	16.7	19.9	19.7	18.2	17.6
Cockpit TAV flow <lb/min>	1.2	1.1	1.8	1.6	0.0	1.0	5.2	0.0	2.3	2.1	0.0	0.5
DTS Aft Cabin <°C>	5.0	4.4	29.4	30.5	7.8	7.5	-8.1	13.6	28.4	28.5	12.6	9.5
DTS Cockpit <°C>	17.0	14.7	40.0	40.6	7.2	16.7	18.1	13.7	37.2	37.4	12.7	15.8
DTS Fwd Cabin <°C>	5.2	4.6	28.7	30.5	8.0	7.9	-6.1	13.2	27.9	27.9	12	9.9
Fwd Cabin Flow <lb/min>	73.1	67.0	57.9	66.0	79.9	56.6	75.9	57.3	69.6	68.9	62.6	61.2
Fwd Cabin TAV flow <lb/min>	0	0	0	0	0.75	0	5.36	0.0	0	0	0	0.0
MIXM Pressure <psia>	13.2	11.6	8.7	11.2	15.0	9.6	13.7	13.7	14.9	14.9	14.9	13.2
MIXTS <°C>	6.1	5	34	34.2	6.2	9.6	-15	11.9	32.3	32.3	9.2	11.3
PDTS <°C>	-3	-4.2	38.3	39.8	-2.9	5.8	-22.7	-2.4	38.7	38.9	-5.5	1.8
TCV flow <lb/min>	22.5	15.32	27.08	29.93	0.51	22.21	33.06	0.01	60.35	55.77	0	27.26
Total Aft Cabin Heat loads <W>	10901	11037	-2488	-3440	11552	7442	1113	7248	-2488	-2488	9063	6922
Total Cockpit Heat loads <W>	1092	1344	-2023	-2390	3467	883	-1231	2397	-2023	-2023	3259	1092
Total Fwd Cabin Heat loads <W>	10401	10512	-2107	-2635	10950	7106	1279	7199	-2110	-2107	8778	6858
Turbine Power <W>	13130	19127	11494	7227	38345	11930	1692	16808	10180	12384	62650	32643
VTS Aft Cabin <°C>	23.9	25.3	23.9	23.9	23.9	24.1	-6.2	29.7	23.9	23.9	31	23.9
VTS Cockpit <°C>	23.9	23.9	23.9	23.9	23.9	23.9	10.5	32.6	23.9	23.9	36.2	23.9
VTS Fwd Cabin <°C>	23.9	25.2	23.9	23.9	23.9	24.4	-3.9	29.7	23.9	23.9	30.4	24.6

Table 43 Absolute deviations from expected values

Output Parameter	HO22ISA2P2BAI	CR38HD2P	GI15CD2P	CR41CD2P	APU0HD2P	APU15ISA2P	APU17XCD2P	APU16XHD2P	APU0CD1P	GI10CD1P	GI0XHD1B1P	H022ISA1P2BAI
ACM Rotational Speed <rpm>	172	222	-719	-130	-147	-1042	71.60	-1016	-1912	-378	-1912	1197
Aft Cabin Flow <lb/min>	0.08	0.14	0.81	-0.03	-0.07	-0.05	-0.07	0.02	-0.22	-0.01	-0.04	-0.04
Aft Cabin TAV flow <lb/min>	0.00	0.00	0.02	-0.02	-0.01	0.00	-0.06	0.00	0.00	-0.02	0.01	0.00
Cockpit Flow <lb/min>	-0.01	-0.26	-0.58	0.07	-0.09	0.00	0.01	-0.02	-0.11	0.03	0.04	0.03
Cockpit TAV flow <lb/min>	-0.01	-0.01	-0.01	-0.04	0.00	0.05	-0.06	0.00	0.00	-0.04	0.01	0.03
DTS Aft Cabin <°C>	-0.64	-2.96	1.11	1.70	-19.97	0.21	0.06	-10.65	0.98	1.35	-5.92	-0.60
DTS Cockpit <°C>	-0.48	-2.68	1.01	1.40	-20.72	0.28	-0.06	-10.78	0.81	1.15	-6.00	-0.73
DTS Fwd Cabin <°C>	-0.61	-3.10	1.22	0.47	-20.16	0.28	0.11	-10.97	1.06	1.51	-6.22	-0.63
Fwd Cabin Flow <lb/min>	0.05	0.19	-0.22	-0.07	0.05	0.08	0.05	-0.09	-0.39	-0.08	-0.02	-0.04
Fwd Cabin TAV flow <lb/min>	0.00	0.00	0.00	0.00	0.00	0.00	0.02	0.00	0.00	0.00	0.01	0.00
MIXM Pressure <psia>	0.61	0.69	0.88	0.79	-0.79	-0.23	0.28	0.34	1.24	0.61	0.49	0.14
MIXTS <°C>	-0.65	-3.25	1.59	2.17	-23.61	0.39	0.12	-12.46	1.26	1.76	-6.91	-0.63
PDTS <°C>	-0.94	-3.52	-1.00	-0.29	-27.39	-0.78	-0.18	-15.78	-0.94	-0.54	-11.83	-1.42
TCV flow <lb/min>	0.03	0.01	0.00	-0.03	0.00	0.02	-0.01	0.00	-0.01	-0.04	0.01	0.02
Total Aft Cabin Heat loads <W>	5.00	23.30	0.12	0.40	5.00	24.35	-0.58	7.96	0.12	0.12	11.65	4.96
Total Cockpit Heat loads <W>	3.42	2.39	-0.31	0.33	3.41	3.73	-1.65	1.85	-0.31	-0.31	4.56	3.42
Total Fwd Cabin Heat loads <W>	3.80	-8.90	0.17	0.33	3.90	-0.71	2.22	16.34	3.17	0.17	2.70	16.84
Turbine Power <W>	-295	-675	-550	-337	-1073	-586	-37	-935	-1184	-551	-5271	-24
VTS Aft Cabin <°C>	-0.67	-3.01	1.24	1.68	-17.77	0.28	0.01	-10.72	0.93	1.37	-5.96	-0.67
VTS Cockpit <°C>	-0.47	-2.56	0.46	1.51	-17.83	0.25	-0.11	-10.83	0.72	1.21	-6.06	-0.69
VTS Fwd Cabin <°C>	-0.67	-3.21	1.23	1.83	-18.11	0.20	0.12	-10.94	1.07	1.50	-6.23	-0.60

CHAPTER 5 GENERAL DISCUSSION AND CONCLUSION

5.1 Steady-state results discussion

XCD, CD and ISA cases

By looking at the deviation for ISA cases in Table 46, it can be noticed that the pack discharge temperature (PDTS) matches the data very well with a deviation of less than 1°C while TCV and TAV flows are practically identical. This means that for XCD, XD and ISA cases, the pack model is well calibrated. Therefore, the increased temperature deviation at the cabin vents (VTS) in G15CD2P, CR41CD2P and G10CD1P cases can be attributed to the cabin model as the recirculation flow and recirculation heat loss were simplified.

Moreover, deviations in heat loads are negligible and they are primarily due to the error created by digitizing the solar intensity chart and interpolation of the OAT. Rotational speed is also negligible with a relative error not higher than 5.23 % (APU0CD1P). The turbine power output deviation is acceptable although it reaches -1184 W in flight case APU0CD1P. The pack discharge temperature (PDTS) doesn't seem to be affected nevertheless, only the mix manifold pressure is 1.24 psi above the reference.

Cold days (CD) flight cases results in an overheating of approximately 1.5°C. To reach the ideal temperature of 23.9°C, our model would suggest to reduce TAV. It is important to highlight however, that the discrepancy happens at the distribution and the PDTS measure is in better agreement with the reference. Then, it is possible that the thermal losses in the recirculation and cabin ducts were less conservative than the simplifications assumed for the model, i.e. a loss of 1.5°C in recirculation ducting.

Pressure at mix manifold (outlet) also seems to be in agreement with data. Pressure downstream the mix manifold is not indicated because it has not been modeled due to unavailability of pressure loss data.

HD and XHD cases

Hot days (HD) and extreme hot days (XHD) flight cases fail to reach cabin ideal temperature appallingly. The pack (1P or 2P) is unable to converge to the PDTS temperature reference. The problem concerns the heat-exchangers. First, it's important to highlight what is common in all flight cases where the model failed. These are cases with the greatest specific humidity and where water condensation should occur at some point downstream the SHX. Therefore, it is not a coincidence that failed cases are HD and XHD. In fact, according to the OAH model (Table 17) these are the most humid conditions. Unfortunately, liquid water is not taken into consideration by the heat-exchangers. Flowmaster can model humid air up to a 100% relative humidity. When humid air reaches its dew point and pressure is increased or temperature drops, Flowmaster will correctly assume a 100% RH but ignore condensation, and therefore water latent heat. This explains why the ECS model fails and will fail to predict cabin temperature for cases where condensation in heat-exchangers is supposed to happen. When saturated air loses a given amount of heat, part of it stems from latent heat of the water vapor turning into liquid. Flowmaster incorrectly associates the total thermal loss to air sensible heat. This explains why the model predicts a temperature way below the reference in the simulation results.

The argument can be easily verified in Flowmaster by extracting heat from saturated air flow using the heater-cooler component. For instance, consider 50 lb/min (0.37799 kg/s) flow of saturated air at 20°C and 1 atm. The specific humidity is then 0.0144 kg_{water}/kg_{mix}. Since water latent heat of vaporization is 2454 kJ/kg_{water} at 20°C, it would require 13.36 kW heat extraction to obtain dry air. The heater-cooler is set to extract 10 kW. In principle, at equilibrium we should not obtain a change in temperature because the heat comes from condensation of water vapor, yet FM's results show otherwise (Table 44).

Table 44 Water condensation assessment

	Inlet	**Outlet**
Temperature [°C]	20.0°C	-6.0°C
Pressure [kPa]	101.325	101.325
Relative humidity [%]	100	100

Specific humidity [kg_{water}/kg_{mix}]	0.014478	0.014478
Thermal loss [kW]	10	

Handling FM's limitation with regard to condensation and evaporation negligence could be realised in two different ways. First, a new feature where humidity could be included in heat-exchangers performance maps can be put forward (this would also require FM to compute the latent heat of water vapor in the energy balance equation). However, this method would result in building an arduous 4D performance map where exhaustive data would be required. The second approach would be to build a dynamic (transient) model. [11] This model wouldn't require a performance map as it would compute the outlet temperatures by solving the differential modeling equations. The drawback of this approach is that internal geometric data of the cross-flow heat-exchangers (heat transfer area and length, fin efficiencies, internal geometry data, etc.) would be required and assumptions on convective heat transfer and mass transfer coefficients would have to be made [12-14] without being able to validate them.

5.2 Ram air limitation

A very important limitation within the model could not be overcome, that is the model is unable to match the ram air flow based on ambient inlet and outlet pressures, pressure drops within the channel and fan drive. Despite accurate pressure drop modeling within the ram channel (RARV, HXs and NACA scoops) and acceptable ram air fan mapping, fan bypass flow could not be matched. Although, a closer look to LTS data shows dubious numbers. Figure 54 is an example of steady-state ram air data from LTS (flight case APU8ISA2P). The first column indicates the flow rate (lb/min) whereas the second column indicates absolute pressure (psia). It can be noticed that the flow splits at the collector inlet where 95.20 lb/min goes through the fan, while 116.13 lb/min bypasses it through a check valve (PLCKV). Finally, the two streams mix at the bypass junction.

RAM AIR CHANNEL								
Ambient	211.14	12.470	9.7	9.7	33.6	0.0		
Intake Scoop outlet	211.14	11.818	9.7	9.7	33.6	0.0		
Sprayer inlet	211.14	11.603	9.7	9.7	33.6	0.0		
SHX inlet (cold side)	211.14	11.603	8.6	8.6	36.6	0.0		
SHX outlet (cold side)	211.14	11.348	21.1	21.1	36.6	0.0		
PHX outlet (cold side)	211.14	11.174	67.4	67.4	36.6	0.0		
Plenum inlet	211.14	11.174	67.4	67.4	36.6	0.0		
Collecter inlet	95.20	11.107	67.3	67.3	36.6	0.0		
Fan inlet	95.20	11.107	67.3	67.3	36.6	0.0		
Fan outlet	95.20	11.476	72.0	72.0	36.6	0.0		
PLCKV outlet	116.13	11.450	67.3	67.3	36.6	0.0		
Bypass junction	211.33	11.450	69.4	69.4	36.6	0.0		
Plenum outlet	211.33	11.243	69.4	69.4	36.6	0.0		
RARV outlet	211.33	11.180	69.4	69.4	36.6	0.0		
Discharge scoop inlet	211.33	10.712	69.4	69.4	36.6	0.0		
Ambient	211.33	12.470	69.4	69.4	36.6	0.0		
RECIRCULATION								

Figure 54 APU8ISA2P ram air data

It can be argued that bypass flow seems to violate the second law. In fact, the pressure at the plenum inlet (11.174 psia) is inferior to the pressure at the PLCKV outlet or at the bypass junction (11.450 psia). Yet, fluids flow from high to low pressure. In other words, if the pressures are accurate, then one would expect reverse flow at the bypass stream. It is not surprising then that Flowmaster's flow and fan power consumption solutions deviate from the reference.

In order to validate the pack model and cabin distribution, ram air flow rates were assigned as inputs as well as the fan power consumption. Indeed, flow through the fan must match the data very closely because it modifies the power consumption, which in turn determines the ACM operating point. Moreover, data points (flight cases) were discarded when fan was mapped (section 4.1.2) because of aberrant efficiencies. Therefore, setting the ram mass flow as an input for those cases was expected.

Finally, it should be noted that this discrepancy in bypass flow and pressure was found in almost all flight cases whether they were ground or in-flight.

5.3 Heat-exchanger calculation improvement

Heat-transfer calculation in wet or partially wet heat exchangers is more complicated than dry cases. Yet it was really surprising that FM was unable to predict accurate outlet temperatures and

condensed/evaporated water flows because of latent heat omission. This limitation being significant, a calculation method for wet heat-exchangers (steady-state) is proposed here. This method assumes that the total heat flow rate and pressure drop are known, either as a user input or by mapping. Inlet conditions must also be known. Pressure drop mapping was achieved successfully in this project and no additional improvement is necessary. However, there is still room for further research in efficient mapping of wet heat-exchangers heat-transfer.

Wet heat-exchanger approach

The methodology consists on discretizing the flow stream inside the heat-exchanger in *n* elements and solving the energy balance equation in each one of them. In the stream being cooled down, when the temperature reaches the dew point, the enthalpy of the condensed water is added to the energy equation until the humidity ratio reaches zero. Once the thermal process is solved, the pressure drop is taken into account and the algorithm tries to find liquid-vapor equilibrium state. The calculation on the heated stream is similar except there might be water evaporation instead of condensation if liquid water is present at the inlet.

By proceeding as explained above, it is assumed that the pressure drops linearly in the direction of the flow and that the heat flux in each element is constant. In reality, the process is more complex. The thermodynamic path assumed within this methodology from the initial to the final thermodynamic state is an ideal one. However, the real thermodynamic process path is unimportant to us as we are only concerned in finding the final flow state. Ultimately, the temperature found will be at thermal equilibrium where both phases (liquid and vapor) are at the same temperature.

To apply the method, the reference enthalpy state must be defined for each species. Usually, water zero enthalpy is set at the liquid phase at 0°C. For dry air it is also 0°C. Air and vapor are assumed to be ideal gases and their enthalpies are only function of temperature.

When inlet stagnation temperature and pressure are known, the static values must be first calculated using Equations 7, 8 and 11. Then, the vapour partial pressure is calculated:

$$P_{vapor} = \left(\frac{\dot{m}_{vapor}}{\dot{m}_{vapor} + \frac{M_{water}}{M_{air}} \dot{m}_{air}} \right) P_{s\ inlet}$$

The dew point is given by Goff's relation [44]

$$T_{dew} = 164.630366 + 1.832295 \cdot 10^{-3} P_{vapor} + 4.27215 \cdot 10^{-10} {P_{vapor}}^2 + 3.738954 \cdot 10^{3} {P_{vapor}}^{-1} - 7.01204 \cdot 10^{5} {P_{vapor}}^{-2} + 16.161488 \ln P_{vapor} - 1.437169 \cdot 10^{-4} P_{vapor} \ln P_{vapor}$$

The energy balance around the element is

$$\frac{\dot{Q}}{n} = \left[\dot{m}_{air} \cdot C_{p_{air}}\left(T_{out} - T_{ref}\right) + \dot{m}_{vapor}\left(h_{latent@T_{ref}} + C_{p_{vapor}}\left(T_{out} - T_{ref}\right)\right)\right] - \left[\dot{m}_{air} \cdot C_{p_{air}}\left(T_{in} - T_{ref}\right) + \dot{m}_{vapor}\left(h_{latent@T_{ref}} + C_{p_{vapor}}\left(T_{in} - T_{ref}\right)\right)\right]$$

$\dot{Q}$ and n are the total heat duty and the number of elements, respectively. The temperature T_{out} is solved in the equation above and the process is repeated in the next element where T_{in} is set as T_{out} found previously until the temperature reaches the dew point or all the heat has been transferred.

At the dew point, water vapor condenses and its latent heat is transferred while the static temperature stays constant. Hence, the energy equation becomes the enthalpy difference between the element outlet and inlet.

$$\frac{\dot{Q}}{n} = \left[\dot{m}_{air} \cdot C_{p_{air}}\left(T_{dew} - T_{ref}\right) + \left(\dot{m}_{vapor} - \dot{m}_{cond}\right)\left(h_{latent@T_{ref}} + C_{p_{vapor}}\left(T_{dew} - T_{ref}\right)\right) + \left(\dot{m}_{liq} C_{pl} + \dot{m}_{cond} C_{pl}\right)\left(T_{dew} - T_{ref}\right)\right] - \left[\dot{m}_{air} \cdot C_{p_{air}}\left(T_{dew} - T_{ref}\right) + \dot{m}_{vapor}\left(h_{latent@T_{ref}} + C_{p_{vapor}}\left(T_{dew} - T_{ref}\right)\right) + \dot{m}_{liq} C_{pl}\left(T_{dew} - T_{ref}\right)\right]$$

The flow of condensed water m_{cond} is solved until the vapor flow rate reaches zero or all the heat is transferred. When all the vapor has condensed but there's still heat to be transferred (the calculation has not reached the last element), the energy equation is

$$\frac{\dot{Q}}{n} = \left[\dot{m}_{air} \cdot C_{p_{air}}\left(T_{out} - T_{ref}\right) + \dot{m}_{l} C_{p_{l}}\left(T_{out} - T_{ref}\right)\right] - \left[\dot{m}_{air} \cdot C_{p_{air}}\left(T_{in} - T_{ref}\right) + \dot{m}_{l} C_{p_{l}}\left(T_{in} - T_{ref}\right)\right]$$

It should be noted that in reality, at the dew point, the heat flow rate comprises latent and sensible heat, that is the temperature still decreases even though not all the water vapor has condensed, but

once again we are not concerned with the real process path in a steady-state process. When the temperature is below the dew point but there's still water vapor or when the temperature is above the dew point but there's still liquid water present, the state has not reached thermal equilibrium yet. Eventually, it will and the final state will be the same as the one obtained with our calculation.

A Matlab script (see Appendix A) was written to compute wet heat-exchanger outlet conditions and three computed examples are presented below to better illustrate the method.

Table 45 Heat-exchanger calculation improvement inputs

		Inputs		
		Example 1	**Example 2**	**Example 3**
$\mathbf{P_{t\ inlet}}$	Pa	323963	271101	295722
$\mathbf{T_t}$	K	385.15	369.55	391.9
$\dot{\mathbf{m}}_{\mathbf{air}}$	kg/s	0.3538	0.29029	0.31297
$\dot{\mathbf{m}}_{\mathbf{vapor}}$	kg/s	0.00668686	0.00343797	0.00312085
$\Delta \boldsymbol{P_t}$	Pa	-15775	-12252	-13934
$\dot{\boldsymbol{Q}}$	J/s	-38485	-24649	-23562
A	m^2	0.005641472	0.005641472	0.005641472
n		600	600	600

Table 46 Heat-exchanger calculation improvement outputs

		Outputs		
		Example 1	**Example 2**	**Example 3**
$\dot{\mathbf{m}}_{\mathbf{vapor}}$	kg/s	0.0032	0.002149	0.003121
$\dot{\mathbf{m}}_{\mathbf{liquid}}$	kg/s	0.0035	0.001288	0
$\mathbf{T_s}$	K	303.55	297.46	318.6
$\mathbf{T_{dew}}$	K	303.55	297.46	303.9
$\mathbf{P_{s\ outlet}}$	Pa	307 480	311 329	281186
Rel. Hum.		100.0	100.0	45.2

5.4 Transient simulation and control

Transient simulation was out of scope for this project. However, discussion on its feasibility and advantages were explored and are presented here.

Valve pressure loss coefficients, which can be thought as the valve opening, were assigned as inputs to the model. These coefficients are very important because they determine the pressure drop through the valve (FCV) or the flow rate (TAPRV and TAVs). Yet, these values are unknown a priori.

Transient ECS models have been reported in literature. [8, 10, 11, 45]. Therefore, our model was run with FM's transient solver and proved to converge to a steady-state solution after random disturbances to the system. Now, a transient simulation can prove to be most useful determining valve openings. In fact, controllers can be used to find the optimal openings so as to reach a set point, a certain temperature in one of the cabins for example. Controllers can even be used to control flow split by changing the cabins coefficient of discharges.

As mentioned in the introduction, control of the most important cabin parameters, pressure and temperature, should be carried out by manipulation of the outflow valve (OFV) and TCV, respectively. A steady-state control approach was first attempted in order to converge to the optimal valve openings and reach temperature and pressure set points. This can be done using PID controllers and setting the Integral constant to any value, instead of "Not Set", while running a *steady-state simulation*. Flowmaster will then attempt to reach the set point by iterating through the valve opening parameter. Assessment of this approach was undertaken for TCV control. Most of the time, TCV converged. However, this approach was unsuccessful in every attempt when additional valves were considered. The model failed to converge and did not provide any evaluation of system performance. Failed convergence could be due to the fact that, while the controllers' tolerance and weighting factor can be changed in the settings, it applies to all the controllers. However, the valves do not have the same sensitivity and some might need iterations that are of different magnitudes.

This is where transient simulation can be most useful. While running that type of simulation, PIDs controllers can reach their set points (or not) and there is no limitation with the number of valves that can be on automatic control. Cockpit temperature control by TCV opening was attempted for

case H022ISA1P2BAI. Figure 55 shows the cockpit temperature as a function of time in a transient simulation where the PI controller set point was defined at 24.16°C.

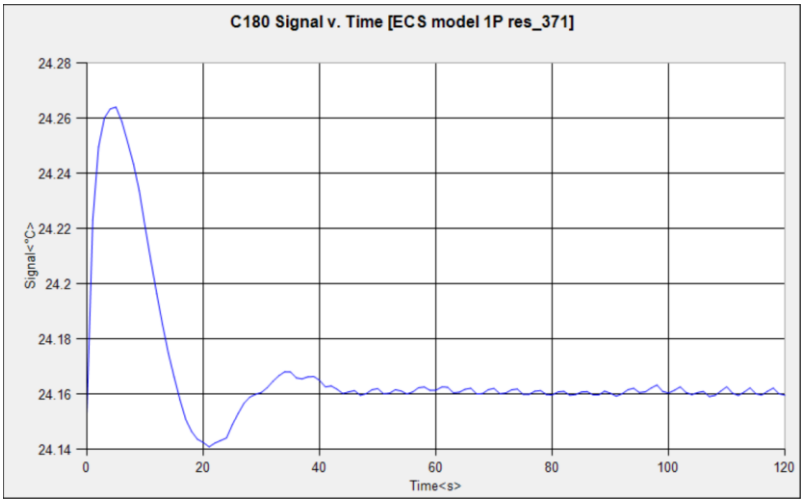

Figure 55 Cockpit temperature (VTS) in transient simulation

Also, transient simulation could allow cabin pressure control by switching the flow source downstream the cabins (boundary condition) for an outflow valve and adding a controller.

While there is no limitation on the number of valves, before integrating full cabin temperature control into the model, there is a need to define a control philosophy and logic in order to implement Trim air valve (TAV) control that needs to be investigated further.

Finally, a very important point must be pointed out in transient simulation. ECS dynamic behaviour (time response) from our model must not be considered. Our ECS model is essentially a steady-state model – ECS components are not dynamic models and cannot provide accurate time response behaviour. Nevertheless, we can apply a transient solver in order to find the optimal valve openings.

In addition, if steady-sate cabin heat sources/sinks are substituted by a dynamic cabin temperature model described by equations 57 and 58, then the dynamics of the ECS could be analysed *while* aircraft descending or climbing under the assumption that ECS packs dynamics are much faster than cabin dynamics. This seams reasonable since cabin volume is much larger than the packs.

$$\boldsymbol{m_{furniture} \cdot Cp_{furniture} \frac{dT_{furniture}}{dt} = UA_{furniture}\left(T_{cabin} - T_{furniture}\right)} \quad (57)$$

$$V_{cabin} \cdot \rho_{air} \cdot Cp_{air} \frac{dT_{cabin}}{dt} = UA_{cabin}(T_{skin} - T_{cabin}) + W_{electrical} + W_{metabolic} + UA_{furniture}(T_{furniture} - T_{cabin}) \quad (58)$$

5.5 Conclusion

An aircraft ECS comprising pack and distribution was modeled with Flowmaster. The main components were mapped based on flight data and used by the model to compute temperature, pressure, flow and humidity throughout the system. The model was validated for XCD, CD and ISA cases at all altitudes (ground or in-flight). In other words, the model could be validated for cases where condensation did not take place within the heat-exchangers. Nonetheless, two important limitations were found within the model.

First, a software limitation prevents to predict cabin conditions where water condensation occurs in HD and XHD cases. Unfortunately, humid air condensation and evaporation are neglected in heat transfer components. Thereby, the cabin temperature is lower than in reality. A method was proposed to overcome this issue: improved heat-exchanger calculation.

Second, a limitation encountered in our data made it impossible for the model to match ram air flow and thus fan power consumption. Nevertheless, the model can run when these variables are set as inputs.

Finally, the model was run in transient mode successfully. Additionally, transient mode allows control implementation by classical PID controllers. The latter can be used to find optimal valve openings and for temperature control.

BIBLIOGRAPHY

[1] A.P.P. Santos, C.R. Andrade, and E. L. Zaparoli, "A Thermodynamic Study of Air Cycle Machine for Aeronautical Applications," *International Journal of Thermodynamics,* vol. 17, p. 10, September 2014 2014.

[2] H. L. Zhao, Y. Hou, Y. F. Zhu, L. Chen, and S. T. Chen, "Experimental study on the performance of an aircraft environmental control system," *Applied Thermal Engineering,* vol. 29, pp. 3284-3288, Nov 2009.

[3] "Cabin Environmental Control Systems," in *Aviation Maintenance Technician Handbook* vol. 2, ed: FAA, 2012.

[4] D.V.Mahindru and P. Mahendru, "Environmental Control System for Military & Civil Aircraft," *Global Journal of researches in engineering: Aerospace Engineering,* vol. 11, August 2011 2011.

[5] M. Dechow and C. A. H. Nurcombe, "Aircraft Environmental Control Systems," in *Air Quality in Airplane Cabins and Similar Enclosed Spaces*, M. Hocking, Ed., ed Berlin, Heidelberg: Springer Berlin Heidelberg, 2005, pp. 3-24.

[6] "T-20209-DAC-0001 ECS Performance Report."

[7] "T-20209-DAC-0004 Required data for Zonal Temperatures, Pressures & Ventilation Flow Rate."

[8] J. Eichler, "Simulation Study of an Aircraft's Environmental Control System Dynamic Response," *Journal of Aircraft,* vol. 12, pp. 757-758, 1975/10/01 1975.

[9] S. Conceição, Zaparoli, E., and Turcio, W., "Thermodynamic Study of Aircraft Air Conditioning Air Cycle Machine: 3-wheel × 4-wheel," *SAE Technical Paper 2007-01-2579,* 2007.

[10] Y. Tu and G. P. Lin, "Dynamic Simulation of Aircraft Environmental Control System Based on Flowmaster," *Journal of Aircraft,* vol. 48, pp. 2031-2041, 2011/11/01 2011.

[11] Y. Tu and G. P. Lin, "Dynamic Simulation of Humid Air Environmental Control System," in *40th International Conference on Environmental Systems*, ed: American Institute of Aeronautics and Astronautics, 2010.

[12] J. V. C. Vargas, A. Bejan, and D. L. Siems, "Integrative thermodynamic optimization of the crossflow heat exchanger for an aircraft environmental control system," *Journal of Heat Transfer-Transactions of the Asme,* vol. 123, pp. 760-769, Aug 2001.

[13] J. V. C. Vargas and A. Bejan, "Thermodynamic optimization of finned crossflow heat exchangers for aircraft environmental control systems," *International Journal of Heat and Fluid Flow,* vol. 22, pp. 657-665, 12// 2001.

[14] T. Shiba and A. Bejan, "Thermodynamic optimization of geometric structure in the counterflow heat exchanger for an environmental control system," *Energy,* vol. 26, pp. 493-512, 5// 2001.

[15] I. Pérez-Grande and T. J. Leo, "Optimization of a commercial aircraft environmental control system," *Applied Thermal Engineering,* vol. 22, pp. 1885-1904, 12// 2002.

[16] G. C. G. Croce, "CONVECTIVE HEAT AND MASS TRANSFER IN TUBE-FIN EXCHANGERS UNDER DEHUMIDIFYING CONDITIONS," *Numerical Heat Transfer, Part A: Applications,* vol. 40, pp. 579-599, 2001/11/01 2001.

[17] G. Comini and S. Savino, "Latent and sensible heat transfer in air-cooling applications," *International Journal of Numerical Methods for Heat & Fluid Flow,* vol. 17, pp. 608-627, 2007.

[18] T. Walters. (January 2000) Gas-flow calculations don't choke. *Chemical Engineering*. Available: http://www.chemengonline.com/issues/

[19] J. A. Olsen, Walters, Trey, "Modeling Highly Compressible Flows in Pipe Networks Using A Graphical User Interface," presented at the ASME International Joint Power Generation Conference, 1997.

[20] M. A. Saad, *Compressible Fluid Flow*: Prentice Hall, 1993.

[21] C. Borgnakke and R. E. Sonntag, *Fundamentals of Thermodynamics, 8th Edition*: Wiley Global Education, 2012.

[22] A. K. S. Jain, P K, "Explicit equations for pipeflow problems," *Journal of the Hydraulics Division,* vol. 102, p. 8, 2013.

[23] T. L. Bergman, F. P. Incropera, D. P. DeWitt, and A. S. Lavine, *Fundamentals of Heat and Mass Transfer*: Wiley, 2011.

[24] R. L. Webb, "Heat Exchanger Design Methodology for Electronic Heat Sinks," *Journal of Heat Transfer,* vol. 129, pp. 899-901, 2006.

[25] SAE, "Heat and Mass Transfer and Air-Water Mixtures," ed: SAE International, 2001.

[26] A. H. Shapiro, *The dynamics and thermodynamics of compressible fluid flow*: Ronald Press Co., 1954.

[27] A. International, "AMCA Publication 201 Fans and Systems," in *Fan application manual*, ed.

[28] W. Cory, "Fans and Ventilation - A Practical Guide," ed: Elsevier.

[29] S. L. Dixon and C. A. Hall, "Chapter 2 - Dimensional Analysis: Similitude," in *Fluid Mechanics and Thermodynamics of Turbomachinery (Seventh Edition)*, ed Boston: Butterworth-Heinemann, 2014, pp. 39-67.

[30] ISO, "Industrial fans - Performance testing using standardized airways," ed, 2007, p. 228.

[31] S. L. Dixon and C. A. Hall, "Chapter 1 - Introduction: Basic Principles," in *Fluid Mechanics and Thermodynamics of Turbomachinery (Seventh Edition)*, ed Boston: Butterworth-Heinemann, 2014, pp. 1-37.

[32] M. Bolemant and D. Peitsch, *An Alternative Compressor Modeling Method within Gas Turbine Performance Simulations*: Deutsche Gesellschaft für Luft-und Raumfahrt-Lilienthal-Oberth eV, 2014.

[33] P. Walsh and P. Fletcher, *Gas Turbine Performance*: Wiley, 2008.

[34] J. G. Samuels, B, "Effect of humidity on performance of turbojet engines," National Advisory Committee for Aeronautics NACA-TN-2119, 1950.

[35] "Performance Products Catalog," in *Product Catalog* vol. 5, Garret, Ed., ed.

[36] M. Martinez-Sanchez, "16.50 Introduction to Propulsion Systems," ed: Massachusetts Institute of Technology: MIT OpenCourseWare, 2012.

[37] "T-C08110300-SP-0001 Cabin Pressure Control System Technical Specification."

[38] SAE, "Thermodynamics of Incompressible and Compressible Fluid Flow," ed: SAE International, 2011.

[39] SAE, "Aerothermodynamic Systems Engineering and Design," ed: SAE International, 2011.

[40] A. F. L. C. M. Center, "MILITARY SPECIFICATION: ENVIRONMENTAL CONTROL, ENVIRONMENTAL PROTECTION, & ENGINE BLEED AIR SYSTEMS, AIRCRAFT, GENERAL SPECIFICATION FOR," ed, 1971.

[41] "T-C08110400-DD-0002 AIR CONDITIONING SYSTEM DESCRIPTION DOCUMENT."

[42] (2010). *Surface Fitting using gridfit*. Available: http://www.mathworks.com/matlabcentral/fileexchange/8998-surface-fitting-using-gridfit

[43] (2014). *RegularizeData3D*. Available: http://www.mathworks.com/matlabcentral/fileexchange/46223-regularizedata3d

[44] D. G. Kröger, "Air-Cooled Heat Exchangers and Cooling Towers - Thermal-Flow Performance Evaluation and Design, Volume 1," ed: PennWell.

[45] C. Müller, D. Scholz, and T. Giese, "Dynamic Simulation of Innovative Aircraft Air Conditioning," presented at the 1st CEAS European Air and Space Conference, Berlin, Germany, 2007.

APPENDIX A WET HEAT-EXCHANGER SCRIPTS

Main code

```
clear all;
clc

%CONSTANTS
y = 1.4;
Mw = 18.015/1000; %kg/mol
Mair = 28.965/1000; %kg/mol
R = 8.3145498; %J/mol K

%INPUTS
n=600;
dP0= 13934; %Pa
Q= -23562; %J/s
ma= 0.31297; %kg/s
mv= 0.00312085;
ml=0;
A=0.005641472; %m^2
P0= 295722; %Pa
T0= 391.9; %K

dP0i=dP0/n;
Qi=Q/n;
Mmix = 1/(mv/(mv+ma)/Mw + ma/(mv+ma)/Mair);
Rmix = R/Mmix;

%Initialisation
i=0;
options = optimoptions('fsolve','TolFun',1e-9);
```

```
Mi = fsolve(@(Mi)(ma+mv-A*P0*sqrt(y/Rmix/T0)*Mi*(1+(y-1)/2*Mi^2)^(-3)),0);
j=Mi; %save value for reference
P = P0*(1+(y-1)/2*Mi^2)^(-y/(y-1));
Pin = P;  %save value for reference
T = T0*(1+(y-1)/2*Mi^2)^(-1);
Tin=T; %save value for reference
w= mv/ma;
Pv = (mv/(mv+Mw*ma/Mair))*P;
Pvs = Goff(T);

if Pv<=Pvs
    fprintf('La limite de saturation n''a pas été atteinte');
    HumRel = Pv/Pvs*100;
    HumRat= Mw/Mair*(Pv/(P-Pv));
else
    fprintf('Il devrait avoir de l''eau condensée à l''entrée-équilibre liquide vapeur');
    HumRel = 100;
end

%Point de rosée initial - Dew point

if (mv > 0)&& Pv<=Pvs
    Tdew = Goffinv(Pv);
else
    Tdew = inf;
end

%Échange thermique
while i<n

    % Température au-dessus du point de rosée et il n'y a pas de
    % liquide
```

```
if T > Tdew

    T = fsolve(@(x)(Qi-ma*(Cpa(T,x)+ mv/ma*Cpv(T,x))),273.15);

    if T<Tdew
        dT=T-Tdew;
        T=Tdew;
    end
    i=i+1;
end

 % Température égale au point de rosée et il n'y a pas de
 % liquide

if (T==Tdew) && (mv>0)

    m_cond = -Qi/(hfg(273.15)+Cpv(273.15,T)-Cpl(273.15,T));
    ml = ml + m_cond;
    mv = mv - m_cond;

    if mv<=0
        dmv = mv; %save value for reference
        mv=0;
    end
    i=i+1;
end


% Température en dessous du point de rosée

if T<=Tdew && mv==0
    Qii = (n-i)*Qi;
```

```
        % Static temperature after heat transfer
        T = fsolve(@(x)(Qii - ma*Cpa(T,x) - ml*Cpl(T,x)),307);
        i=n;
    end
end
Tj = T;
ml_i=ml;
mv_i=mv;
% Mi = fsolve(@(Mi)(ma+mv-A*P0*sqrt(y/Rmix/(T*(1+(y-1)/2*Mi^2)))*Mi*(1+(y-1)/2*Mi^2)^(-
(y+1)/2/(y-1))),0);
% T0 = (T*(1+(y-1)/2*Mi^2));
Pv_end = (mv/(mv+Mw*ma/Mair))*P;
Pvs_end = Goff(T);
HumRel_i = Pv_end/Pvs_end*100;

%Pressure drop
P = P - n*dP0i;

Pv_end = (mv/(mv+Mw*ma/Mair))*P;
Pvs_end = Goff(T);
HumRel_j = Pv_end/Pvs_end*100;
%Tdew = Goffinv(Pv_end);

% Is there liquid water while the Pv<Psaturation
k=20000;
while ml>0 && Pv_end/Pvs_end<1
    %If yes, then we need to flash the liquid water. Note that the latent
    %heat required will come from the air.

    mevap = -Qi*n/k/(hfg(273.15)+Cpv(273.15,T)-Cpl(273.15,T));
    mv = mv + mevap;
```

```
    ml = ml - mevap;

    T = fsolve(@(x)(Qi*n/k-ma*(Cpa(T,x)+ mv/ma*Cpv(T,x))), T);
    Pv_end = (mv/(mv+Mw*ma/Mair))*P; %Pv_end augmente
    Pvs_end = Goff(T); %Pvs_end diminue

    if Pv_end<Pvs_end
        Tx = T;
    end
end

% mv = mv-mevap;  %only if mevap exist
% ml = ml+mevap;
% T = Tx;

Mi = fsolve(@(Mi)(ma+mv-A*P*(1+(y-1)/2*Mi^2)^(y/(y-1))*sqrt(y/Rmix/(T*(1+(y-
1)/2*Mi^2)^(1)))*Mi*(1+(y-1)/2*Mi^2)^(-(y+1)/2/(y-1))),0);
T0 = T*(1+(y-1)/2*Mi^2)^(1);
P0 = P*(1+(y-1)/2*Mi^2)^(y/(y-1));

Pv_end = (mv/(mv+Mw*ma/Mair))*P;
Pvs_end = Goff(T);

%Outputs
Tend=T
Pend=P
mv
ml
wend= mv/ma
HumRel = Pv_end/Pvs_end*100
HumRat= Mw/Mair*(Pv_end/(Pend-Pv_end))
Tdew = Goffinv(Pv_end)
```

Latent heat function

```
function y=hfg(T)

%Gives the water laten heat J/kg []
y = (3.4831814e6 - 5.8627703e3*T + 12.139568*T^2 - 1.40290431e-2*T^3); %J/kg
```

Dew point function

```
function T = Goffinv(Pv)
%Computes the dew point
%Pv in Pa; T in K

T = 164.630366 + 1.832295e-3*Pv + 4.27215e-10*Pv^2 + 3.738954e3/Pv - 7.01204e5/Pv^2 + 16.161488*log(Pv) -
1.437169e-4*Pv*log(Pv);
```

Dry air heat capacity

```
function y = Cpa(Ta,Tb)
%Computes dry air enthalpy by integration of the heat capacity function
%between temperature Ta and Tb.

ya = 1.045356e3*Ta - 3.161783e-1*Ta^2/2 + 7.083814e-4*Ta^3/3 - 2.705209e-7*Ta^4/4;
yb = 1.045356e3*Tb - 3.161783e-1*Tb^2/2 + 7.083814e-4*Tb^3/3 - 2.705209e-7*Tb^4/4;

y = yb-ya;

end
```

Water vapor heat capacity

```
function y = Cpv(Ta,Tb)
%Computes water vapor enthalpy by integration of the heat capacity function
%between temperature Ta and Tb.

yb = 1.3605e3*Tb + 2.31334*Tb^2/2 - 2.46784e-10*Tb^6/6 + 5.91332e-13*Tb^7/7;
```

```
ya = 1.3605e3*Ta + 2.31334*Ta^2/2 - 2.46784e-10*Ta^6/6 + 5.91332e-13*Ta^7/7;

y = yb - ya;
```

Liquid water heat capacity

```
function y = Cpl(Ta,Tb)
%Computes liquid water enthalpy by integration of the heat capacity function
%between temperature Ta and Tb.

ya = 8.15599e3*Ta - 2.80627e1*Ta^2/2 + 5.11282e-2*Ta^3/3 - 2.17582e-13*Ta^7/7;
yb = 8.15599e3*Tb - 2.80627e1*Tb^2/2 + 5.11282e-2*Tb^3/3 - 2.17582e-13*Tb^7/7;

y= yb - ya;
```